A Report on the Comparison of Unmanned Aerial Vehicle Data with Field Data over Reclaimed Wellsites in the Boreal Forest

Prepared for:
Anne McIntosh
Applications Centre, Alberta Biodiversity Monitoring Institute

Prepared by:
Jennifer Hird and Greg McDermid
Geospatial Centre Research Team, Alberta Biodiversity Monitoring Institute

About This Document

Acknowledgements
We wish to thank the following individuals for their valuable contributions to this work: Allison Cully and Tobias Tan (UAV operators), Taylor McKeeman (UAV image pre-processing), Alessandro Montaghi (UAV point cloud pre-processing), Jerome Cranston (GIS support), and Anne McIntosh, Delinda Ryerson and the field crews of the Ecological Recobvery Monitoring Project. Ancillary data was provided by Alberta Environment and Sustainable Resource Development.

Title
A Report on the Comparison of Unmanned Aerial Vehicle Data with Field Data over Reclaimed Wellsites in the Boreal Forest

Authors
Jennifer Hird, Greg McDermid

Purpose
This report summarizes the preliminary results of a study investigating the relationships between data collected by unmanned aerial vehicles and that collected by ground crews over a series of reclaimed wellsites in Alberta's boreal forest.

Suggested Citation
Alberta Biodiversity Monitoring Institute Geospatial Centre Research Team. (2015). A Report on the Comparison of Unmanned Aerial Vehicle Data with Field Data over Reclaimed Wellsites in the Boreal Forest. Department of Geography, University of Calgary, Alberta, Canada.

Contact Information
If you have questions or concerns regarding this report, please contact:
Dr. Greg McDermid
Department of Geography, University of Calgary
Earth Sciences Rm. 356, 2500 University Dr. NW
Calgary, Alberta, Canada T3C 3J6
Email: mcdermid@ucalgary.ca
Phone: 1 (403) 220-4780

Table of Contents

List of Tables

List of Figures

1.0 Introduction

The Alberta government's Environmental Protection and Enhancement Act requires industrial companies to return their decommissioned industrial developments (e.g., oil and gas facilities) located on Alberta soil to "equivalent land capability". In other words, the ability of the land to support various equivalent (though not identical) land uses must be restored, after which a reclamation certificate is issued [1]. Once a decommissioned industrial site has been certified, the rate of its ecological recovery to a natural state is neither currently documented nor monitored, and may continue for decades following decommission and reclamation [2]. In response to the need for a greater understanding and knowledge of recovery rates over reclaimed land, the Ecological Recovery Monitoring (ERM) Project was initiated by the Alberta Biodiversity Monitoring Institute. In addition to rigorous field studies designed to assess historical wellsite ecological recovery rates, the ERM aims to develop a framework for a sustainable and scientifically sound, long-term monitoring program for tracking ecological recovery at certified industrial sites. A key component of the latter is the investigation of current technologies that may offer a cost-efficient, repeatable source of ecological information. One such technology that has garnered great interest in the field of ecology, among many others, is the use of unmanned aerial vehicles (UAVs). With their ability to provide detailed, spatially explicit, local views of the Earth's surface on short time scales and at a greatly reduced cost, when compared to more traditional field data collection or LiDAR acquisition, UAVs offer significant potential as an additional data source for long-term ecological recovery monitoring.

The objective of this study was to compare UAV-derived datasets with data collected by ground field crews over a series of reclaimed wellsites in Alberta's boreal forest as a means of assessing the potential value of UAV data as an additional source for ecological recovery indicators. This is one component of the larger ERM Project. The following provides a short background and introduction to UAVs, followed by a description of the study area, the methods used in the study, the results, and finally, discussion and conclusion sections.

2.0 Background

The growing availability of small, lightweight unmanned aerial vehicles (UAVs), also commonly referred to as unmanned aerial systems or 'drones'[3], has lead to an explosion of interest in their value for a diversity of applications, including ecology and resource management. Commercial UAVs are generally divided into two main types: fixed-wing and rotary-wing [3]. The former generally offer more stability and longer flights (they are often larger), while the latter are generally more maneuverable. UAVs range in size, flight duration, payload, level of automation, etc., and the choice of which to use and what sensor or sensors to employ is highly dependent upon one's application. Detailed reviews of UAV technology and application are provided by [4], [5] and [3]. Regardless of which unit and sensor are employed, however, each offers a means of acquiring detailed, remotely-sensed data over a variety of landscapes at user-defined temporal scales. Also advantageous is that these data are acquired for a fraction of the costs associated with traditional field data collection or manned aircraft-borne sensors [6]. UAVs are thus particularly useful in locations with limited accessibility, or where long-term, repeating measurements are necessary, such as in monitoring programs.

While UAV technology is generally still considered to be 'new' and many of its applications and limitations continue to be explored, numerous publications outlining the results of recent investigations are showing considerable promise and potential. Current applications include precision agriculture and crop monitoring [6]–[11], deriving forest structure [12]–[14], conducting wildlife surveys [15], [16], mapping and monitoring geology and Earth processes [17], [18], topographic and structural surveying [19]–[22], and many others.

One noteworthy advantage of UAV remote sensing datasets is their potential to produce three-dimensional point clouds that rival those obtained using LiDAR (Light Detection and Ranging) sensors. These are the product of the multiple photographic views captured by a UAV-borne sensor, which, in combination with current photogrammetric knowledge and recent advances in computing power and technology, have led to an increased understanding and use of Structure from Motion (SfM) techniques [23]. SfM, in basic terms, works much like a stereo-pair of overlapping aerial photographs but employs multiple overlapping digital images of an object or surface of interest to build a full three-dimensional structure in the form of a point cloud [24].

Photogrammetric point clouds offer enormous potential for providing an incredibly detailed, three-dimensional view of the Earth's surface. Information regarding the heights and external structure of vegetation and anthropogenic infrastructures can be very meticulously mapped. One drawback of UAV-derived point clouds is that internal structures (e.g., sub-canopy forest vegetation structures) are captured only where line of sight exists. In other words, unlike LiDAR, which comprises multiple laser returns including ground returns, the optically-based data from which photogrammetric point clouds are built cannot penetrate below a forest canopy, especially in densely-vegetated areas [25]. This difficulty is often addressed by combining UAV point clouds with a recent LiDAR-based digital terrain model, thus providing a sub-canopy 'ground' reference. A number of studies have used these combined datasets to produce canopy height models (CHMs), with which the authors then derive a series of forest structure metrics.

For instance, [26] demonstrated the successful estimation of tree heights, stem volumes, and basal area from a photogrammetric point cloud constructed over a study area in southern Sweden, concluding their techniques to produce results comparable to LiDAR-derived metrics. More recently, [12] promoted the use of UAV-acquired imagery and the derived point clouds in identifying smaller forest gaps than are detected with more traditional remote sensing datasets, thereby offering a means of mapping and monitoring an important structural attribute related to overall forest structure and understory biodiversity. The currently literature supports the potential that UAVs possess for providing an invaluable, cost-effective source of information on ecological indicators within the framework of a long-term monitoring program.

3.0 Methods

3.1 Study Area

The study area comprises a set of 17 reclaimed wellsites scattered across an area of approximately 22,000 km^2, covering the Swan Hills within west-central Alberta, Canada (Fig. 1). The area encompasses environments within both the Boreal Forest and Foothills regions of Alberta, as described by the Natural Regions and Subregions of Alberta [27]. Both regions are characterized by deciduous, mixedwood and coniferous forests, but the Boreal Forest region,

which covers more than half the province of Alberta, also contains extensive wetlands and comprises a greater variety in topographical, climatic and vegetative community characteristics than the Foothills [27]. Nevertheless, each experiences short summers and long, cold winters and is home to a wide variety of flora and fauna.

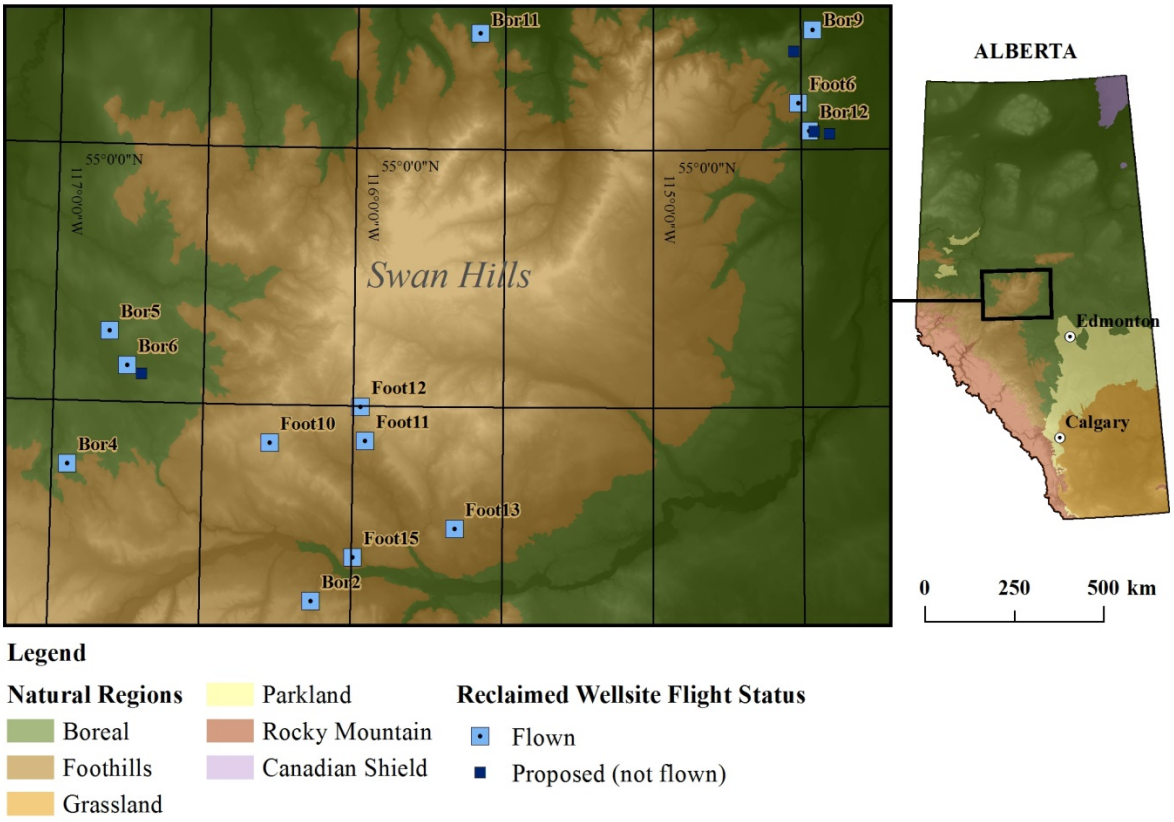

Fig. 1. Study area map showing the location of all flown and proposed (for flight) reclaimed wellsites within the west-central Alberta region. Site IDs are provided for the flown sites. Alberta's Natural Regions and the location of the study area within Alberta itself are also shown.

3.2 Data

3.2.1 *Field Data Collection*

In summer 2014, field crews collected a variety of information at each of the wellsites included in this study. At each, a series of 5 x 5 m, 10 x 10m and 25 x 25 m plots as well as 5 m, 10 m and 25 m transects were marked both within the wellsite itself, and within nearby, natural (undisturbed) reference sites. Fig. 2 shows the layout of these plots and transects followed at each wellsite. Different types of data were collected for the various types and sizes of sample unit. As the current study reflects only one component of the larger ERM Project, the field data used in this study was collected and intended for use in a broader research context. Thus not all data collected by ground crews in the summer of 2014 was employed here. Table 1 lists the set of field data measurements that were compared with concurrent UAV data, and the sample units over which they were collected. These include general shrub, herb and forb ground cover,

canopy cover, tree diameters (at breast height), and tree heights. For a full and detailed description of the field protocols followed by the ERM ground crews, please refer to [28].

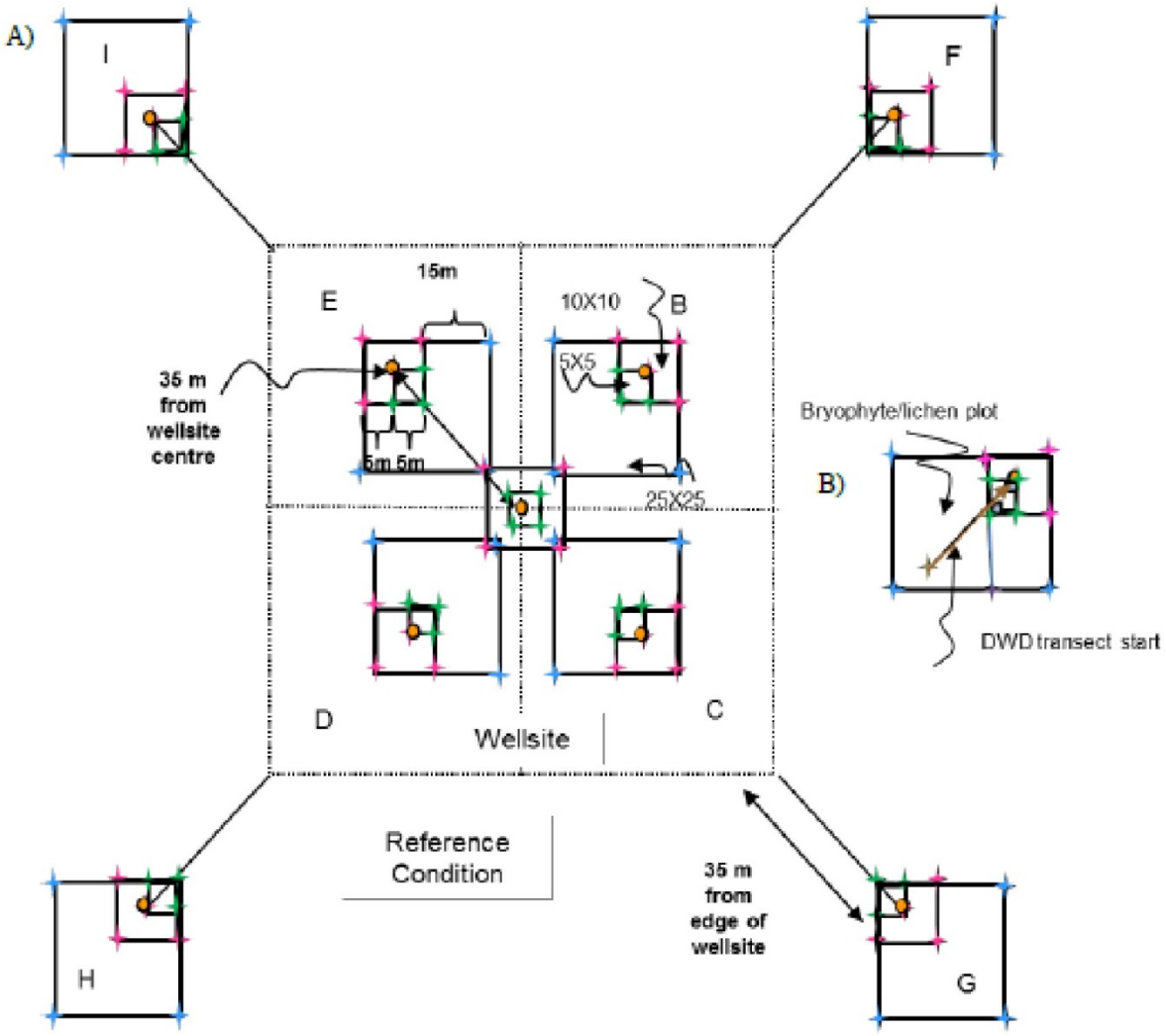

Fig. 2. A) Layout of the 5 x 5 m (green), 10 x 10 m (pink) and 25 x 25 m (blue) nested square sample plots at reclaimed wellsites and adjacent reference sites. The nested plots are labeled by quadrant (A through I). B) Showing the placement of transects (brown) within a plot. Adapted from [28].

Table 1. List of field measurements used in the current study.

Field Data Used in Study	Sample Unit of Collection
2D shrub cover > 2 m (%)	5 x 5 m plots
2D shrub cover 0.5 m to 2 m (%)	5 x 5 m plots
2D shrub cover < 0.5 m (%)	5 x 5 m plots
2D forb & herb cover < 0.5 m (%)	5 x 5 m plots
mean canopy cover (%)	10 x 10 m plots
tree and snag diameter at breast height* (cm)	5 x 5 m, 10 x 10 m, and 25 x 25 m plots
snag decay stage**	5 x 5 m, 10 x 10 m, and 25 x 25 m plots
tree and snag top height (m)	5 x 5 m, 10 x 10 m, and 25 x 25 m plots
coarse woody debris (CWD) diameter (cm)	25 m transects
CWD tally	25 m transects
CWD decay stage	25 m transects
small woody debris (SWD) 1 to 3 cm diameter (tally)	10 m transects
SWD 3 to 5 cm diameter (tally)	10 m transects
SWD 5 to 7 cm diameter (tally)	10 m transects

*1.3 m

**Used to ensure stumps were not included in the analysis

3.2.2 UAV Image Acquisition

Two separate UAVs, each flown by a separate operator, were used to capture digital RGB photos over the reclaimed wellsites and their immediate surroundings (Table 2). One of the models, the Mikrokopter Hexakopter XL, was a commercially-available 'ready-to-fly' model and was used to fly nine wellsites. The other was a custom-built prototype quadcopter and was used to fly four wellsites. In total, 13 of 17 proposed sites were successfully flown. One site (Bor7) could not be accessed by the UAV field crews, while remaining four were not flown due to an end-of-flight crash of the prototype UAV at a previous site, likely as a result of wind turbulence. A series of ground control points (GCPs) were marked, measured, and their coordinates recorded for each wellsite. Further details for each flight survey are found in Appendix A, and in [29].

Table 2. UAV model and camera payload specifications of the UAV units used to acquire imagery in this study.

	UAV Models	
Specifications	**Mikrokopter Hexakopter XL**	**Prototype**
Description	Multi-rotor, commercial 'ready-to-fly' hexcopter	Multi-rotor, custom-built quadcopter
Size	102 cm (l) x 102 cm (w)	45 cm (l) x 45 cm (w)
Weight	2.7 kg	1.5 kg
Max Speed	22 km/h	Not tested
Flight Endurance	25 mins	15 mins
Autonomy	None; manual remote control	Waypoint programming
Operator	Allison Cully (University of Calgary)	Tobias Tan (University of Alberta)
Specifications	**Camera Payloads**	
Model	Panasonic Lumix GX1	Ricoh GR
Resolution	16 megapixels	16 megapixels
Sensor Size	18 mm x 13.5 mm	23.7 mm x 15.7 mm
Weight	420 g	243 g
	Other Information	
Sites Flown	Bor2, Bor4, Bor5, Bor6, Foot10, Foot11, Foot12, Foot13, Foot15	Bor9, Bor14, Foot1, Foot6

3.2.3 Additional Datasets

An additional LiDAR dataset provided by Alberta Environment and Sustainable Resource Development (AESRD) was also used in this study as a means of providing a ground reference for the construction of UAV-based vegetation height models (VHMs). VHMs are not typically used in the literature for studying vertical vegetation structures; canopy height models or CHMs typically provide the base layer from which forest structural information such as canopy cover and forest stand heights is derived ([30]). However, as this study involves forested as well as non-forested (e.g., shrubby) vegetation, a VHM is used rather than a CHM.

The LiDAR was acquired via airborne sensors between 2005 and 2008. It was assumed that the 1 m 'bare earth' digital terrain models (DTMs) provided by AESRD remain relatively accurate representations of the current ground surface over the reclaimed wellsites.

3.2.4 Data Preparation and Pre-processing

3.2.4.1 Field Data

Field data were compiled within a Microsoft Access database, from which the relevant attributes (Table 1) for the 13 flown sites were extracted. Some of these data (e.g., mean canopy cover, 2D shrub cover) were inputted directly into the analysis, while others (e.g, diameter at breast height (DBH) and heights) were compiled into plot- or transect-level statistics using Microsoft Excel, before being included in the analysis. Table 3 lists the final field data variables used in this study.

Table 3. Final field variables used in the study. Where plot- or transect-level statistics are not listed, the variables were used directly in the analysis.

Field Data	Plot- and Transect-Level Statistics
2D shrub cover > 2 m (%)	--
2D shrub cover 0.5 m to 2 m (%)	--
2D shrub cover < 0.5 m (%)	--
2D forb & herb cover < 0.5 m (%)	--
mean canopy cover (%)	--
tree and snag diameter at breast height* (cm)	mean, maximum, minimum, range
tree and snag top height (m)	mean, maximum, minimum, range
coarse woody debris (CWD) diameter (cm)	mean
CWD tally	--
CWD decay stage	mean
small woody debris (SWD) 1 to 3 cm diameter (tally)	--
SWD 3 to 5 cm diameter (tally)	--
SWD 5 to 7 cm diameter (tally)	--

*1.3 m

The various x and y coordinates and the associated bearings recorded by the field crews at each wellsite were used to reconstruct the orientation and layout of the various plots and transects within a digital environment. These data were used to extract UAV-derived height data from within the wellsites, as described further below.

3.2.4.2 UAV Imagery

Agisoft PhotoScan Professional was used to process the sets of UAV images obtained for each reclaimed wellsite, using the x, y and z coordinates of the three GCPs recorded (per site) to georeference the resulting point clouds into WGS 84, UTM zone 11N. Images were first converted to a JPEG format prior to importation into the PhotoScan software. General steps within the software include image alignment, the construction of a dense point cloud, and the manual identification and flagging of GCPs within each individual photo containing a GCP within its extent as a means of georeferencing the resulting point cloud. This procedure was undertaken with all UAV imagery collected by the Mikrokopter Hexakopter XL (Table 2). However, difficulties were encountered when working with the images acquired by the custom-build UAV unit; these data are currently still being processed.

Once the georeferenced, photogrammetric point clouds (PPCs) had been created for the nine reclaimed wellsites flown by the Mikrokopter UAV, they were compared with the AESRD aireborne LiDAR-derived ‘bare earth’ DTMs before being combined in order to produce CHMs. Vertical mismatches were observed, however, in the z coordinate domain between the wellsite PPCs and the LiDAR DTMs, and ranged from sub-metric to upwards of more than 20 m, as estimated through a comparison of the original ground control points z coordinates with their spatial equivalent in the relevant DTM (Table 4). These vertical mismatches posed a challenge in creating reasonable CHMs, since the LiDAR DTMs are meant to offer a reference surface from which to calculate PPC-derived non-ground heights (e.g., of trees, shrubs, other ground cover). A method for aligning the PPCs with the DTMs is currently under development, and involves the

coding of a customized tool within the R programming language. In the interest of conducting an analysis of the UAV PPCs in comparison with ground data, a preliminary analysis was undertaken for the wellsite possessing the lowest mean vertical mismatch: Bor6. This site showed an average GCP vertical mismatch of 0.1 m (Table 4), which is deemed reasonable for an initial exploratory data analysis. It should be noted that the remainder of the Methods section describes the treatment of data from the Bor6 wellsite (Fig. 1).

Table 4. Mean vertical mismatch between wellsite photogrammetric point clouds and the associated LiDAR DTMs.

Reclaimed Wellsite	Vertical Mismatch (m)
Bor2	-22.1*
Bor4	12.1
Bor5	-0.2
Bor6	-0.1
Foot10	4.8
Foot11	2.1
Foot12	4.5
Foot13	-6.5
Foot15	7.6

*Negative numbers indicate the point cloud is below the LiDAR DTM

In order to construct a VHM of the Bor6 site, from which a variety of vegetation structure-related metrics and statistics could be extracted, the Bor6 PPC was first converted to a 0.5 m digital elevation raster within ESRI's ArcGIS 10.3 software. The LiDAR DTM was then subtracted from this PPC-derived raster to produce a 0.5 m VHM, also within ArcGIS 10.3. Though these two datasets did not possess equivalent spatial resolutions (i.e., 0.5 m vs. 1 m), it was assumed that capturing the spatial variation in above-ground surface heights (e.g., vegetation) by using a 0.5 m spatial resolution would out-weigh any detriment caused by the use of a coarser resolution DTM. It should also be noted that because the wellsites involved in this study are reclaimed and are located within relatively uninhabited portions of the province, it was assumed that any above-ground values represent vegetation heights.

Once the VHM was constructed, a variety of metrics and statistics were calculated for each of the 5 x 5 m and 10 x 10 m plots, and the 10 m and 25 m transects (Table 5). The 25 x 25 m plots were not used in this study as the majority of their area fell outside the footprint of the UAV imagery collected at the Bor6 site.

The metrics presented in Table 5 reflect typical metrics as found in the current UAV literature (e.g., [31], [32]), and while many of them are very similar to one another, the exploratory nature of this study supports the use of numerous variables as a means of best assessing possible relationships between such variables and ground-based ecological and vegetation measures. Once extracted from the Bor6 site VHM, the UAV-derived metrics were analyzed following the procedures outlined in the following section.

Table 5. List of the various height and canopy cover variables calculated using the Bor6 site VHM.

Height Variables (m)	Canopy Cover Variables (%)
Mean Height	Canopy Cover = 0 m
Height Standard Deviation	Canopy Cover < 0.25 m
Maximum Height	Canopy Cover 0.25 - 0.5 m
Minimum Height	Canopy Cover < 0.5 m
Median Height	Canopy Cover 0.5 - 1 m
Height Range	Canopy Cover < 1.3 m
Sum of Heights	Canopy Cover >= 1.3 m
First Quartile	Canopy Cover 1 - 2 m
Second Quartile	Canopy Cover < 2 m
Third Quartile	Canopy Cover >= 2 m
50th Percentile	Canopy Cover 2 - 5 m
75th Percentile	Canopy Cover >= 5 m
85th Percentile	Canopy Cover 5 - 10 m
90th Percentile	Canopy Cover 10 - 15 m
95th Percentile	Canopy Cover 15 - 20 m
99th Percentile	Canopy Cover 20 - 25 m
	Canopy Cover > 25 m

3.3 Analysis

The UAV-derived and field-based variables extracted for the Bor6 site were first compared using a statistical correlation analysis, by sampling unit (i.e., plot size and transect size). Kendall's tau-b correlation statistic was run on the data within IBM's SPSS Statistics Version 21 software, using a two-tailed significance level of 0.05. This non-parametric test is designed to handle non-normally distributed data sets and is less prone to sampling error than either Pearson's correlation or Spearman's rho [33]. In addition to a correlation analysis, the Automatic Linear Modeling module of the software was used to conduct a 'best subsets' linear regression analysis wherein all possible combinations of UAV PPC-derived variables were tested as model covariates for each of the field variable. The objective was to derive the best possible linear regression model to describe the variation present within each field variable, and since the number of PPC variables is high and there is likely to be a considerable amount of multicollinearity between them, this was decided as the best approach to modeling the field variables using the PPC data. Model fit was determined using a corrected Akaike information criterion (AICC).

As spatially-explicit rasters of the PPC-derived variables included in the current analysis are not yet available, the models built in the above procedure were not applied over the area of the Bor6 wellsite. This forms a component of the further work described in Section 6.0 below.

4.0 Results

4.1 Data Collection and Processing

Fig. 3 shows the layout of the three sets of plots and two sets of transects over which field data was collected in the summer of 2014 by ERM field crews. While Fig. 2 showed the planned, ideal configuration, field conditions often dictate where plots are actually placed once the crews are arrive at a site in the field (e.g., the reference sites cannot be placed on an anthropogenic disturbance such as a road or seismic cutline).

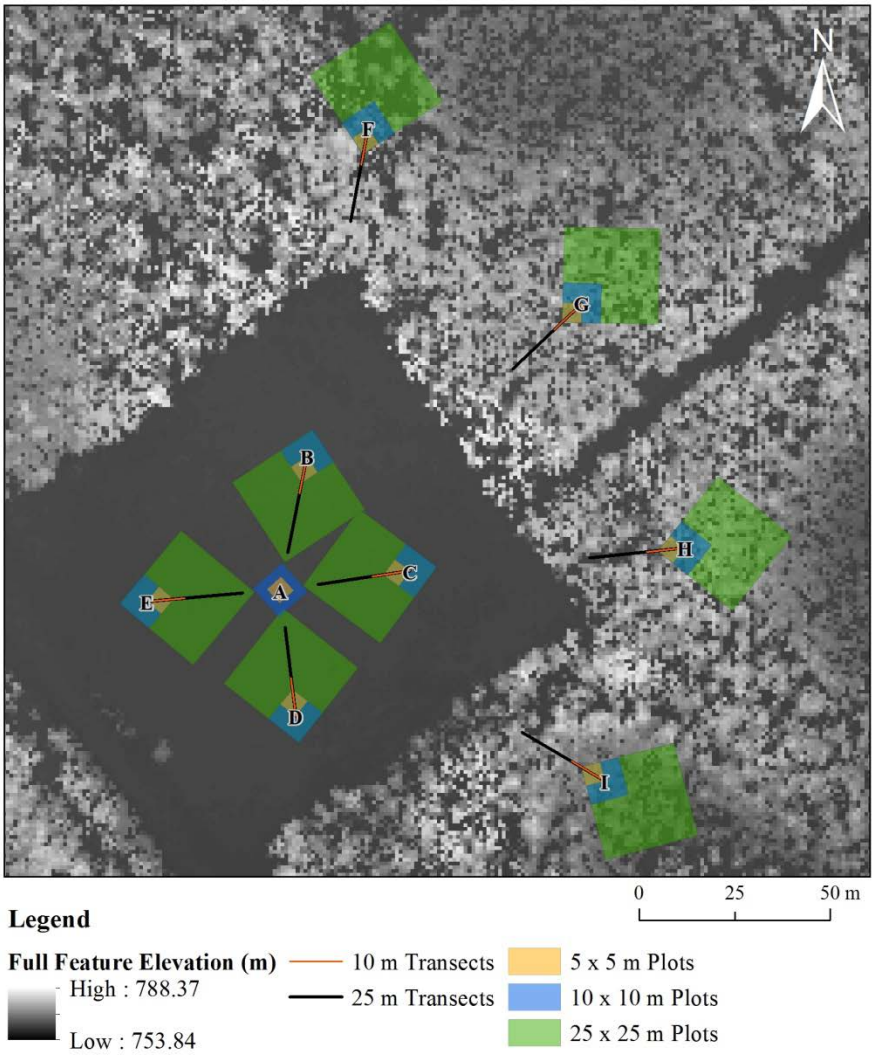

Fig. 3. Layout of the 5 x 5 m, 10 x 10 m, and 25 x 25 m plots and the 10 m and 25 m transects where field data was collected at the Bor6 wellsite, overlain on top of the LiDAR-derived full feature digital surface model provided by AESRD.

Details of the UAV flight and resulting photogrammetric point cloud (PPC) for the Bor6 reclaimed wellsite are presented in Fig. 4. The flight produced more than 700 images, which were processed using more than 2,000,000 tie points to produce a PPC with more than 35 million points. A three-dimensional visualization of the resulting PPC is shown in true colour in Fig. 5. It

is evident that the PPC captures with great precision the incredible details of the surface vegetation in and around wellsite Bor6. One can observe the textures and shapes of much of the vegetation, particularly the trees. For instance, individual aspen tree trunks are clearly visible along the edges of the wellsite, easily identifiable by their white colour and long, straight shapes. The growth of scrubby vegetation over portions of the well pad itself is also clear, suggesting that such a dataset could offer a significant amount of information regarding vegetation recovery over reclaimed wellsites such as this. Further details regarding the Bor6 site and the other sites flown using the Mikrokopter Hexakopter XL are provided in Appendix A.

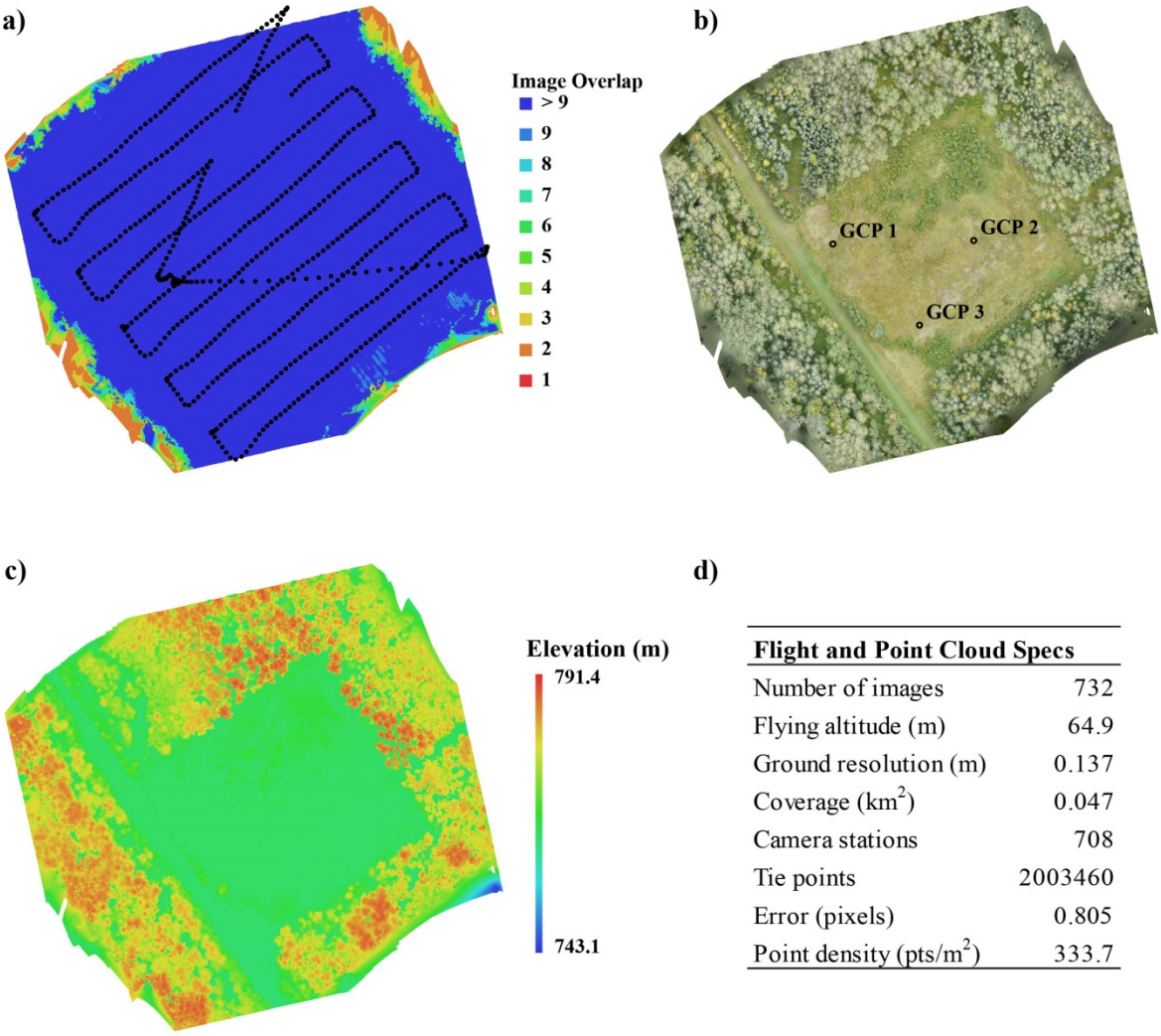

Flight and Point Cloud Specs	
Number of images	732
Flying altitude (m)	64.9
Ground resolution (m)	0.137
Coverage (km^2)	0.047
Camera stations	708
Tie points	2003460
Error (pixels)	0.805
Point density (pts/m^2)	333.7

Fig. 4. Wellsite Bor6 UAV flight information and visuals, showing a) UAV flight camera point layout and image overlap, b) a true colour mosaicked image and location of ground control points (GCPs), c) a digital elevation model derived from the site photogrammetric point cloud, and d) a table summarizing key flight and photogrammetric point cloud details.

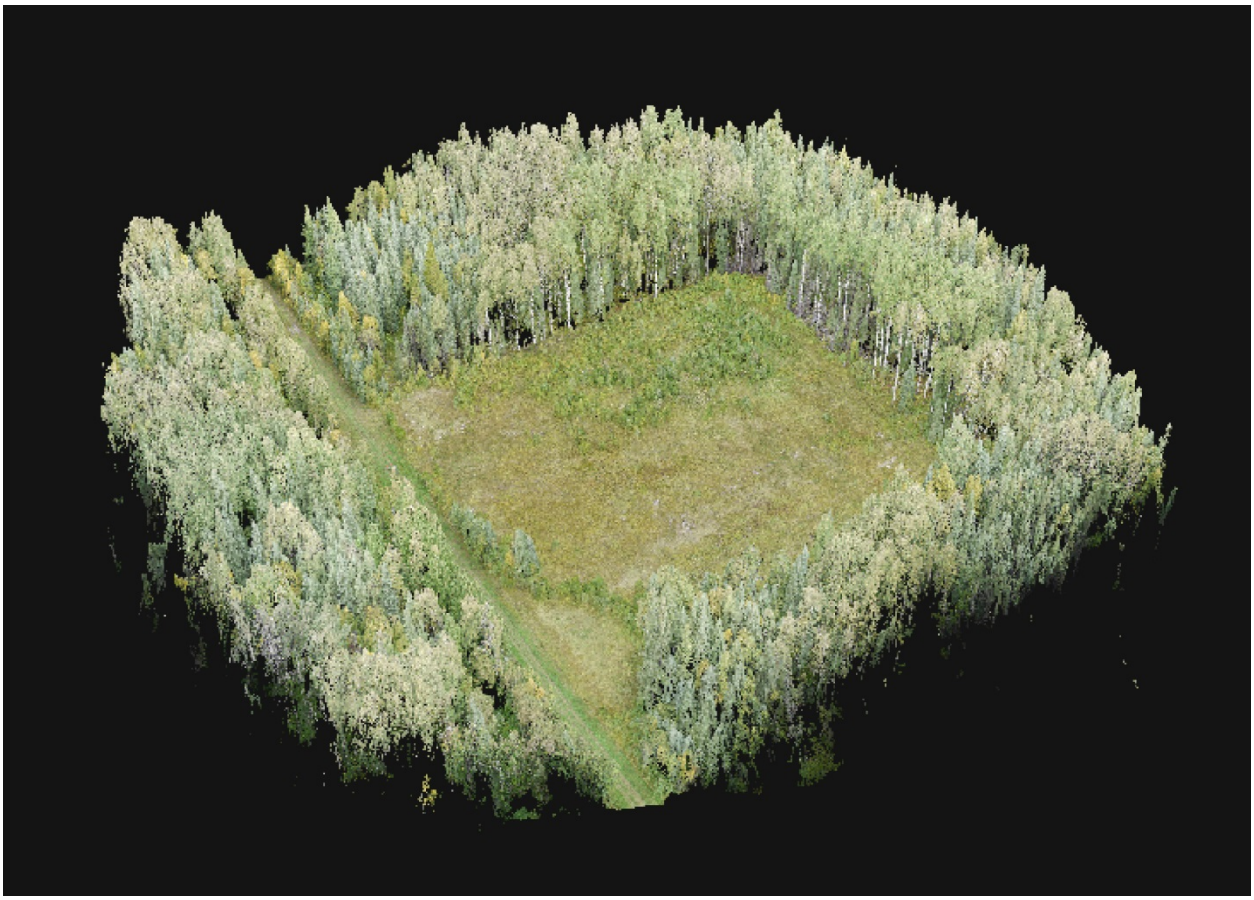

Fig. 5. Three-dimensional view of the UAV photogrammetric point cloud constructed for the Bor6 wellsite.

Fig. 6 provides three profiles showing both the horizontal and vertical distribution of points over three identified transects. The first, profile A, clearly shows both the natural and anthropogenic gaps in the forest and vegetation canopy that one can see in the bird's-eye-view of the wellsite PPC to the left of the figure. One can also clearly see individual trees within parts of this profile, and observe that multiple species can be differentiated simply by the shapes of their crowns (e.g., the very sharp, pointed crowns of the trees to the right in profile A suggest a species of spruce). The same is true of profile B (Fig. 6) – the indications of a long, straight trunks, wide branches, and heterogeneous, asymmetrical crowns of the trees to the left of this PPC profile imply a deciduous species. Profile B also shows the more recent, scrubby vegetation located on the well pad itself. This vegetation is clearly not representative of a forest, but shows that the well pad comprises more than herbaceous-type ground cover. The final profile in Fig. 6 – profile C – demonstrates a PPC profile over a more densely forested section of the Bor6 site. Here, the complexity of the forest canopy is evident, both horizontally and vertically. However, this profile also demonstrates one of the most important disadvantages of this type of point cloud: the technology does not penetrate dense vegetation to provide information about the ground surface underneath as LiDAR pulses are able to do. Only where vegetation is sparse enough to allow line-of-sight to the ground can ground surface information be captured through PPCs.

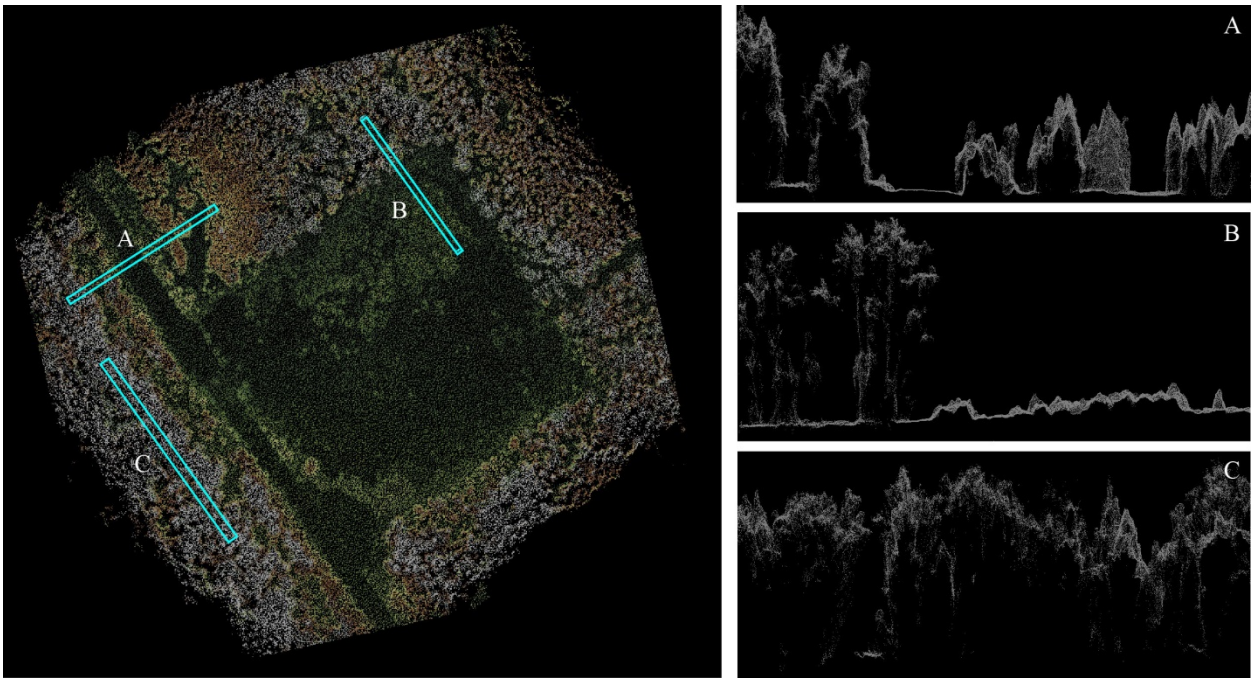

Fig. 6. Three sample photogrammetric point cloud profiles from the Bor6 site. The locations of the profiles (A, B and C) are provided on the photogrammetric point cloud view to the left.

4.2 Statistical Analysis

Thus far, statistical analysis has been applied only to data collected over the 5 m x 5 m plots at the Bor6 wellsite. In anticipation of the removal of the vertical mismatch between the wellsite UAV PPCs and the corresponding LiDAR DTMs within the very near future and the subsequent re-calculation and analysis of the PPC data, further preliminary analysis using the current Bor6 PPC was not undertaken.

Table 6 provides the Kendall's taub-b correlation statistics between field variables measured in the 5 m x 5 m plots at Bor6 and the UAV photogrammetric point cloud (PPC) variables extracted from these plots. Statistically significant correlations range from 0.568 to 0.909, suggesting that where they are significant, correlations between the field and PPC variables are relatively strong. A greater number of strong and significant correlations are observed between field and PPC height variables, while fewer are found for the PPC canopy cover variables (Table 6). In addition, a much greater number of these are seen for the field diameter at breast height (DBH; = 1.3 m) and height variables, than for the two-dimensional shrub and ground cover variables. Nonetheless, the DBH field variables show more significant correlations with canopy cover PPC variables than do the field height variables, though the highest observed significant correlations are between field-measured mean height, maximum height and minimum height and PPC-derived canopy cover at 15 – 20 m (Table 6). No significant correlations were observed for the forb and herb cover < 0.5 m or 0.5 – 2 m field variables, while two significant correlations with the shrub cover > 2 m field variable were observed (i.e., with the canopy cover 0.5 – 1 m and canopy cover 1 – 2 m PPC variables). The shrub cover < 0.5 m field variable showed several significant correlations with both height and canopy cover PPC variables.

Correlation statistics between the UAV PPC variables themselves are given in Table 7. As would be expected, many high, significant correlations exist between the height-related PPC variables while the correlations between these and the canopy cover PPC variables are much more often statistically insignificant and weaker. No correlation results are seen for the PPC canopy cover at heights > 25 m because no data existed for this category at the Bor6 site (i.e., the forest canopy was < 25 m in height).

Table 6. Kendall's tau-b correlation statistics, comparing field variables with UAV point cloud-derived variables for the 5 m x 5 m field plots.

		Field Variables											
UAV Variables		**2D Forbs/Herbs < 0.5 m**	**2D Shrub < 0.5 m**	**2D Shrub 0.5 m - 2 m**	**2D Shrub > 2 m**	**Mean DBH[1]**	**Maximum DBH**	**Minimum DBH**	**DBH Range**	**Mean Height**	**Maximum Height**	**Minimum Height**	**Height Range**
Height (m)	Mean	.261	.589*	.261	.036	.725*	.645*	.564	.645*	.806**	.806**	.806**	.725*
	Std. Dev.	.327	.648*	.196	.182	.806**	.725*	.645*	.725*	.725*	.725*	.725*	.806**
	Max	.261	.589*	.261	.109	.725*	.645*	.564	.645*	.806**	.806**	.806**	.725*
	Min	-.154	.312	-.346	-.514	.227	.318	.409	.318	.318	.318	.318	.227
	Median	.232	.568*	.298	.037	.739*	.656*	.574	.656*	.821**	.821**	.821**	.739*
	Range	.261	.589*	.261	.109	.725*	.645*	.564	.645*	.806**	.806**	.806**	.725*
	Sum	.261	.589*	.261	.036	.725*	.645*	.564	.645*	.806**	.806**	.806**	.725*
	1st Quartile	.143	.742**	.179	-.239	.768*	.682*	.597	.682*	.853**	.853**	.853**	.768*
	2nd Quartile	.232	.568*	.298	.037	.739*	.656*	.574	.656*	.821**	.821**	.821**	.739*
	3rd Quartile	.196	.530	.327	.036	.725*	.645*	.564	.645*	.806**	.806**	.806**	.725*
	50th Percentile	.232	.568*	.298	.037	.739*	.656*	.574	.656*	.821**	.821**	.821**	.739*
	75th Percentile	.196	.530	.327	.036	.725*	.645*	.564	.645*	.806**	.806**	.806**	.725*
	85th Percentile	.196	.530	.327	.036	.725*	.645*	.564	.645*	.806**	.806**	.806**	.725*
	90th Percentile	.196	.530	.327	.036	.725*	.645*	.564	.645*	.806**	.806**	.806**	.725*
	95th Percentile	.196	.530	.261	.109	.725*	.645*	.564	.645*	.806**	.806**	.806**	.725*
	99th Percentile	.261	.589*	.261	.109	.725*	.645*	.564	.645*	.806**	.806**	.806**	.725*
Canopy Cover (%)	< 0.25 m	-.410	-.708*	0.000	.190	-.725*	-.725*	-.810**	-.725*	-.554	-.554	-.554	-.725*
	0.25 - 0.5 m	-.104	-.563*	.035	.270	-.740*	-.740*	-.827**	-.740*	-.566	-.566	-.566	-.740*
	< 0.5 m	-.273	-.585*	-.068	.114	-.725*	-.725*	-.810**	-.725*	-.554	-.554	-.554	-.725*
	0.5 - 1 m	.115	-.243	.115	.642*	-.151	-.251	-.251	-.251	-.352	-.352	-.352	-.151
	1 - 2 m	.214	-.501	.086	.667*	-.473	-.473	-.473	-.473	-.473	-.473	-.473	-.473
	< 1.3 m	-.133	-.508	.066	.258	-.615*	-.698*	-.780*	-.698*	-.533	-.533	-.533	-.615*
	>= 1.3 m	.168	.424	-.034	.037	.627*	.711*	.794*	.711*	.544	.544	.544	.627*
	< 2 m	-.101	-.515	.101	.299	-.615*	-.698*	-.780*	-.698*	-.533	-.533	-.533	-.615*
	>= 2 m	.078	.566	-.118	-.262	.698*	.791*	.884**	.791*	.605	.605	.605	.698*
	2 - 5 m	.416	.500	.277	.309	.564	.403	.403	.403	.242	.242	.242	.564
	5 - 10 m	.263	.593	-.088	0.000	.776*	.672*	.776*	.672*	.465	.465	.465	.776*
	>= 5 m	0.000	.495	-.039	-.349	.605	.698*	.791*	.698*	.698*	.698*	.698*	.605
	10 - 15 m	.077	.589*	-.115	-.257	.636*	.727*	.818*	.727*	.545	.545	.545	.636*
	15 - 20 m	.154	.728*	.269	-.171	.818*	.727*	.636*	.727*	.909**	.909**	.909**	.818*
	20 - 25 m	-.069	.375	.416	-.231	.242	.242	.081	.242	.564	.564	.564	.242
	> 25 m	--	--	--	--	--	--	--	--	--	--	--	--
	= 0 m	.109	-.328	.073	.324	-.364	-.455	-.455	-.455	-.545	-.545	-.545	-.364

[1]Diameter at breast height: 1.3 m

*Significant at the 0.05 level (two-tailed)

**Significant at the 0.01 level (two-tailed)

Table 7. Kendall's tau-b correlation statistics, comparing UAV point cloud-derived variables with one another for the 5 m x 5 m field plots.

UAV Variables	Sum	Mean	Std. Dev.	Max	Min	Median	Range	1st Quartile	2nd Quartile	3rd Quartile	50th Percentile	75th Percentile	85th Percentile	90th Percentile	95th Percentile	99th Percentile	< 0.25 m	0.25 - 0.5 m	0.5 - 1 m	1 - 2 m	2 - 5 m	5 - 10 m	10 - 15 m	15 - 20 m	20 - 25 m	> 25 m	= 0 m	< 0.5 m	< 2 m	>= 2 m	>= 5 m	< 1.3 m	>= 1.3 m
Sum	1.000																															
Mean	1.000**	1.000																														
Std. Dev.	.833**	.833**	1.000																													
Max	.889**	.889**	.944**	1.000																												
Min	.327	.327	.131	0.196	1.000																											
Median	.986**	.986**	.817**	.873**	0.331	1.000																										
Range	.889**	.889**	.944**	1.000**	0.196	.873**	1.000																									
1st Quartile	.852**	.852**	.669*	.730**	0.430	.864**	.730**	1.000																								
2nd Quartile	.986**	.986**	.817**	.873**	0.331	1.000**	.873**	.864**	1.000																							
3rd Quartile	.944**	.944**	.778**	.833**	0.327	.986**	.833**	.852**	.986**	1.000																						
50th Percentile	.986**	.986**	.817**	.873**	0.331	1.000**	.873**	.864**	1.000**	.986**	1.000																					
75th Percentile	.944**	.944**	.778**	.833**	0.327	.986**	.833**	.852**	.986**	1.000**	.986**	1.000																				
85th Percentile	.944**	.944**	.778**	.833**	0.327	.986**	.833**	.852**	.986**	1.000**	.986**	1.000**	1.000																			
90th Percentile	.944**	.944**	.778**	.833**	0.327	.986**	.833**	.852**	.986**	1.000**	.986**	1.000**	1.000**	1.000																		
95th Percentile	.944**	.944**	.889**	.944**	0.261	.930**	.944**	.791**	.930**	.889**	.930**	.889**	.889**	.889**	1.000																	
99th Percentile	.889**	.889**	.944**	1.000**	0.196	.873**	1.000**	.730**	.873**	.833**	.873**	.833**	.833**	.833**	.944**	1.000																
< 0.25 m	-.551*	-.551*	-.609*	-.551*	-0.444	-0.530	-.551*	-0.540	-0.530	-0.493	-0.530	-0.493	-0.493	-0.493	-0.493	-.551*	1.000															
0.25 - 0.5 m	-.295	-.295	-.471	-0.412	-0.312	-0.299	-0.412	-0.420	-0.299	-0.295	-0.299	-0.295	-0.295	-0.295	-0.354	-0.412	.739**	1.000														
0.5 - 1 m	-.065	-.065	-.131	-0.196	-0.192	-0.066	-0.196	-0.179	-0.066	-0.065	-0.066	-0.065	-0.065	-0.065	-0.131	-0.196	0.341	.624*	1.000													
1 - 2 m	-.255	-.255	-.109	-0.109	-0.514	-0.295	-0.109	-.598*	-0.295	-0.327	-0.295	-0.327	-0.327	-0.327	-0.182	-0.109	0.418	0.540	0.385	1.000												
2 - 5 m	.354	.354	.471	0.354	-0.277	0.359	0.354	0.387	0.359	0.354	0.359	0.354	0.354	0.354	0.354	0.354	-0.369	-0.375	0.139	-0.231	1.000											
5 - 10 m	.522	.522	.596*	0.522	0.351	0.529	0.522	0.572	0.529	0.522	0.529	0.522	0.522	0.522	0.522	0.522	-.701*	-.712*	-0.175	-0.439	0.632	1.000										
10 - 15 m	.458	.458	.523	0.458	.615*	0.464	0.458	0.501	0.464	0.458	0.464	0.458	0.458	0.458	0.458	0.458	-.785**	-.797**	-0.423	-0.514	0.277	.702*	1.000									
15 - 20 m	.850**	.850**	.784**	.850**	0.308	.862**	.850**	.931**	.862**	.850**	.862**	.850**	.850**	.850**	.850**	.850**	-.580*	-.589*	-0.346	-0.514	0.416	0.614	0.538	1.000								
20 - 25 m	.471	.471	.354	0.471	0.139	0.478	0.471	0.516	0.478	0.471	0.478	0.471	0.471	0.471	0.471	0.471	-0.123	-0.125	-0.277	-0.231	-0.125	-0.237	0.139	0.555	1.000							
> 25 m	--	--	--	--	--	--	--	--	--	--	--	--	--	--	--	--	--	--	--	--	--	--	--	--	--	1.000						
= 0 m	-.588*	-.588*	-.402	-0.464	-.728*	-.628*	-0.464	-.610*	-.628*	-.650*	-.628*	-.650*	-.650*	-.650*	0.526	-0.464	0.356	0.197	0.000	0.486	0.000	-0.332	-0.583	-0.510	-0.328	--	1.000					
< 0.5 m	-.435	-.435	-.609*	-.551*	-0.307	-0.412	-.551*	-0.413	-0.412	-0.377	-0.412	-0.377	-0.377	-0.377	-0.493	-.551*	.879**	.862**	0.478	0.342	-0.369	-.701*	-.785**	-.580*	-0.123	--	0.226	1.000				
< 2 m	-.286	-.286	-.457	-0.400	-0.370	-0.261	-0.400	-0.344	-0.261	-0.229	-0.261	-0.229	-0.229	-0.229	-0.343	-0.400	.776**	.940**	.639*	0.449	-0.243	-.614*	-.841**	-0.505	-0.121	--	0.223	.896**	1.000			
>= 2 m	.500	.500	.567*	0.500	0.588	0.507	0.500	0.548	0.507	0.500	0.507	0.500	0.500	0.500	0.500	0.500	-.801**	-.813**	-0.431	-0.524	0.283	.716*	.981**	0.588	0.141	--	-0.594	-.801**	-.857**	1.000		
>= 5 m	.567*	.567*	.500	.567*	.667*	.575*	.567*	.621*	.575*	.567*	.575*	.567*	.567*	.567*	.567*	.567*	-.731*	-.742*	-0.510	-0.524	0.141	0.626	.902**	.667*	0.283	--	-.669*	-.731*	-.789**	.920**	1.000	
< 1.3 m	-.310	-.310	-.479	-0.423	-0.365	-0.286	-0.423	-0.339	-0.286	-0.254	-0.286	-0.254	-0.254	-0.254	-0.366	-0.423	.794**	.896**	.597*	0.406	-0.239	-.605*	-.829**	-0.497	-0.120	--	0.220	.912**	.986**	-.845**	-.778**	1.000
>= 1.3 m	.572*	.572*	.743**	.686*	0.404	.551*	.686*	0.376	.551*	0.514	.551*	0.514	0.514	0.514	.629*	.686*	-.716**	-.637*	-0.303	-0.112	0.243	.614*	.841**	0.505	0.121	--	-0.510	-.776**	-.735**	.857**	.789**	-.754**	1.000

*Significant at the 0.05 level (two-tailed)

**Significant at the 0.01 level (two-tailed)

The results of the Automated Linear Modeling procedure using 'best subsets', as applied to the field variables measured over the 5 m x 5 m plots at the Bor6 site are presented in Table 8. The selected variables, their coefficients, standard errors, and significance, as well as the F-statistics and *p*-values for the best models as determined for each field variable through an AICC statistic are listed. The shrub cover field variables are generally best modeled using UAV PPC canopy cover variables, while DBH and height variables were often best explained using PPC height statistics (Table 8). Both the 0.5 – 2 m and > 2 m shrub cover field variable models comprised PPC canopy cover at low heights. In contrast, the < 0.5 m shrub cover variable model comprised two PPC canopy cover variables equivalent to much taller vegetation.

Table 8. List of the selected UAV-derived variables, their coefficients, standard errors and *p*-values, and the model F-statistics and model *p*-values for the best models selected for each field variable measured at the 5 m x 5 m plots.

	Best Model					
Dependent Variable (Field Variable)[1]	**Selected Independent Variables[2] (UAV Point Cloud-Derived Variables)**	**Coefficient**	**Std. Error**	***p*-value**	**F-statistic**	***p*-value (F)**
2D Shrub < 0.5 m	CC_ge5m	26.798	0.100	0.000	68600.167	0.000
	CC_10m-15m	12.196	0.199	0.000		
2D Shrub 0.5 m - 2 m	CC_1m-2m	-19.600	0.980	0.000	400.167	0.000
2D Shrub > 2 m*	CC_1m-2m	-20.000	0.000	--	--	0.000
	CC_0m	204.000	0.000	--		
Mean Diameter at Breast Height (DBH)	Ht_3Qrt	0.766	0.103	0.005	56.318	0.005
Maximum DBH	Ht_95Pctl	0.323	0.212	0.008	39.121	0.008
Minimum DBH	CC_15m-20m	9.326	0.228	0.001	1067.026	0.001
	Ht_minimum	0.193	0.012	0.004		
DBH Range	Ht_95Pctl	1.035	0.145	0.006	50.814	0.006
Mean Height	Ht_85Pctl	0.964	0.112	0.003	73.757	0.003
Maximum Height	Ht_95Pctl	1.171	0.149	0.004	61.719	0.004
Minimum Height	Ht_85Pctl	0.680	0.153	0.021	19.703	0.021
Height Range	Ht_stdev	3.440	0.248	0.001	192.773	0.001

[1]Note: The 2D Forbs/Herbs < 0.5 m field variable could not be modeled because of problems with the data.

[2]CC = Canopy cover; Ht = Height; gt = greater than; ge = greater than or equal to; lt = less than; le = less than or equal to; Qrt = quartile; Ptcl = percentile

*This model was determined to have perfect fit; for this reason it does not have an F-statistic or a model *p*-value.

The 85th and 95th height percentile PPC variables best explained the mean height and minimum height, and maximum height, minimum DBH and DBH range field variables, respectively (Table 8). Field-measured mean DBH was modeled using the PPC 3rd quartile height while minimum field DBH was best modeled using both the minimum PPC height variable and PPC canopy cover at 15 – 20 m. PPC height standard deviation best explained field height ranges. Each model was statistically significant suggesting that the variation observed in these types of field measurements can be explained with some level of confidence using UAV PPC-derived height and canopy cover metrics. The directness of this power of explanation is further supported by the

large number of single-variable models listed in Table 8 – finding a very parsimonious model was easily accomplished, at least in the current case.

5.0 Discussion

Our results indicate that significant relationships exist between statistical height and canopy cover metrics derived from UAV-based photogrammetric point clouds (PPCs) and ground data collected by field crews at the 5 m x 5 m plots of the Bor6 wellsite. They also indicate that these relationships show predictive potential with regard to modeling vegetation structural measurements on the ground.

All of the field height variables show numerous strong, significant correlations with height-based PPC variables, which is a very encouraging result (Table 6). This suggests that there is a lot of similarity between heights measured in the field and those captured by UAV. A number of such correlations are also observed between the height range field variable and canopy cover PPC variables, but few significant correlations are found between these PPC variables and the other height-based field variables (Table 6). In contrast, the DBH field variables showed a greater number of significant correlations with canopy cover PPC variables, perhaps reflecting a relationship between crown size and tree diameter on the ground. These field variables, with the exception of minimum DBH, also all show numerous significant correlations with height-related PPC variables (Table 6). It is probable that this is a reflection of a tree height vs. tree diameter relationship.

The shrub and herb/forb percent cover variables do not show nearly as many significant correlations with the PPC variables as do the other height and DBH field variables (Table 6). It is probable that the data simply do not capture enough of the variability in shrub and herb/forb cover in order to fully evaluate possible correlations, and/or, that a portion of the PPC data do not reflect shrub cover where the field measurement counterparts do. This is very likely given that four of the nine 5 x 5 m plots were located at reference sites outside the Bor6 well pad and were thus in forest-covered locations where UAV below-canopy line-of-sight is minimal at best. In these cases, the PPC variables would reflect the characteristics of forest canopy vegetation and not those of the shrub layers below, while ground crews are able to collect information about these sub-canopy layers. The lower sample size resulting from this situation is likely one reason for the higher number of insignificant and/or weak correlations between shrub and herb/forb ground cover and the PPC data. It is suggested that these forest-covered plots be removed from future analyses involving shrub and herb/forb cover ground data.

Statistically significant, parsimonious models were built for all but one of the field variables measured at the Bor6 5 m x 5 m plots (Table 8). Many of the field height variables could be explained by one of two PPC height variables: 85th percentile and 95th percentile, suggesting both of these height statistics are more important for explaining variations in vegetation structure and height distributions across the Bor6 wellsite than any of the other height-related PPC variables. Nevertheless, the 3rd quartile height, minimum height and height standard deviation PPC variables were included in other models listed in Table 8.

The SPPS Statistics software was not able to build a model for the herb/forb cover < 0.5 m field variable. This may be a result of the lack of significant or even moderately strong correlations between this variable and any of the UAV PPC variables (Table 6). However, the shrub cover 0.5 – 2 m field variable shows the same pattern in Table 6, but the analysis did provide a significant model for this variable based on the PPC canopy cover 1 – 2 m variable. Perhaps there is more variability present in the latter variable, which enables the construction of a reasonable model for this variable but not for the former.

One of the largest challenges which limited the scope of the current preliminary study was the vertical mismatch observed between the UAV-derived PPCs and the AESRD LiDAR digital terrain models (DTMs), which were intended as a ground reference for the line-of-sight dependent PPCs, and the subsequent creation of vegetation height models (VHM). This mismatch did not allow for a direct comparison and must be removed in order for appropriate and suitable VHMs to be generated for each of the reclaimed wellsites. In the Bor6 wellsite, where the mismatch was below 1 m and was the smallest calculated from all available wellsite PPCs, it is likely that the above analysis contains a level of error and/or bias related to this mismatch, however small it was estimated to be. It is suggested that further such studies employ higher-precision GPS units (particularly in the vertical domain) and a greater number of fixed targets of known height when conducting flight missions using a UAV.

Another likely source of error in the current study relates to the very small sample size of the dataset used in the analysis. The above preliminary analysis comprises data from nine 5 m x 5 m field plots located at one reclaimed wellsite. It is probably that the great number of strong, statistically-significant correlations observed in the data and the parsimony and high significance level of the models built for the wellsite field variables are at least partially over-estimated as a result of this small sample size. It is suggested that a much larger analysis involving data from many more field plot and wellsite PPCs be conducted in order to test the reliability and accuracy of the preliminary results presented here.

Despite the challenges encountered in this study and the preliminary nature of its results, the results themselves show considerable potential and suggest that UAV PPCs have the ability to offer a reliable and precise source of information on vegetation structural characteristics, and thus, on ecological recovery indicators. UAV-collected data is also a more cost-effective source than more traditional sources (e.g., airborne), and is available at user-defined temporal scales. With their affordability, flexibility, and promising datasets, UAVs could be a valuable tool for supporting the long-term monitoring of non-permanent human footprint features such as reclaimed wellsites.

6.0 Next Steps

As discussed above, the vertical mismatch observed between the UAV PPCs and the LiDAR DTMs offered a considerable challenge to further analysis in the current study. In order to address this issue, a custom-coded algorithm is currently under development, using the R programming language, to address this issue. The algorithm aims to divide the PPC into smaller tiles and align each of the tiles with the corresponding piece of the LiDAR DTM as a means of minimizing the vertical difference between the two. Once completed, this will be used to correct

the vertical mismatch between the two datasets. Once they are aligned, the LiDAR DTMs and UAV PPCs can be combined appropriately to produce VHMs for each of the wellsites. Following this, new height and canopy cover metrics can be extracted and full-scale statistical analyses comprising correlation and regression analysis can be conducted with data from multiple wellsites. It is anticipated that this will produce a more reliable and accurate understanding of the various relationships between ground and UAV-derived data, and how the latter might be used in future to model and predict the former.

An addition to this analysis will be the use of the visible colour optical data component of the UAV PPC datasets – since these PPCs are derived from images, they also contain RGB values. These did not form a component of the current analysis as their extraction from the PPC datasets following the software and methods used here proved difficult. These spectral data are expected to enhance the prediction power of the UAV height and canopy cover metrics, however.

The creation of spatially-explicit UAV PPC-based height, canopy cover and RGB statistic rasters is also an anticipated step once appropriate VHMs exist for the wellsites in our study area. These will enable application of the developed models to the entire UAV-flown area surrounding each wellsite as a means of predicting field-measured vegetation structural characteristics beyond the field plots.

The expanded, more rigorous analysis as represented by the steps above is anticipated to provide a clearer understanding of the potential and value of UAV datasets for studying, mapping, and monitoring vegetation structures.

7.0 Conclusions

While the results presented here are preliminary in nature, it is evident thus far that these methods and results offer proof of concept, and possess great potential for supporting a greater understanding of the relationship between unmanned aerial vehicle- (UAV-) based photogrammetric point cloud (PPC) datasets and ground data collected by field crews over reclaimed wellsites within Alberta's boreal forest. Many significant and strong correlations were observed between various field-measured variables and PPC-derived variables using the 5 m x 5 m plots at the Bor6 wellsite, particularly with regard to height- and diameter at breast height-related measures. Shrub and herb/forb cover were not as well captured by the PPC variables, but this was not surprising given that almost half of the plots were located in forested areas and shrub cover was thus not visible to the UAV camera and not represented by the PPC data in these locations.

Statistically significant models were built for all but one of the field variables, indicating that the spatially-exhaustive prediction of these variables would be possible and could be reliably conducted using UAV-derived datasets. Challenges, such as a vertical mismatch between wellsite PPCs and ancillary LiDAR-derived digital terrain models limited the scope of the current study – statistical analyses have thus far only been conducted on one of the wellsites included in the study area. Nevertheless, the preliminary analysis described here offers a framework for the further work described above and is encouraging in showing early potential in demonstrating the potential of UAV datasets as a valuable tool supporting the long-term

monitoring of ecological recovery over Alberta's reclaimed wellsites and other non-permanent human footprint features.

References Cited

[1] P. of Alberta, "ENVIRONMENTAL PROTECTION AND ENHANCEMENT ACT: Revised Statutes of Alberta 2000, Chapter E-12," Edmonton, Alberta, 2000.

[2] Alberta Biodiversity Monitoring Institute, "Ecological Recovery Monitoring of Dry Mixedgrass Wellsites: Results of vegetation and soil indicator analyses," Edmonton, Alberta, Canada, 2014.

[3] I. Colomina and P. Molina, "Unmanned aerial systems for photogrammetry and remote sensing: A review," *ISPRS J. Photogramm. Remote Sens.*, vol. 92, pp. 79–97, 2014.

[4] A. C. Watts, V. G. Ambrosia, and E. a. Hinkley, "Unmanned aircraft systems in remote sensing and scientific research: Classification and considerations of use," *Remote Sens.*, vol. 4, pp. 1671–1692, 2012.

[5] E. Salamí, C. Barrado, and E. Pastor, "UAV flight experiments on the remote sensing of vegetation areas," pp. 1–25, 2014.

[6] C. C. D. Lelong, P. Burger, G. Jubelin, B. Roux, S. Labbe, and F. Baret, "Assessment of unmanned aerial vehicles imagery for quantitative monitoring of wheat crop in small plots," *Sensors*, vol. 8, pp. 3557–3585, 2008.

[7] J. Baluja, M. P. Diago, P. Balda, R. Zorer, F. Meggio, F. Morales, and J. Tardaguila, "Assessment of vineyard water status variability by thermal and multispectral imagery using an unmanned aerial vehicle (UAV)," *Irrig. Sci.*, vol. 30, pp. 511–522, 2012.

[8] S. K. von Bueren, A. Burkart, A. Hueni, U. Rascher, M. P. Tuohy, and I. J. Yule, "Deploying four optical UAV-based sensors over grassland: Challenges and limitations," *Biogeosciences*, vol. 12, pp. 163–175, 2015.

[9] A. Verger, N. Vigneau, C. Chéron, J. M. Gilliot, A. Comar, and F. Baret, "Green area index from an unmanned aerial system over wheat and rapeseed crops," *Remote Sens. Environ.*, vol. 152, pp. 654–664, 2014.

[10] P. J. Zarco-Tejada, V. González-Dugo, and J. a J. Berni, "Fluorescence, temperature and narrow-band indices acquired from a UAV platform for water stress detection using a micro-hyperspectral imager and a thermal camera," *Remote Sens. Environ.*, vol. 117, pp. 322–337, 2012.

[11] C. Zhang and J. M. Kovacs, "The application of small unmanned aerial systems for precision agriculture: A review," *Precis. Agric.*, vol. 13, pp. 693–712, 2012.

[12] S. Getzin, R. S. Nuske, and K. Weigand, "Using unmanned aerial vehicles to quantify spatial gap patterns in forests," *Remote Sens.*, vol. 6, pp. 6988–7004, 2014.

[13] J. Lisein, M. Pierrot-Deseilligny, S. Bonnet, and P. Lejeune, “A Photogrammetric Workflow for the Creation of a Forest Canopy Height Model from Small Unmanned Aerial System Imagery,” *Forests*, vol. 4, pp. 922–944, 2013.

[14] P. J. Zarco-Tejada, R. Diaz-Varela, V. Angileri, and P. Loudjani, “Tree height quantification using very high resolution imagery acquired from an unmanned aerial vehicle (UAV) and automatic 3D photo-reconstruction methods,” *Eur. J. Agron.*, vol. 55, pp. 89–99, 2014.

[15] D. Chabot and D. M. Bird, “Evaluation of an off-the-shelf Unmanned Aircraft System for surveying flocks of geese,” *Waterbirds*, vol. 35, no. 1, pp. 170–174, 2012.

[16] A. Hodgson, N. Kelly, and D. Peel, “Unmanned aerial vehicles (UAVs) for surveying marine fauna: A dugong case study,” *PLoS One*, vol. 8, no. 11, pp. 1–15, 2013.

[17] W. W. Immerzeel, P. D. A. Kraaijenbrink, J. M. Shea, A. B. Shrestha, F. Pellicciotti, M. F. P. Bierkens, and S. M. de Jong, “High-resolution monitoring of Himalayan glacier dynamics using unmanned aerial vehicles,” *Remote Sens. Environ.*, vol. 150, pp. 93–103, 2014.

[18] Y. Vasuki, E.-J. Holden, P. Kovesi, and S. Micklethwaite, “Semi-automatic mapping of geological structures using UAV-based photogrammetric data: An image analysis approach,” *Comput. Geosci.*, vol. 69, pp. 22–32, 2014.

[19] J. Fernandez-Hernandez, D. Gonzalez-Aguilera, P. Rodriquez-Gonzalvez, and J. Mancera-Taboada, “Image-based modelling from unmanned aerial vehicle (UAV) photogrammetry: An effective, low-cost tool for archaeological applications,” *Archaeometry*, vol. 57, no. 1, pp. 128–145, 2015.

[20] M. Funaki, S. I. Higashino, S. Sakanaka, N. Iwata, N. Nakamura, N. Hirasawa, N. Obara, and M. Kuwabara, “Small unmanned aerial vehicles for aeromagnetic surveys of their flights in the South Shetland Islands, Antarctica,” *Polar Sci.*, vol. 8, pp. 342–356, 2014.

[21] C. Hugenholtz, J. Walker, O. Brown, and S. Myshak, “Earthwork volumetrics with an unmanned aerial vehicle and softcopy photogrammetry,” *J. Surv. Eng.*, vol. 141, no. 1, p. 6014003, 2015.

[22] A. Y.-M. Lin, A. Novo, S. Har-Noy, N. D. Ricklin, and K. Stamatiou, “Combining GeoEye-1 satellite remote sensing, UAV aerial imaging, and geophysical surveys in anomoly detection applied to archaeology,” *IEEE J. Sel. Top. Appl. Earth Obs. Remote Sens.*, vol. 4, no. 4, pp. 870–876, 2011.

[23] N. Snavely, S. M. Seitz, and R. Szeliski, “Modeling the world from Internet photo collections,” *Int. J. Comput. Vis.*, vol. 80, no. December 2007, pp. 189–210, 2008.

[24] M. J. Westoby, J. Brasington, N. F. Glasser, M. J. Hambrey, and J. M. Raynolds, "'Structure-from-Motion' photogrammetry: A low-cost, effective tool for geoscience applications," *Geomorphology*, vol. 179, pp. 300–314, 2012.

[25] J. C. White, M. a. Wulder, M. Vastaranta, N. C. Coops, D. Pitt, and M. Woods, "The utility of image-based point clouds for forest inventory: A comparison with airborne laser scanning," *Forests*, vol. 4, pp. 518–536, 2013.

[26] J. Bohlin, J. Wallerman, and J. E. S. Fransson, "Forest variable estimation using photogrammetric matching of digital aerial images in combination with a high-resolution DEM," *Scand. J. For. Res.*, vol. 27, no. March 2015, pp. 692–699, 2012.

[27] N. R. Committee, "Natural Regions and Subregions of Alberta," Edmonton, Alberta, Canada, 2006.

[28] Alberta Biodiversity Monitoring Institute, "Ecological Recovery Monitoring of Certified Reclaimed Wellsites in Alberta: Field Data Collection Protocols for Forested Lands," Edmonton, Alberta, Canada, 2013.

[29] T. Tan, and S. Nielsen, "Testing UAV-based Remote Sensing for Monitoring Well Pad Recovery: UAV Field Performance, 2014 Summary Report," Edmonton, Alberta, Canada, 2014.

[30] R. Gaulton, and T. Malthus, "LiDAR mapping of canopy gaps in continuous cover forests: A comparison of canopy height model and point cloud based techniques," *Int. J. Remote Sens.*, vol. 31, no. 5, pp. 1193-1211, 2010.

[31] J. P. Dandois and E. C. Ellis, "Remote sensing of vegetation structure using computer vision," *Remote Sens.*, vol. 2, no. 4, pp. 1157–1176, 2010.

[32] B. St-Onge, C. Vega, R. a. Fournier, and Y. Hu, "Mapping canopy height using a combination of digital stereo-photogrammetry and lidar," *Int. J. Remote Sens.*, vol. 29, no. March 2015, pp. 3343–3364, 2008.

[33] P. Y. Chen and P. M. Popovich, *Correlation: Parametric and Nonparametric Measures*. Thousand Oaks, California, USA: Sage Publications, Inc., 2002.

Appendix A

Appendix A-i: Agisoft PhotoScan UAV Image Processing Specifications for the Bor2 Wellsite

Agisoft PhotoScan

Processing Report

20 March 2015

Survey Data

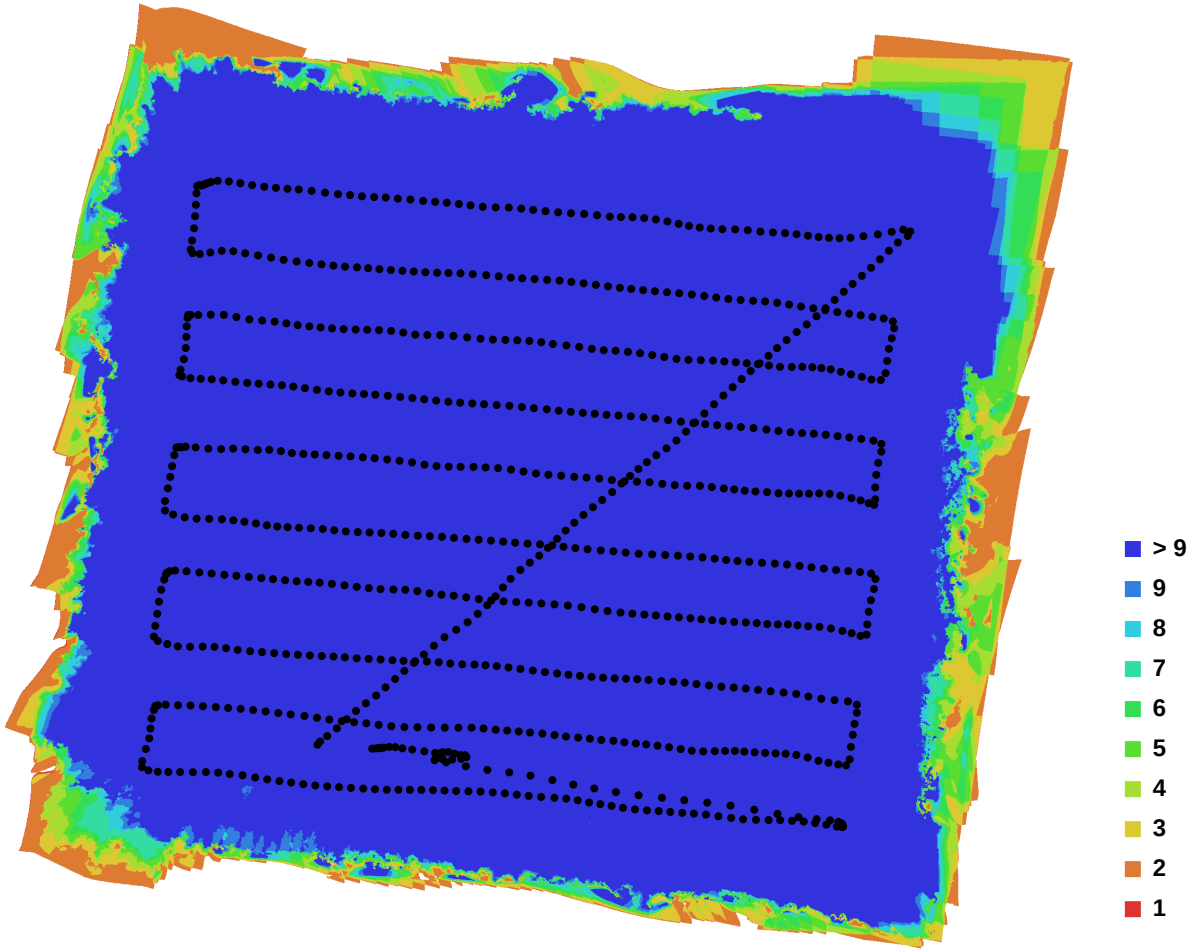

Fig. 1. Camera locations and image overlap.

Number of images:	781	Camera stations:	781
Flying altitude:	65.3684 m	Tie-points:	1971538
Ground resolution:	0.0135722 m/pix	Projections:	5707913
Coverage area:	0.0613487 sq km	Error:	0.553753 pix

Camera Model	Resolution	Focal Length	Pixel Size	Precalibrated
DMC-GF1 (20 mm)	4000 x 3000	20 mm	4.32666 x 4.32666 um	No

Table. 1. Cameras.

Camera Calibration

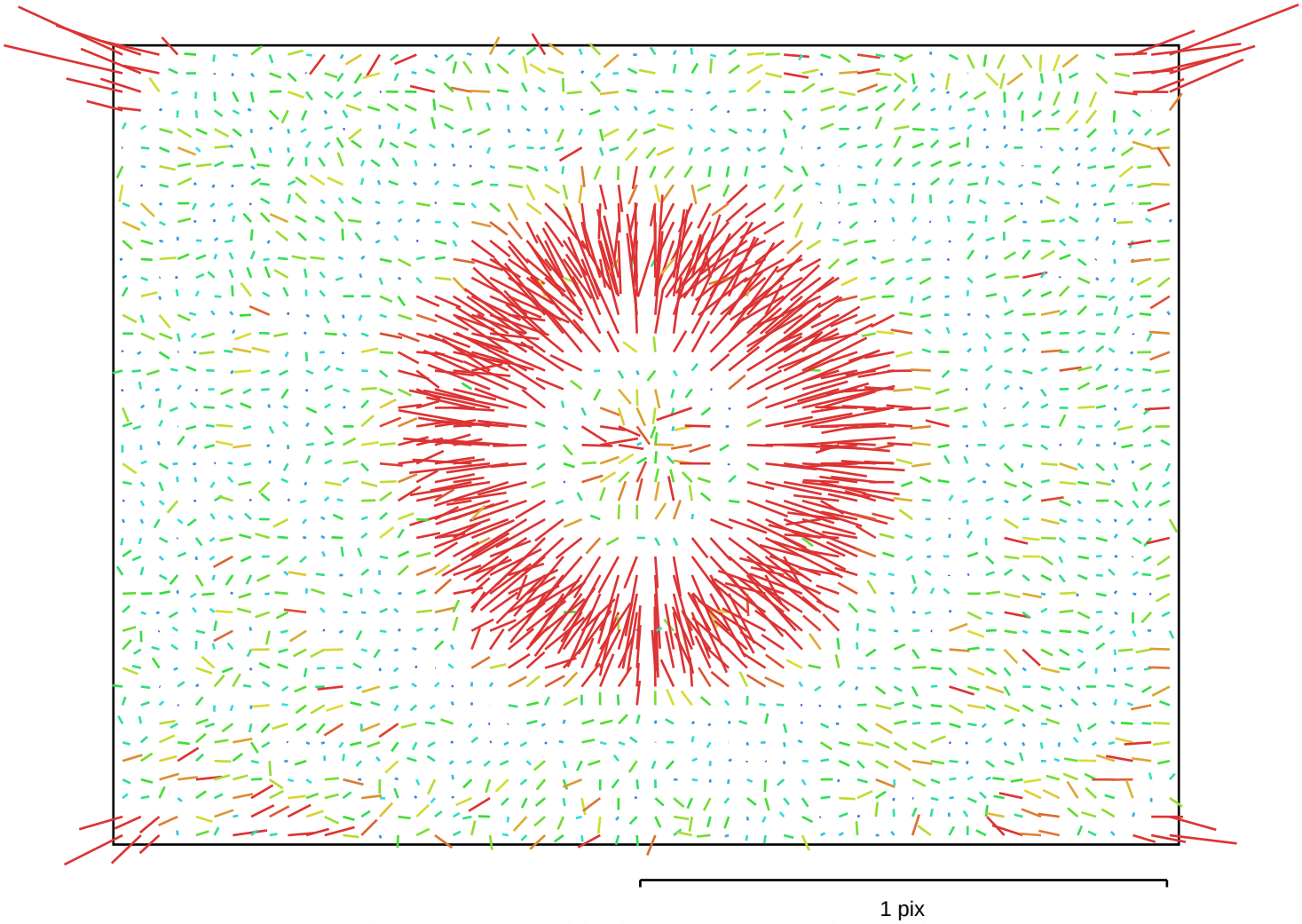

Fig. 2. Image residuals for DMC-GF1 (20 mm).

DMC-GF1 (20 mm)

Type:	Frame	K1:	-0.0203128
Fx:	4461.69	K2:	0.00181282
Fy:	4461.69	K3:	0.0483655
Cx:	2000.36	K4:	0
Cy:	1503.35	P1:	0
Skew:	0	P2:	0

Ground Control Points

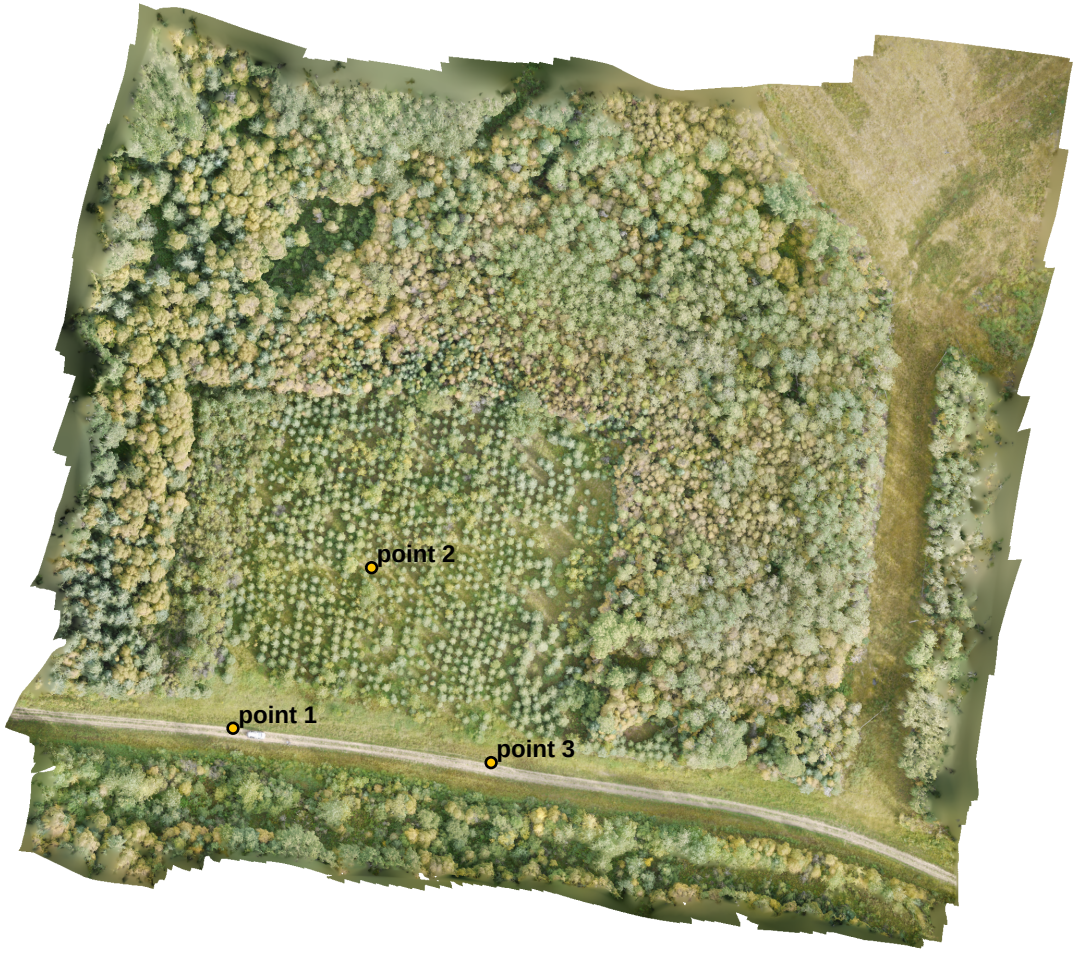

Fig. 3. GCP locations.

Label	X error (m)	Y error (m)	Z error (m)	Error (m)	Projections	Error (pix)
point 1	1.186066	-1.227314	-0.024809	1.706947	36	0.599350
point 2	0.231980	1.930301	-0.014316	1.944243	49	1.046473
point 3	-1.416698	-0.702372	0.032789	1.581592	51	0.326106
Total	**1.075112**	**1.381507**	**0.025137**	**1.750731**	**136**	**0.727686**

Table. 2. Control points.

Digital Elevation Model

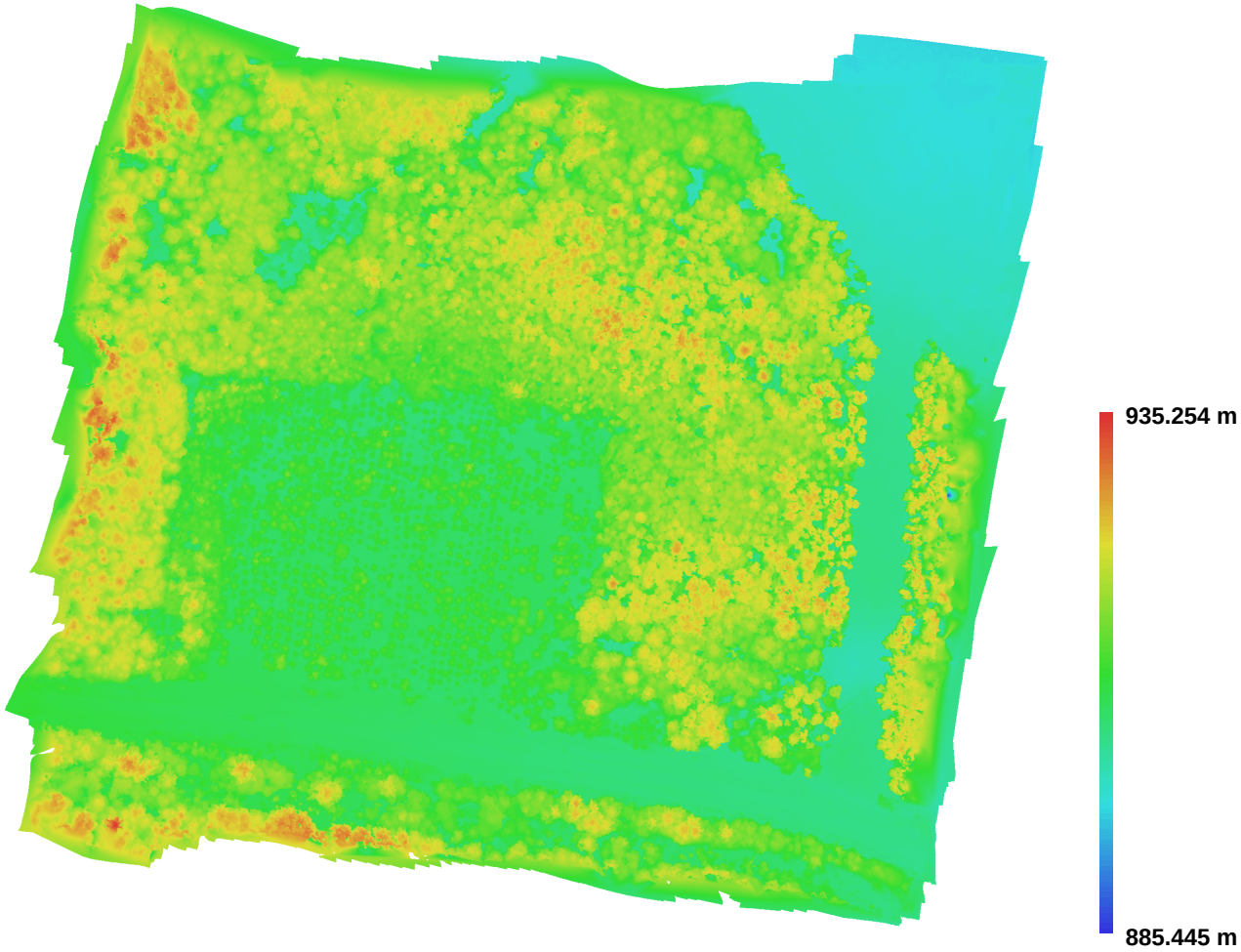

Fig. 4. Reconstructed digital elevation model.

Resolution:	0.0542889 m/pix
Point density:	339.296 points per sq m

Appendix A-ii: Agisoft PhotoScan UAV Image Processing Specifications for the Bor4 Wellsite

Agisoft PhotoScan

Processing Report

20 March 2015

Survey Data

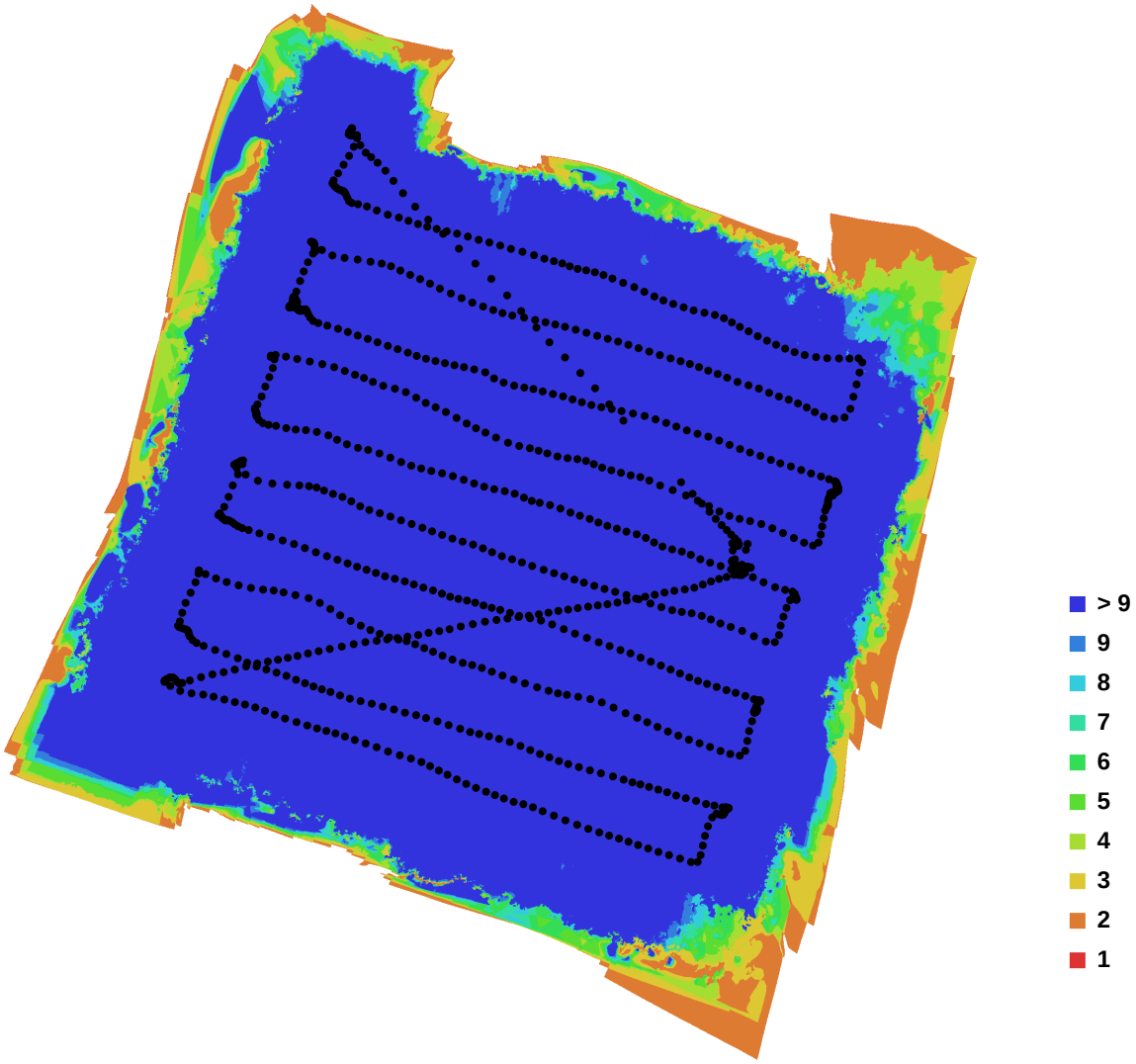

Fig. 1. Camera locations and image overlap.

Number of images:	986	Camera stations:	983
Flying altitude:	74.371 m	Tie-points:	1985075
Ground resolution:	0.0150809 m/pix	Projections:	6192002
Coverage area:	0.0756975 sq km	Error:	0.771297 pix

Camera Model	Resolution	Focal Length	Pixel Size	Precalibrated
DMC-GF1 (20 mm)	4000 x 3000	20 mm	4.32666 x 4.32666 um	No

Table. 1. Cameras.

Camera Calibration

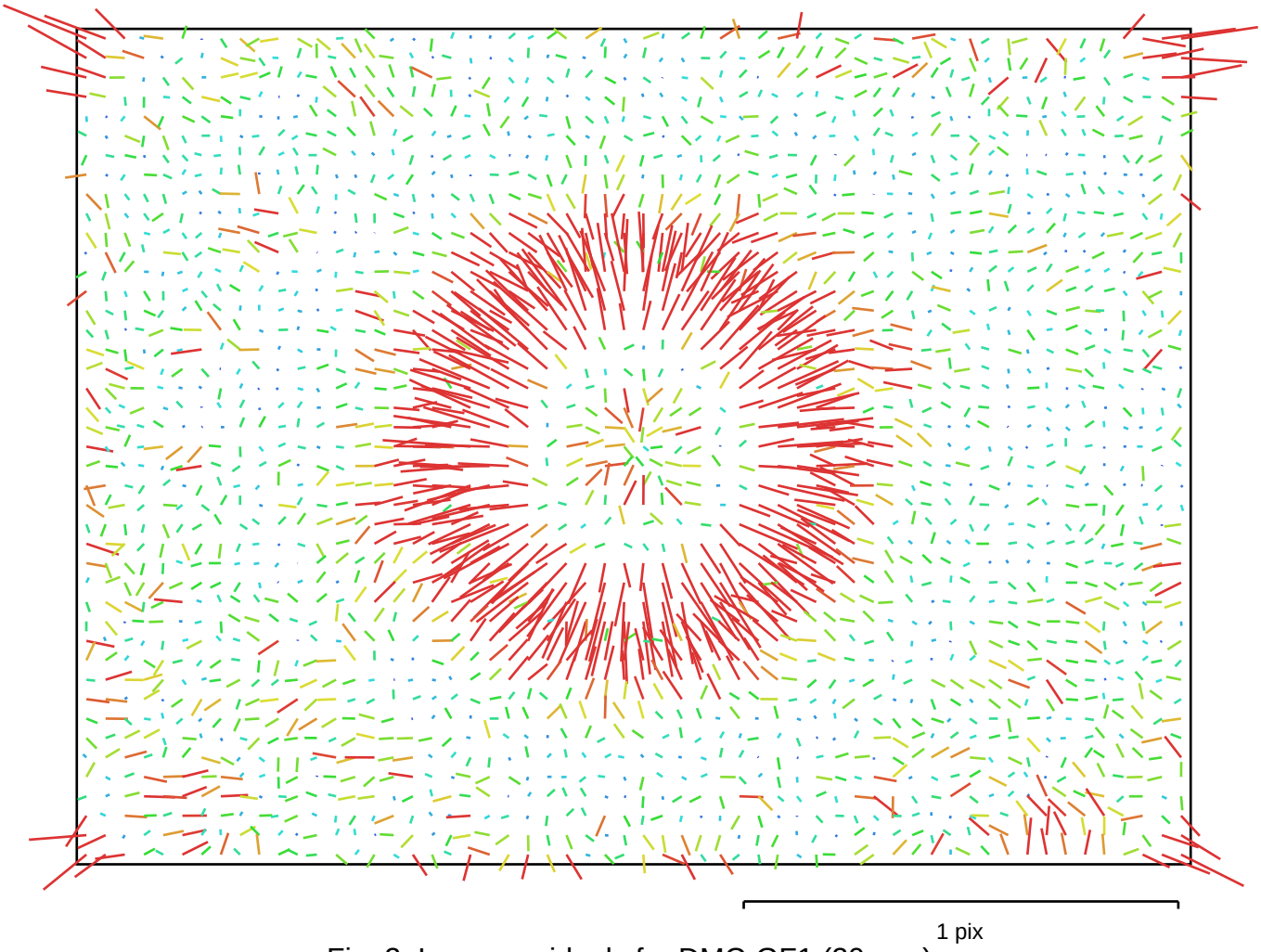

Fig. 2. Image residuals for DMC-GF1 (20 mm).

DMC-GF1 (20 mm)

Type:	Frame	K1:	-0.0165629
Fx:	4459.27	K2:	-0.0219571
Fy:	4459.27	K3:	0.0944984
Cx:	1994.47	K4:	0
Cy:	1498.92	P1:	0
Skew:	0	P2:	0

Ground Control Points

Fig. 3. GCP locations.

Label	X error (m)	Y error (m)	Z error (m)	Error (m)	Projections	Error (pix)
Point 1	-5.123035	5.818740	0.020303	7.752654	78	0.198424
Point 2	7.049651	2.229703	-0.026777	7.393908	45	0.185595
Point 3	-1.916495	-8.051110	-0.003218	8.276070	68	0.304875
Total	**5.151570**	**5.877916**	**0.019490**	**7.815942**	**191**	**0.239344**

Table. 2. Control points.

Digital Elevation Model

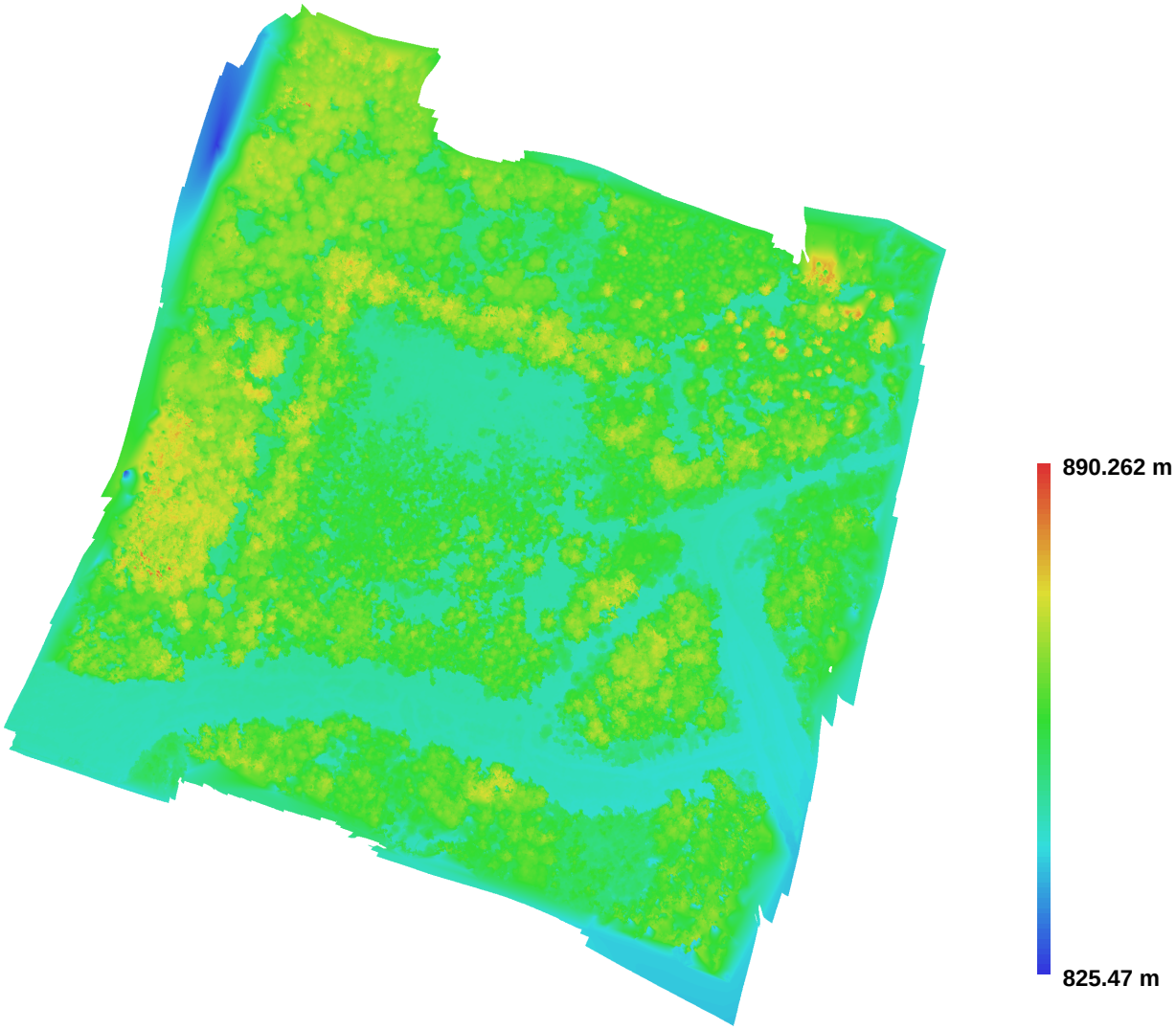

Fig. 4. Reconstructed digital elevation model.

Resolution:	0.0603237 m/pix
Point density:	274.805 points per sq m

Appendix A-iii: Agisoft PhotoScan UAV Image Processing Specifications for the Bor5 Wellsite

Agisoft PhotoScan

Processing Report

20 March 2015

Survey Data

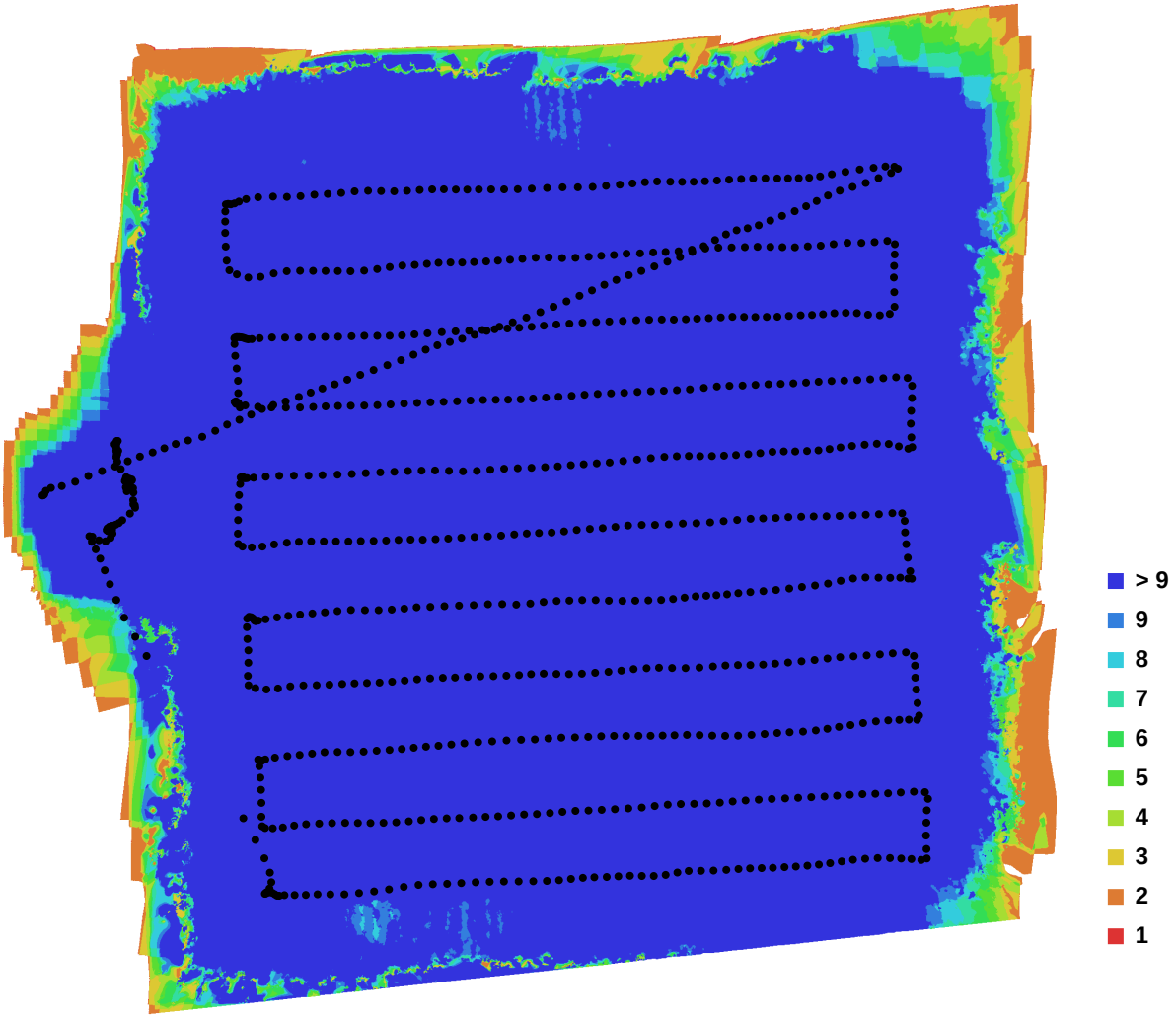

Fig. 1. Camera locations and image overlap.

Number of images:	830	Camera stations:	824
Flying altitude:	65.9208 m	Tie-points:	2782111
Ground resolution:	0.0135194 m/pix	Projections:	9177904
Coverage area:	0.0598695 sq km	Error:	0.504612 pix

Camera Model	Resolution	Focal Length	Pixel Size	Precalibrated
DMC-GF1 (20 mm)	4000 x 3000	20 mm	4.32666 x 4.32666 um	No

Table. 1. Cameras.

Camera Calibration

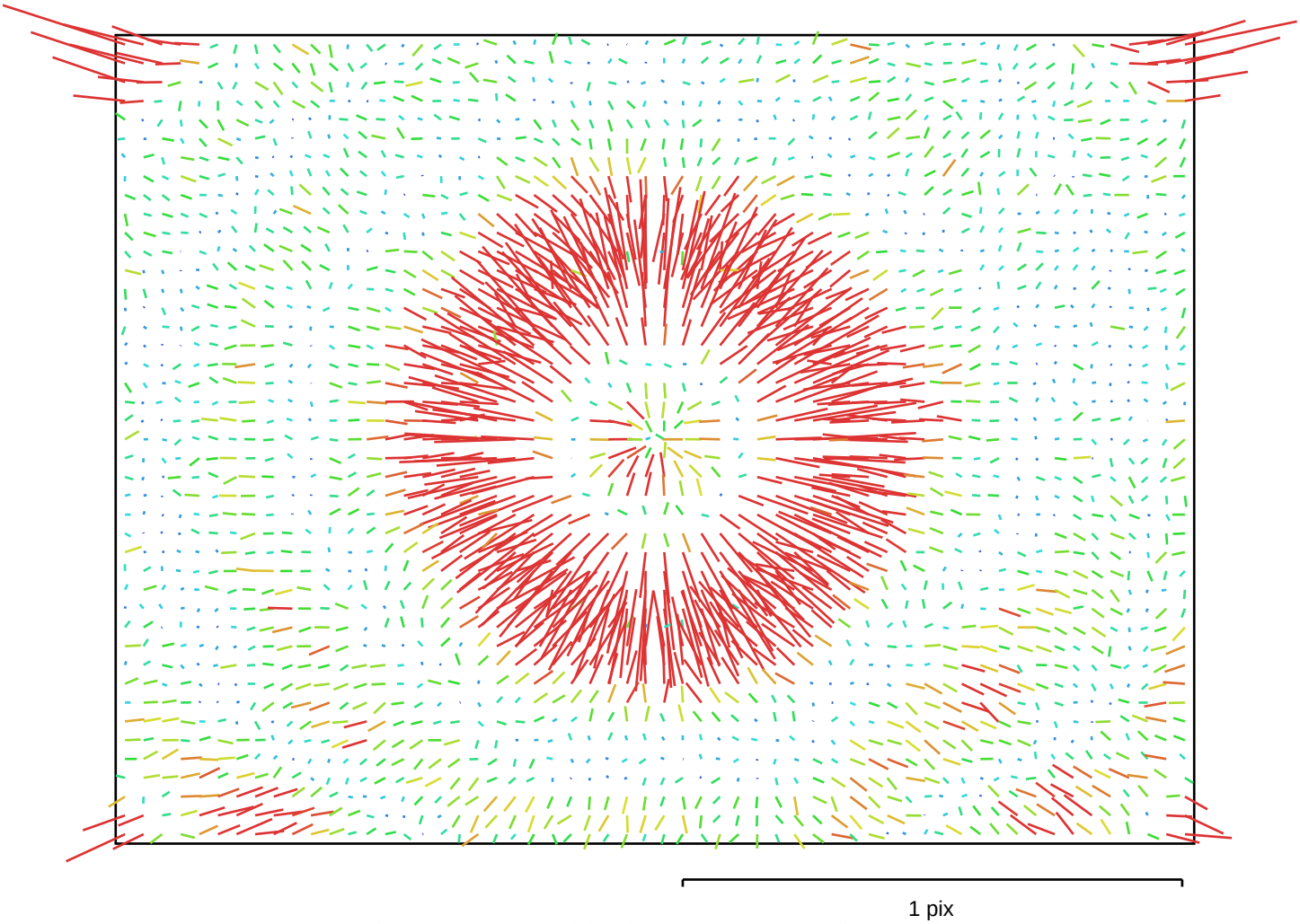

Fig. 2. Image residuals for DMC-GF1 (20 mm).

DMC-GF1 (20 mm)

Type:	Frame	K1:	-0.0206933
Fx:	4470.42	K2:	0.0106016
Fy:	4470.42	K3:	0.0328022
Cx:	2000.55	K4:	0
Cy:	1504.71	P1:	0
Skew:	0	P2:	0

Ground Control Points

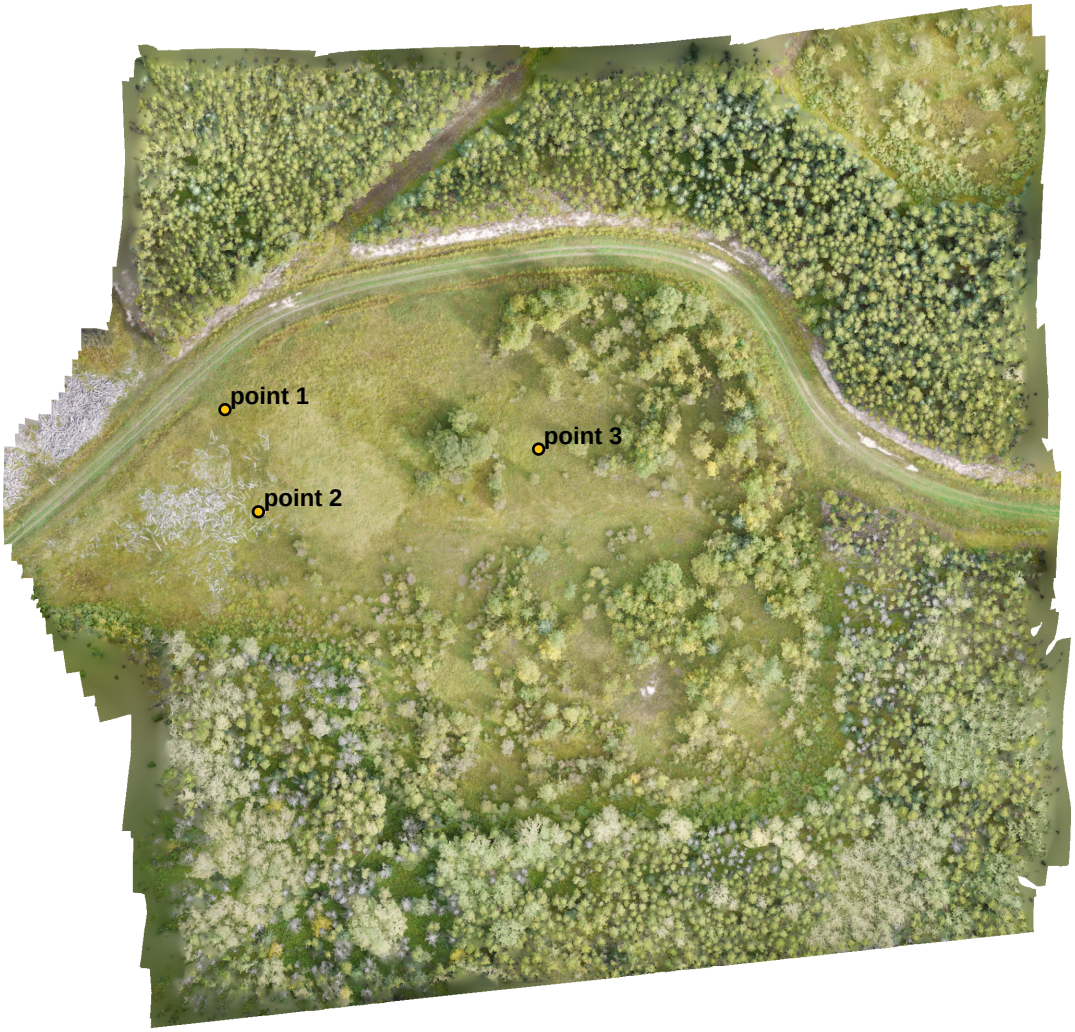

Fig. 3. GCP locations.

Label	X error (m)	Y error (m)	Z error (m)	Error (m)	Projections	Error (pix)
point 1	1.396476	-0.447806	-0.005710	1.466530	64	0.281140
point 2	-1.613186	-0.056362	-0.007347	1.614187	70	0.460085
point 3	0.217221	0.504375	0.015126	0.549371	48	0.811722
Total	**1.238238**	**0.390769**	**0.010253**	**1.298476**	**182**	**0.531961**

Table. 2. Control points.

Digital Elevation Model

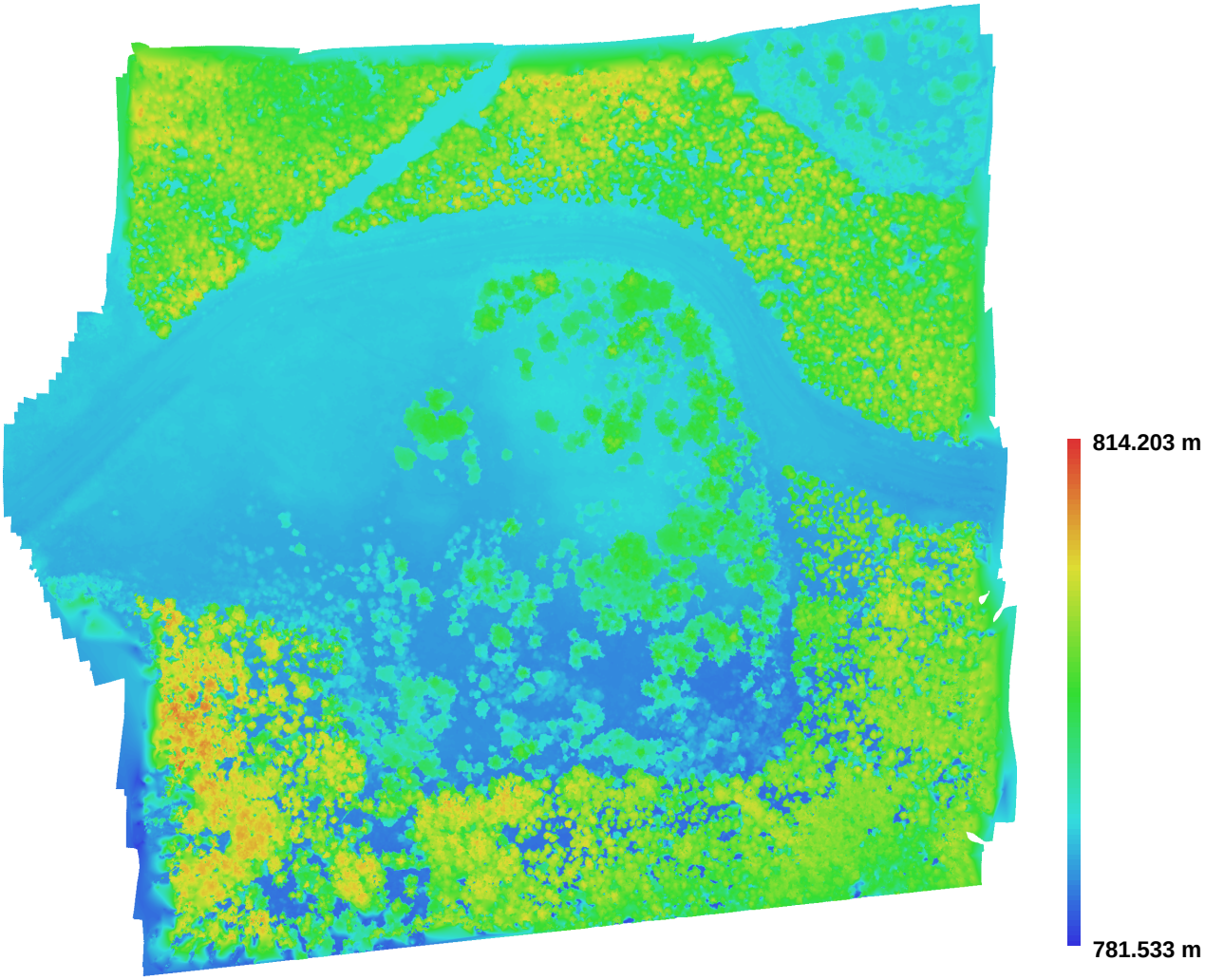

Fig. 4. Reconstructed digital elevation model.

Resolution:	0.0540775 m/pix
Point density:	341.954 points per sq m

Appendix A-iv: Agisoft PhotoScan UAV Image Processing Specifications for the Bor6 Wellsite

Agisoft PhotoScan

Processing Report

20 March 2015

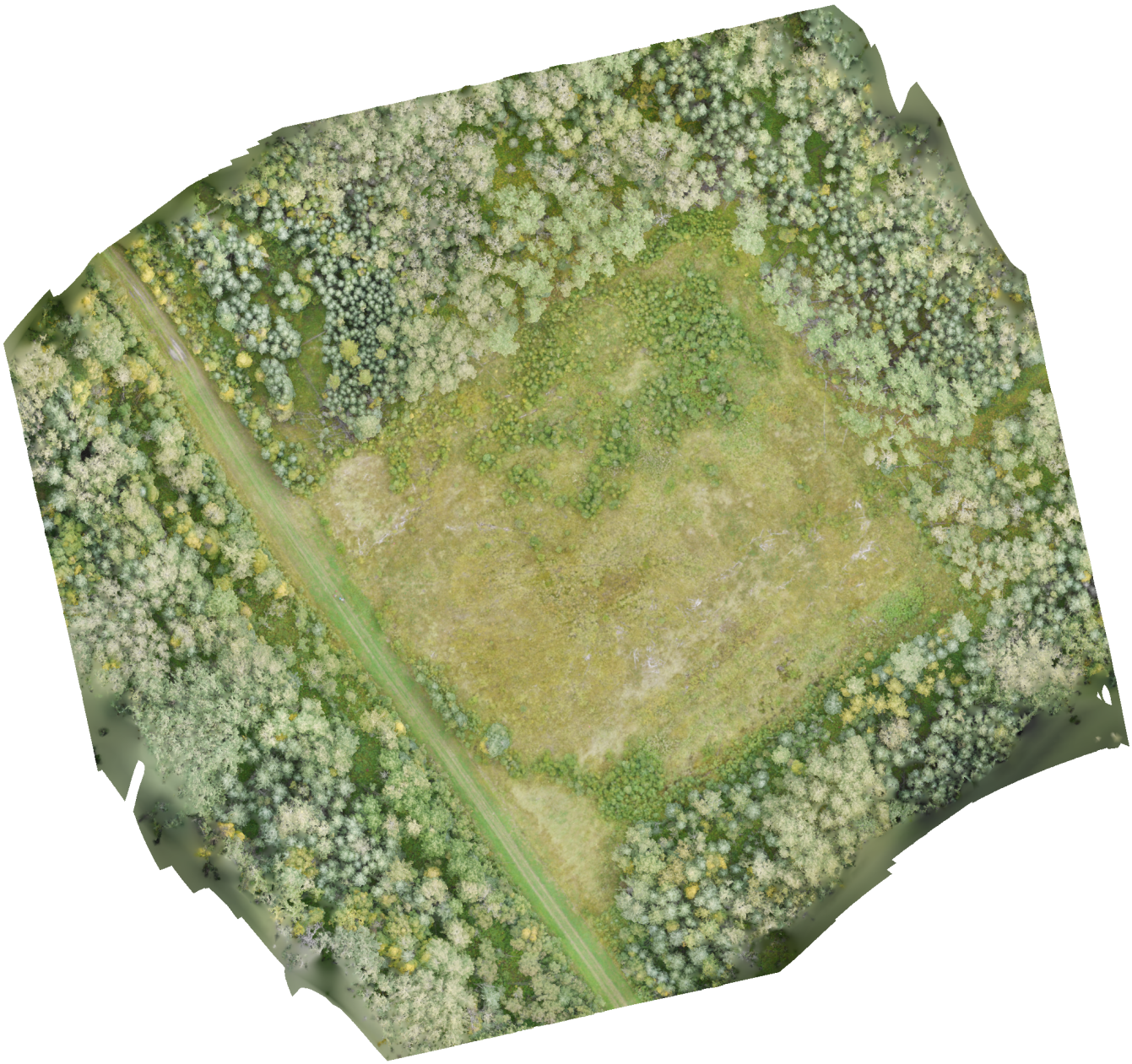

Survey Data

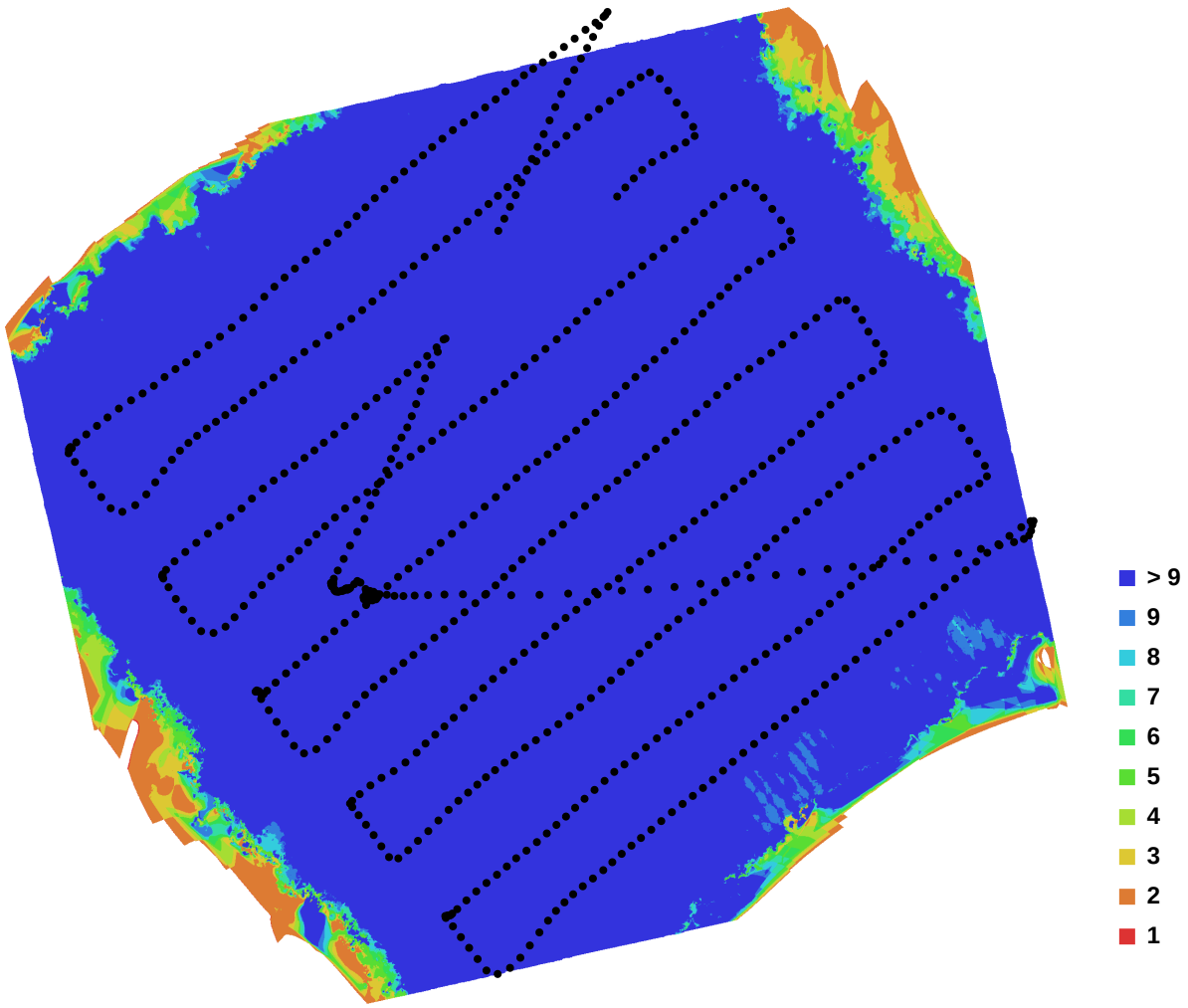

Fig. 1. Camera locations and image overlap.

Number of images:	732	Camera stations:	708
Flying altitude:	64.9172 m	Tie-points:	2003460
Ground resolution:	0.0136855 m/pix	Projections:	6293191
Coverage area:	0.047216 sq km	Error:	0.599069 pix

Camera Model	Resolution	Focal Length	Pixel Size	Precalibrated
DMC-GF1 (20 mm)	4000 x 3000	20 mm	4.32666 x 4.32666 um	No

Table. 1. Cameras.

Camera Calibration

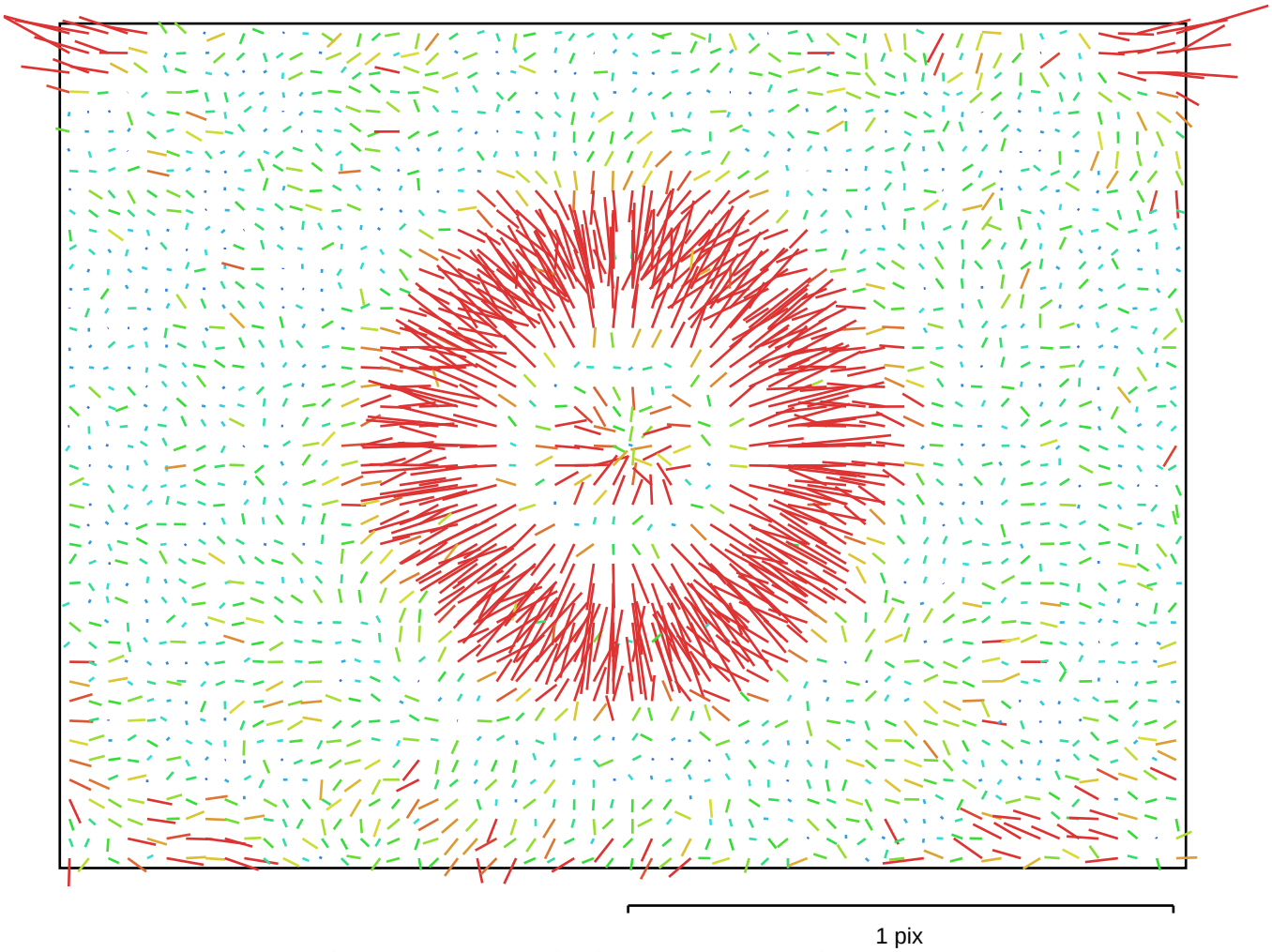

Fig. 2. Image residuals for DMC-GF1 (20 mm).

DMC-GF1 (20 mm)

Type:	Frame	K1:	-0.0256997
Fx:	4457.65	K2:	0.0356223
Fy:	4457.65	K3:	-0.0208891
Cx:	1998.32	K4:	0
Cy:	1508.53	P1:	0
Skew:	0	P2:	0

Ground Control Points

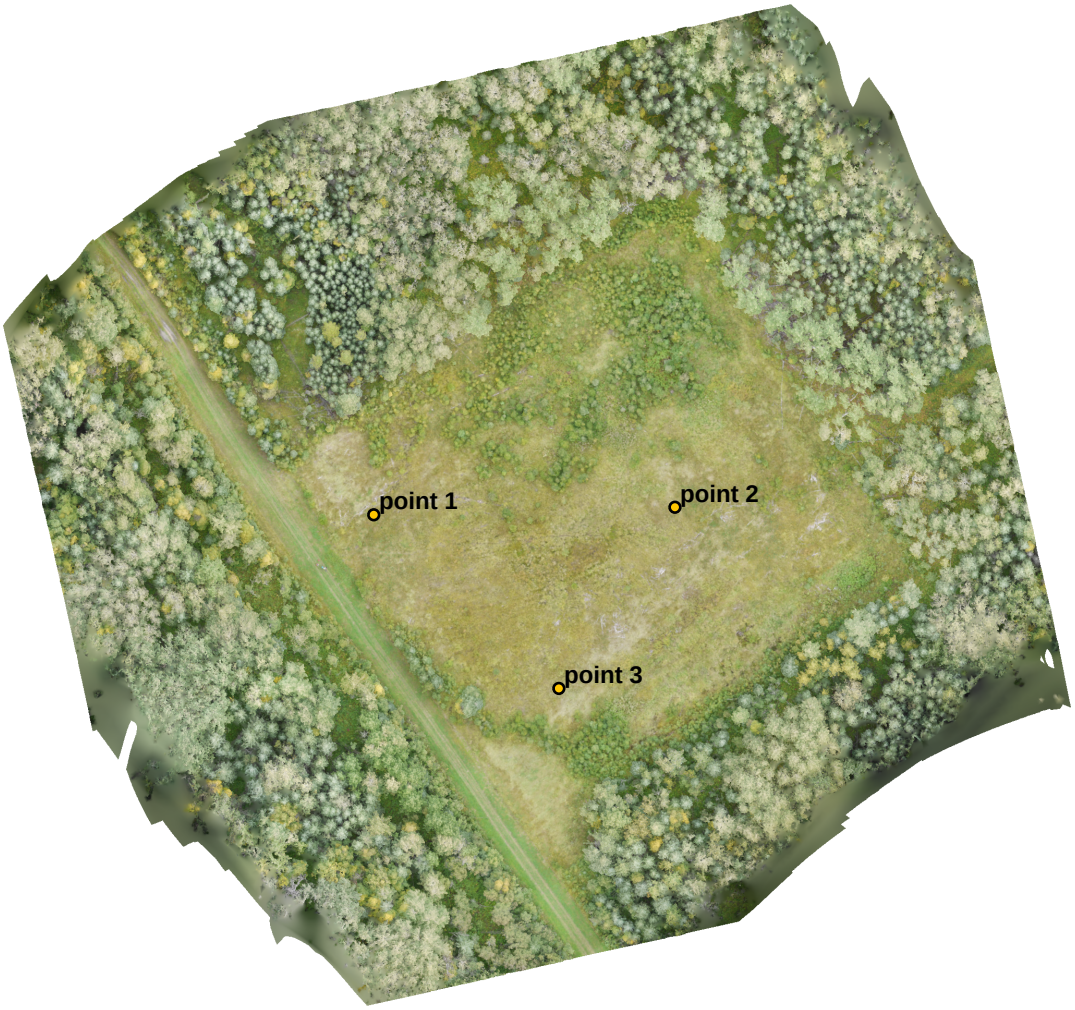

Fig. 3. GCP locations.

Label	X error (m)	Y error (m)	Z error (m)	Error (m)	Projections	Error (pix)
point 1	0.866530	0.182833	0.001242	0.885609	71	0.799766
point 2	-0.398799	0.966601	0.000718	1.045638	50	1.035950
point 3	-0.468449	-1.149498	-0.002783	1.241289	52	0.499210
Total	**0.613558**	**0.873516**	**0.001808**	**1.067468**	**173**	**0.804726**

Table. 2. Control points.

Digital Elevation Model

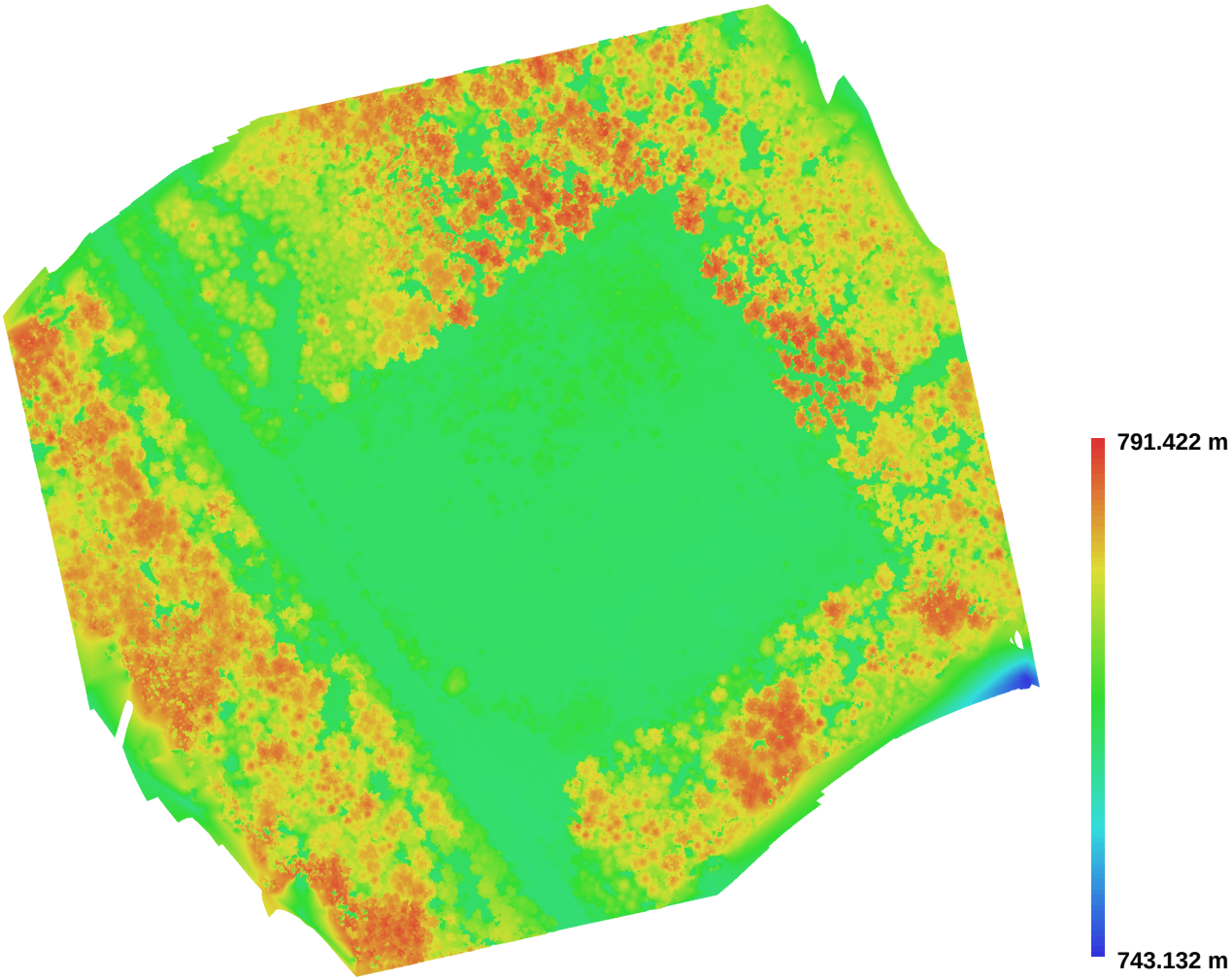

Fig. 4. Reconstructed digital elevation model.

Resolution:	0.0547421 m/pix
Point density:	333.701 points per sq m

Appendix A-v: Agisoft PhotoScan UAV Image Processing Specifications for the Foot10 Wellsite

Agisoft PhotoScan

Processing Report

20 March 2015

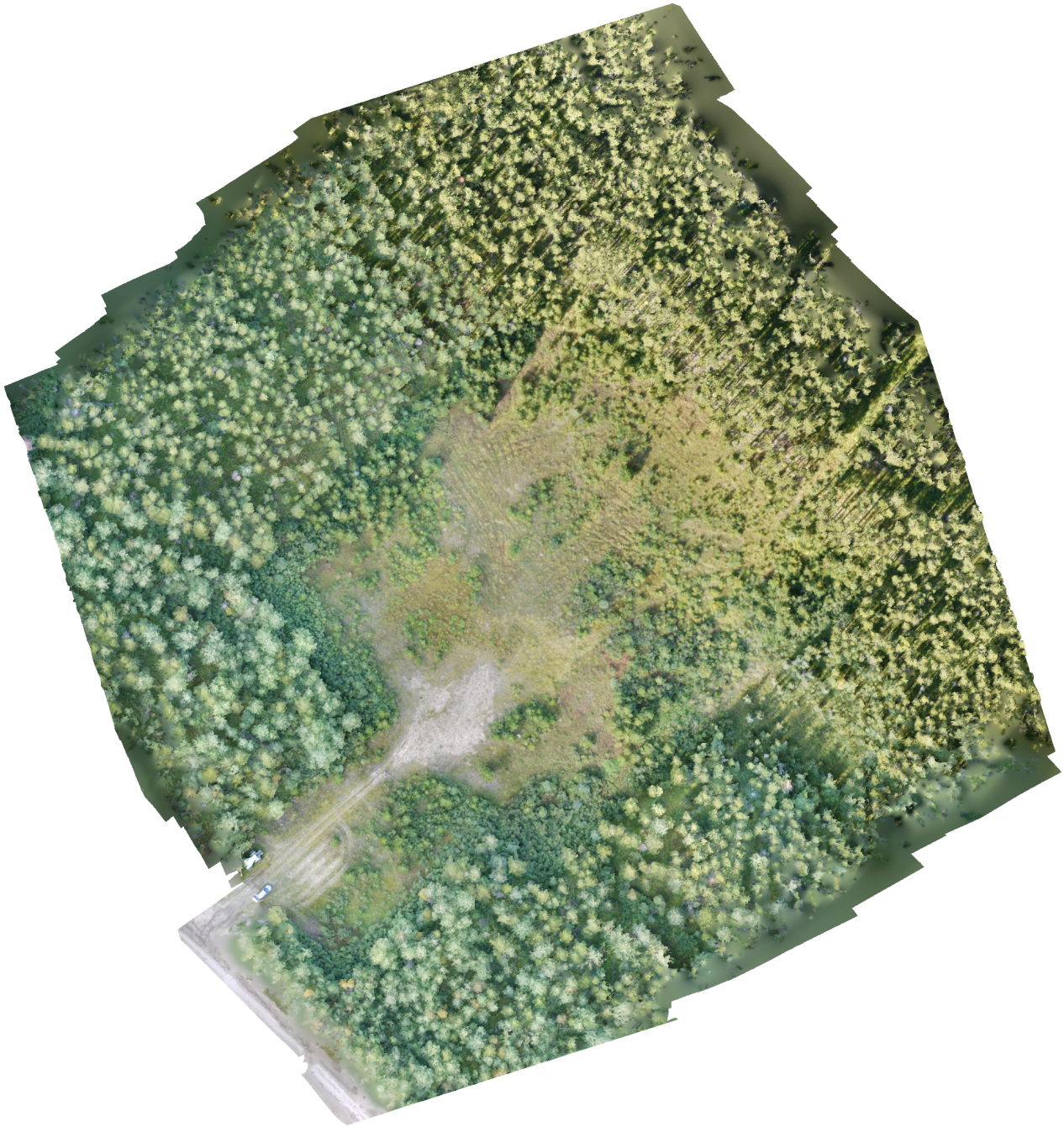

Survey Data

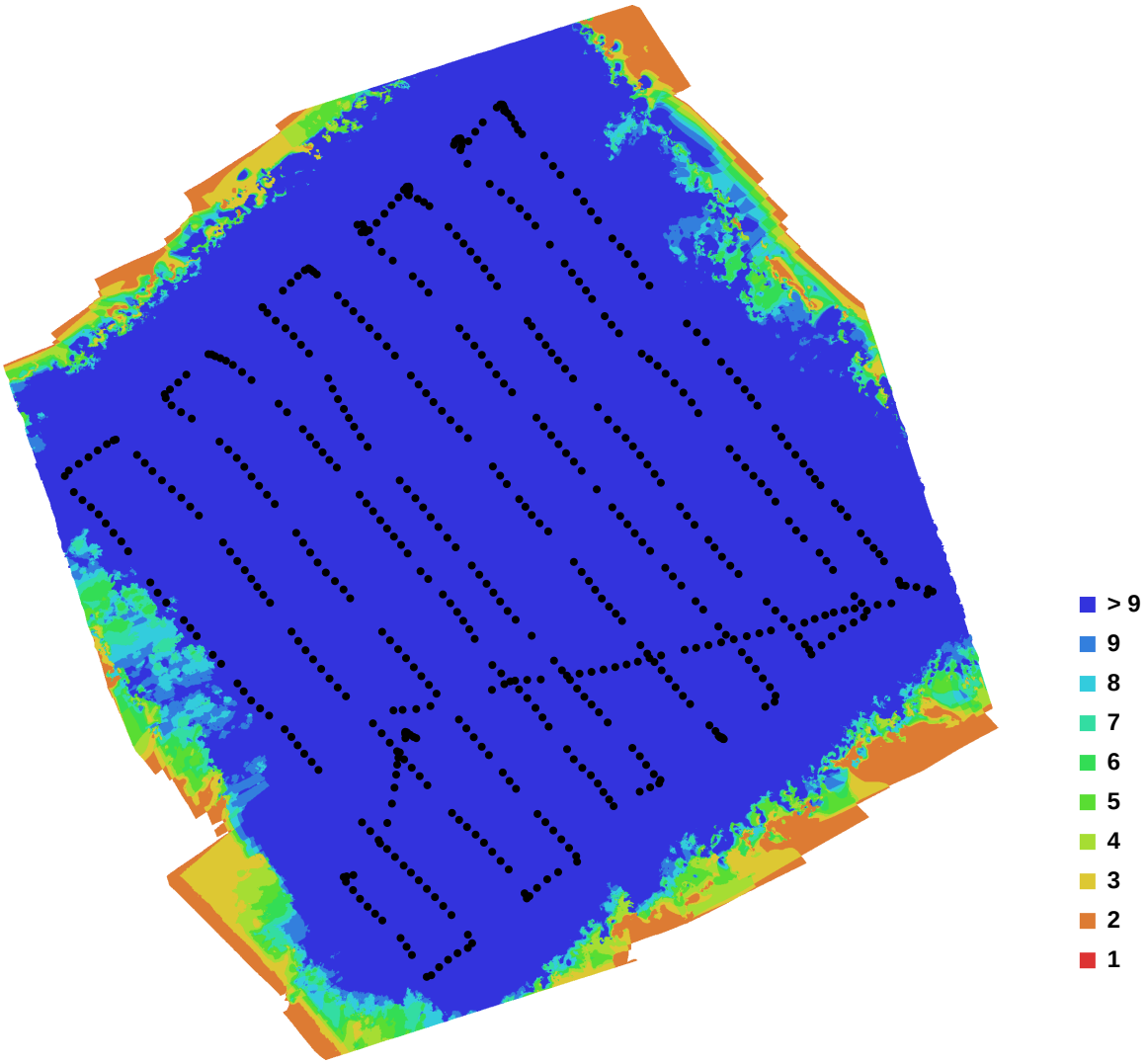

Fig. 1. Camera locations and image overlap.

Number of images:	584	Camera stations:	584
Flying altitude:	70.5305 m	Tie-points:	1693435
Ground resolution:	0.0146193 m/pix	Projections:	5119838
Coverage area:	0.055636 sq km	Error:	0.649379 pix

Camera Model	Resolution	Focal Length	Pixel Size	Precalibrated
DMC-GF1 (20 mm)	4000 x 3000	20 mm	4.32666 x 4.32666 um	No

Table. 1. Cameras.

Camera Calibration

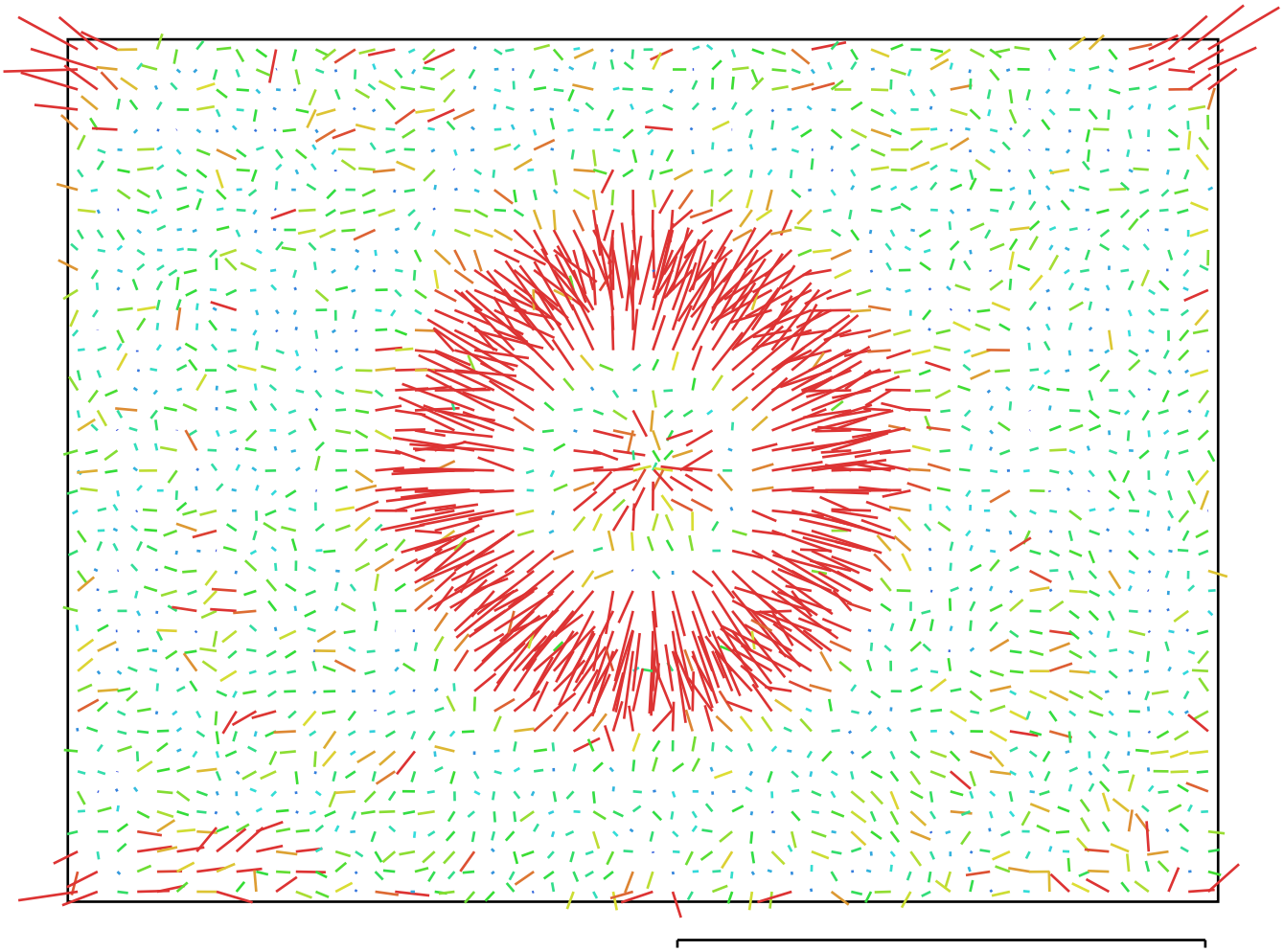

Fig. 2. Image residuals for DMC-GF1 (20 mm).

DMC-GF1 (20 mm)

Type:	Frame	K1:	-0.0270321
Fx:	4458.2	K2:	0.0422929
Fy:	4458.2	K3:	-0.0276945
Cx:	2004.31	K4:	0
Cy:	1504.28	P1:	0
Skew:	0	P2:	0

Ground Control Points

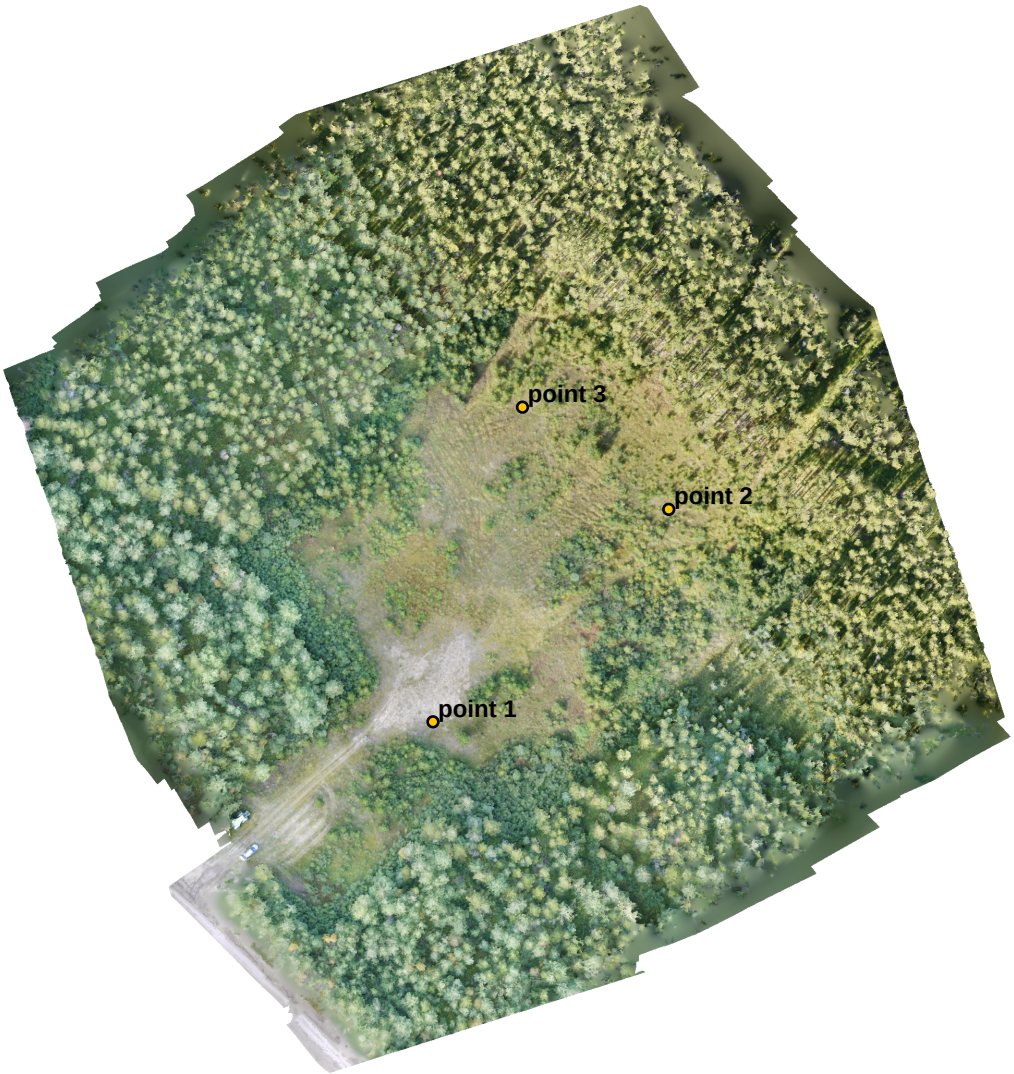

Fig. 3. GCP locations.

Label	X error (m)	Y error (m)	Z error (m)	Error (m)	Projections	Error (pix)
point 1	-0.612180	0.382810	0.007218	0.722053	57	0.316084
point 2	1.030975	0.833098	-0.032796	1.325910	45	0.498290
point 3	-0.418240	-1.217170	0.024902	1.287264	35	0.453258
Total	**0.733167**	**0.879791**	**0.024137**	**1.145491**	**137**	**0.419058**

Table. 2. Control points.

Digital Elevation Model

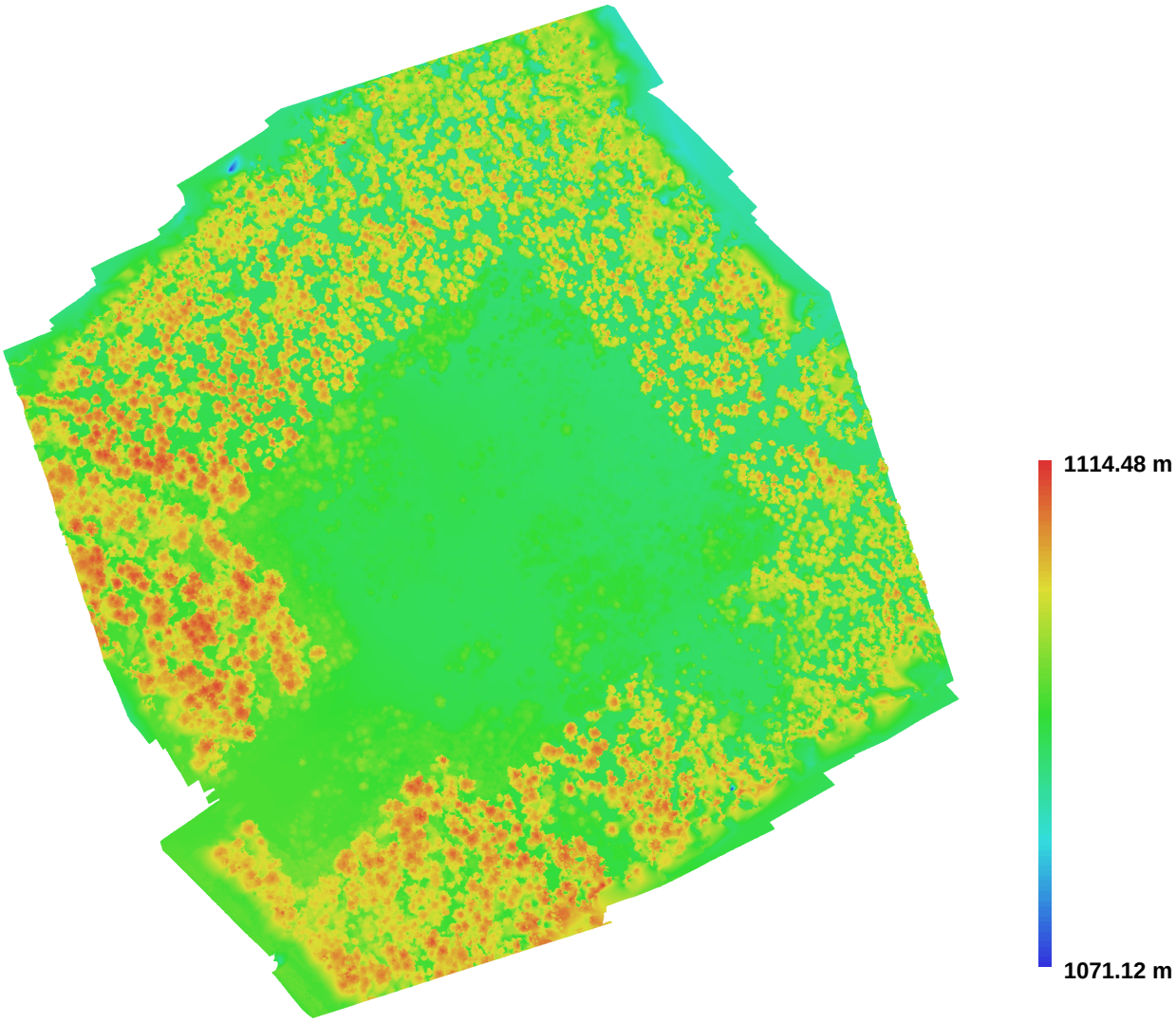

Fig. 4. Reconstructed digital elevation model.

Resolution:	0.0584773 m/pix
Point density:	292.432 points per sq m

Appendix A-vi: Agisoft PhotoScan UAV Image Processing Specifications for the Foot11 Wellsite

Agisoft PhotoScan

Processing Report

20 March 2015

Survey Data

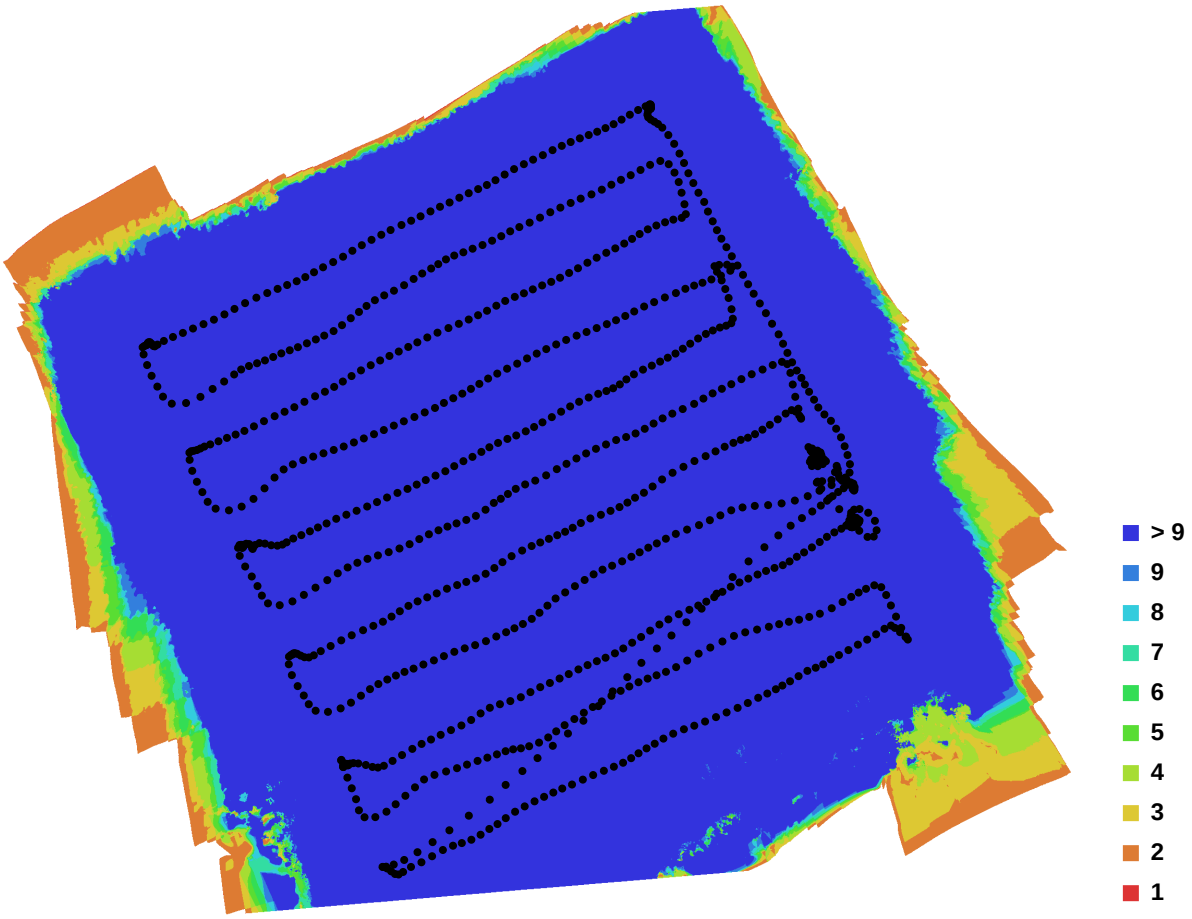

Fig. 1. Camera locations and image overlap.

Number of images:	924	Camera stations:	924
Flying altitude:	74.7271 m	Tie-points:	2533846
Ground resolution:	0.0159413 m/pix	Projections:	7701555
Coverage area:	0.0645517 sq km	Error:	0.764035 pix

Camera Model	Resolution	Focal Length	Pixel Size	Precalibrated
DMC-GF1 (20 mm)	4000 x 3000	20 mm	4.32666 x 4.32666 um	No

Table. 1. Cameras.

Camera Calibration

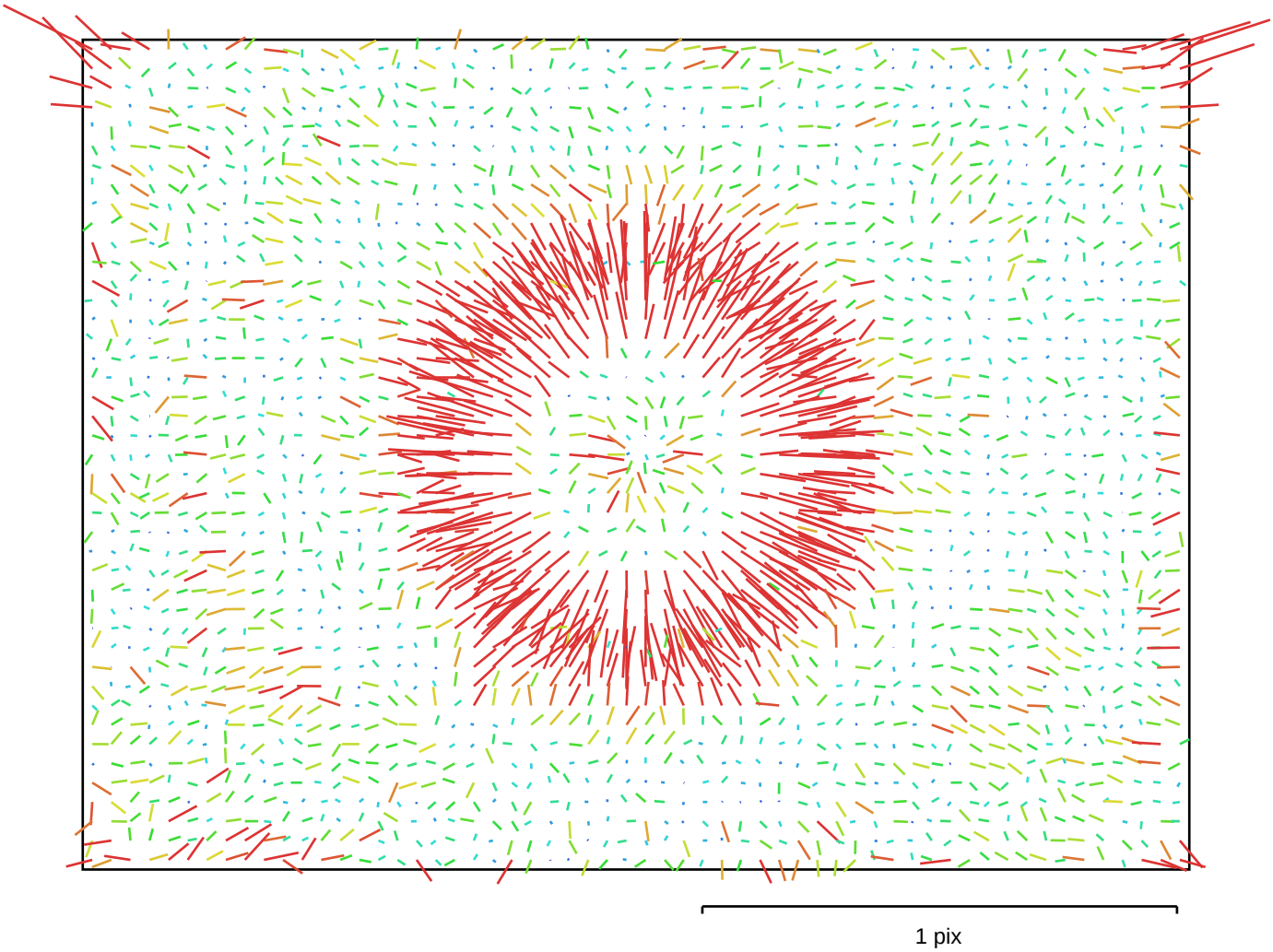

Fig. 2. Image residuals for DMC-GF1 (20 mm).

DMC-GF1 (20 mm)

Type:	Frame	K1:	-0.0205915
Fx:	4472.89	K2:	0.00926525
Fy:	4472.89	K3:	0.0343159
Cx:	1997.2	K4:	0
Cy:	1501.76	P1:	0
Skew:	0	P2:	0

Ground Control Points

Fig. 3. GCP locations.

Label	X error (m)	Y error (m)	Z error (m)	Error (m)	Projections	Error (pix)
point 1	0.520755	0.734860	0.028871	0.901132	81	0.352475
point 2	-0.725672	0.673911	-0.019364	0.990520	99	0.399762
point 3	0.203831	-1.407906	-0.003058	1.422588	56	1.106991
Total	**0.528940**	**0.996055**	**0.020148**	**1.127966**	**236**	**0.632819**

Table. 2. Control points.

Digital Elevation Model

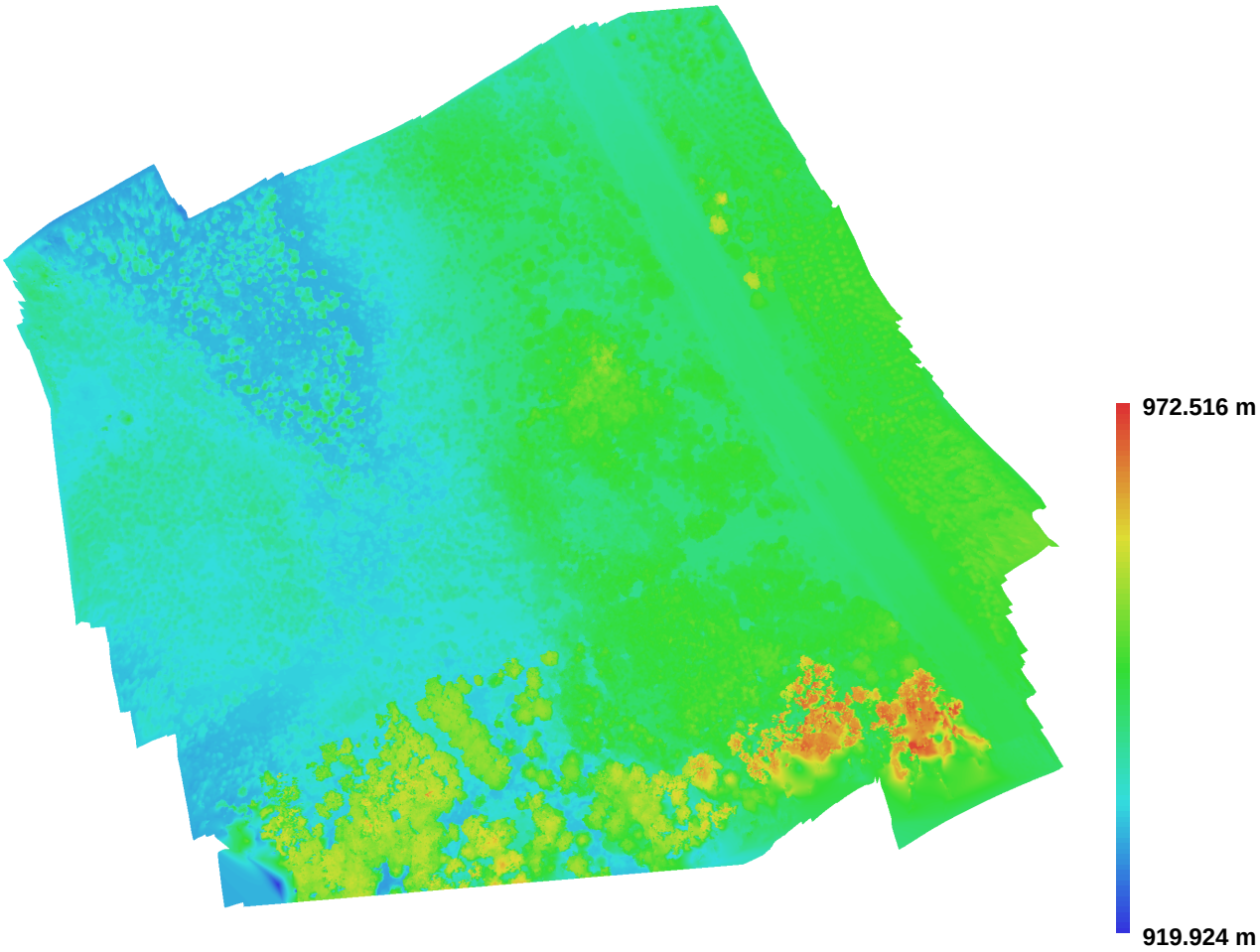

Fig. 4. Reconstructed digital elevation model.

Resolution:	0.0637653 m/pix
Point density:	245.941 points per sq m

Appendix A-vii: Agisoft PhotoScan UAV Image Processing Specifications for the Foot12 Wellsite

Agisoft PhotoScan

Processing Report

20 March 2015

Survey Data

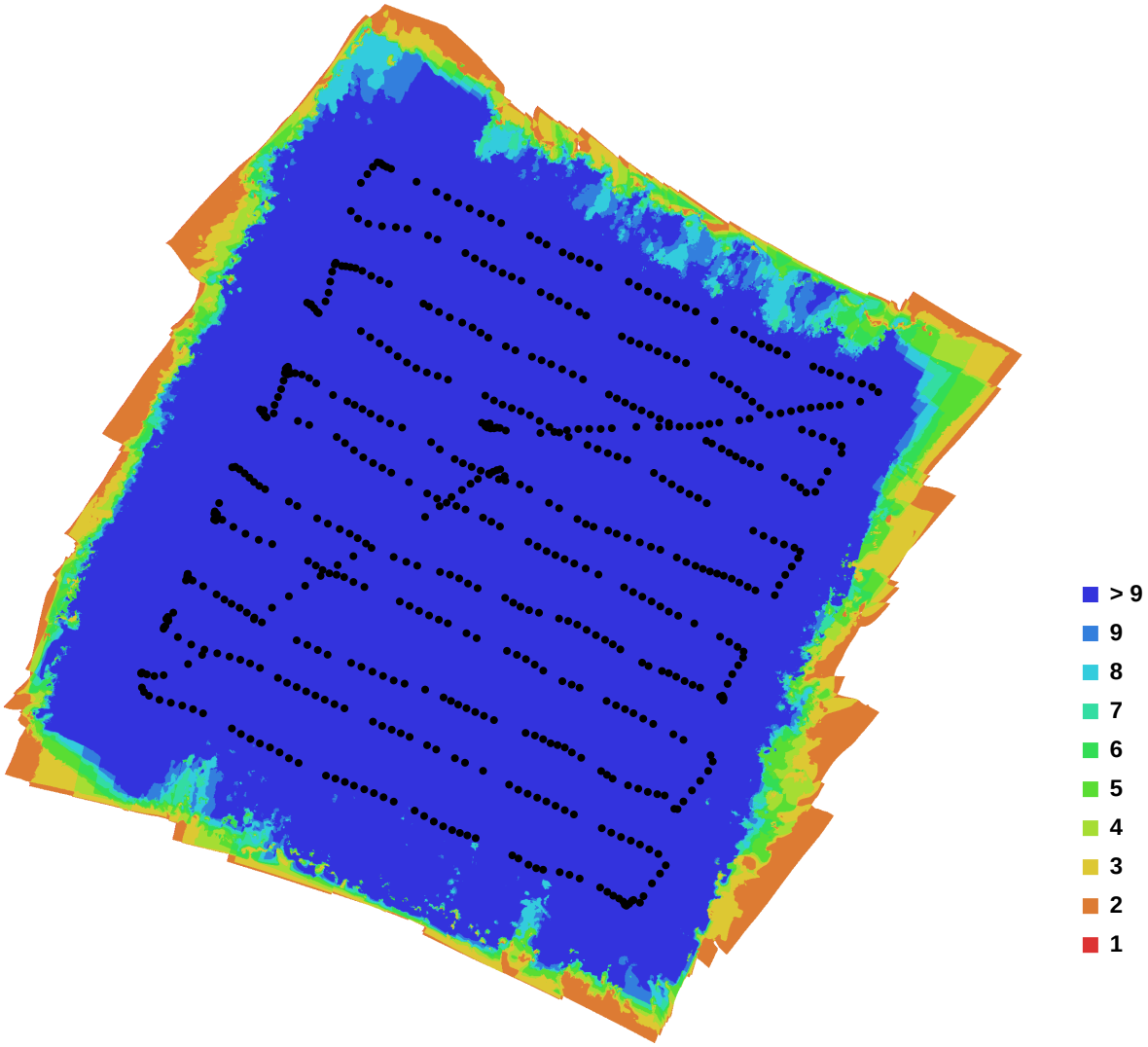

Fig. 1. Camera locations and image overlap.

Number of images:	619	Camera stations:	619
Flying altitude:	66.5539 m	Tie-points:	1698569
Ground resolution:	0.0140302 m/pix	Projections:	5505454
Coverage area:	0.0605587 sq km	Error:	0.71596 pix

Camera Model	Resolution	Focal Length	Pixel Size	Precalibrated
DMC-GF1 (20 mm)	4000 x 3000	20 mm	4.32666 x 4.32666 um	No

Table. 1. Cameras.

Camera Calibration

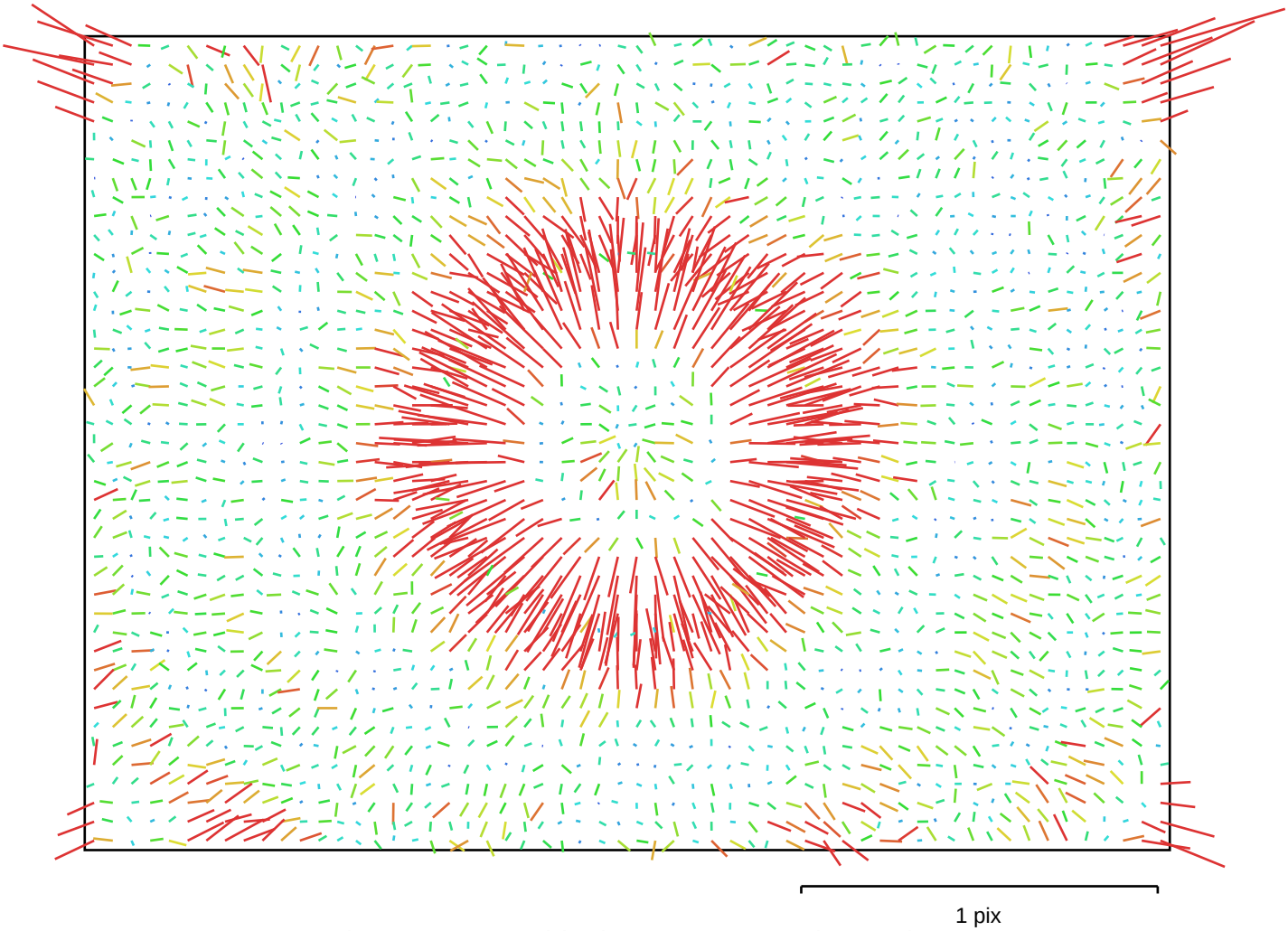

Fig. 2. Image residuals for DMC-GF1 (20 mm).

DMC-GF1 (20 mm)

Type:	Frame	K1:	-0.0151854
Fx:	4469.28	K2:	-0.0273779
Fy:	4469.28	K3:	0.111315
Cx:	1996.71	K4:	0
Cy:	1506.37	P1:	0
Skew:	0	P2:	0

Ground Control Points

Fig. 3. GCP locations.

Label	X error (m)	Y error (m)	Z error (m)	Error (m)	Projections	Error (pix)
point 1	1.573070	-1.171148	0.089286	1.963189	31	0.566822
point 2	-2.424103	-0.825827	-0.106969	2.563144	35	0.879461
point 3	0.852218	1.996491	0.017738	2.170845	35	0.617659
Total	**1.739454**	**1.418867**	**0.081095**	**2.246211**	**101**	**0.706289**

Table. 2. Control points.

Digital Elevation Model

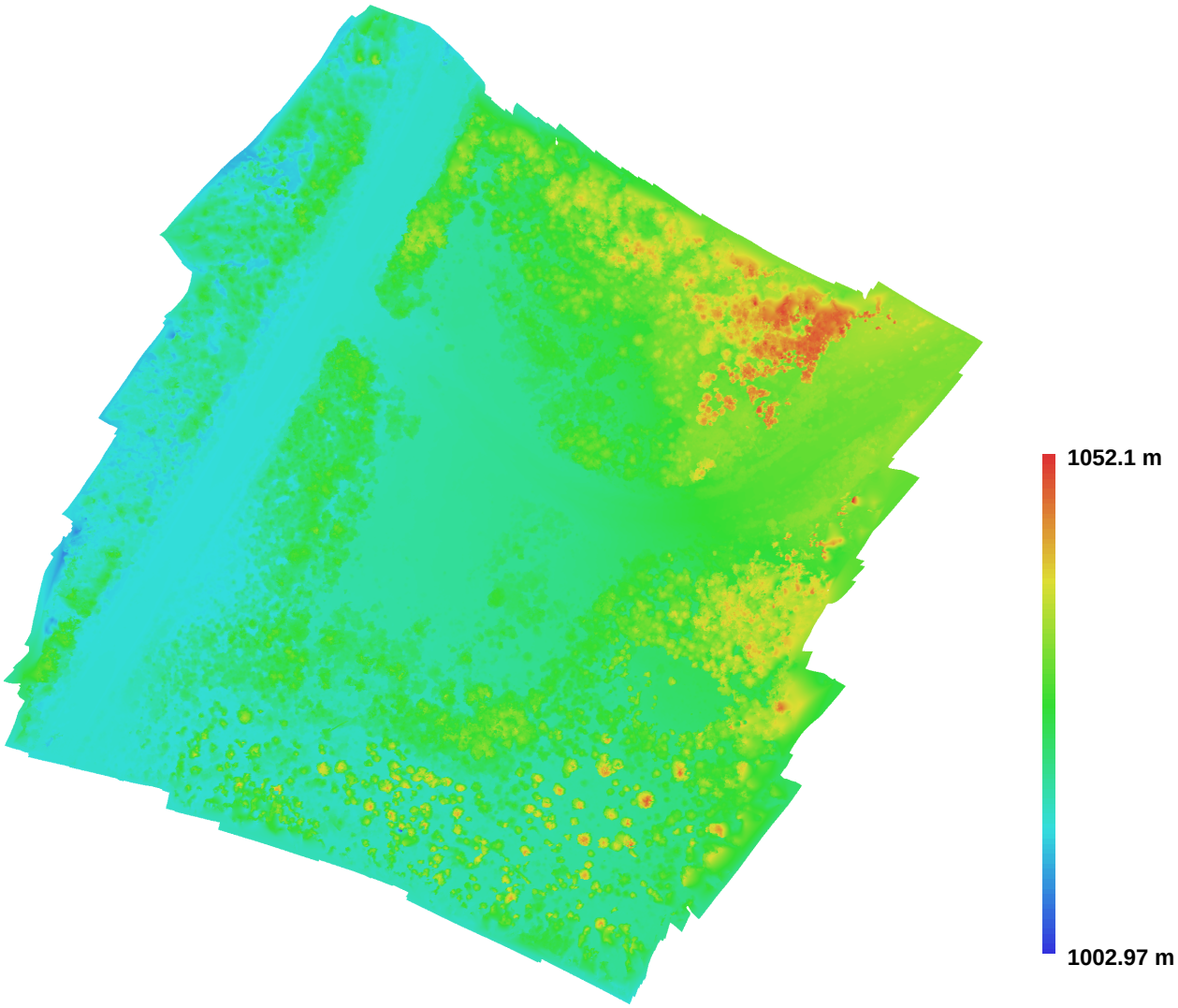

Fig. 4. Reconstructed digital elevation model.

Resolution:	0.0561209 m/pix
Point density:	317.505 points per sq m

Appendix A-viii: Agisoft PhotoScan UAV Image Processing Specifications for the Foot13 Wellsite

Agisoft PhotoScan

Processing Report

20 March 2015

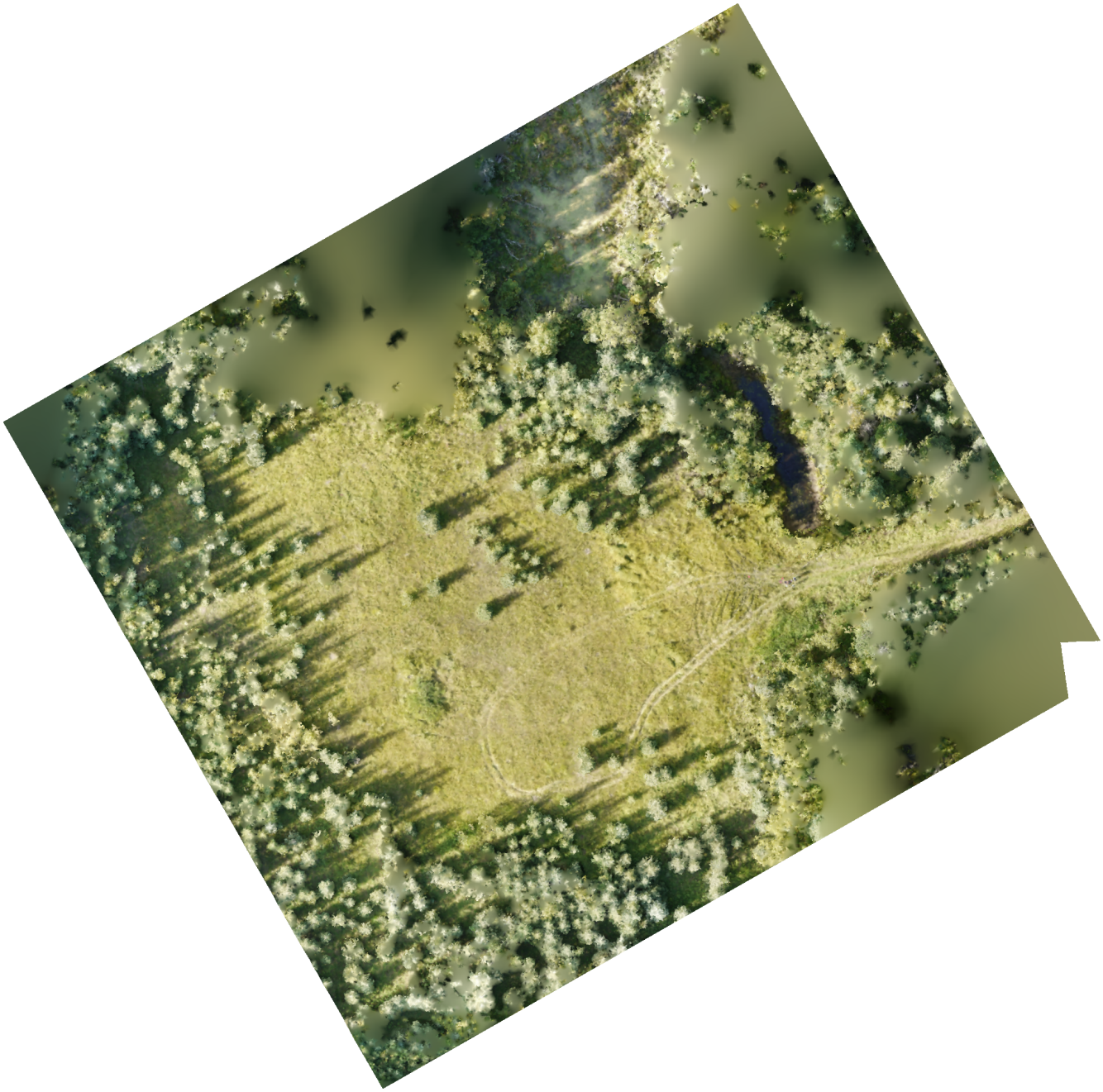

Survey Data

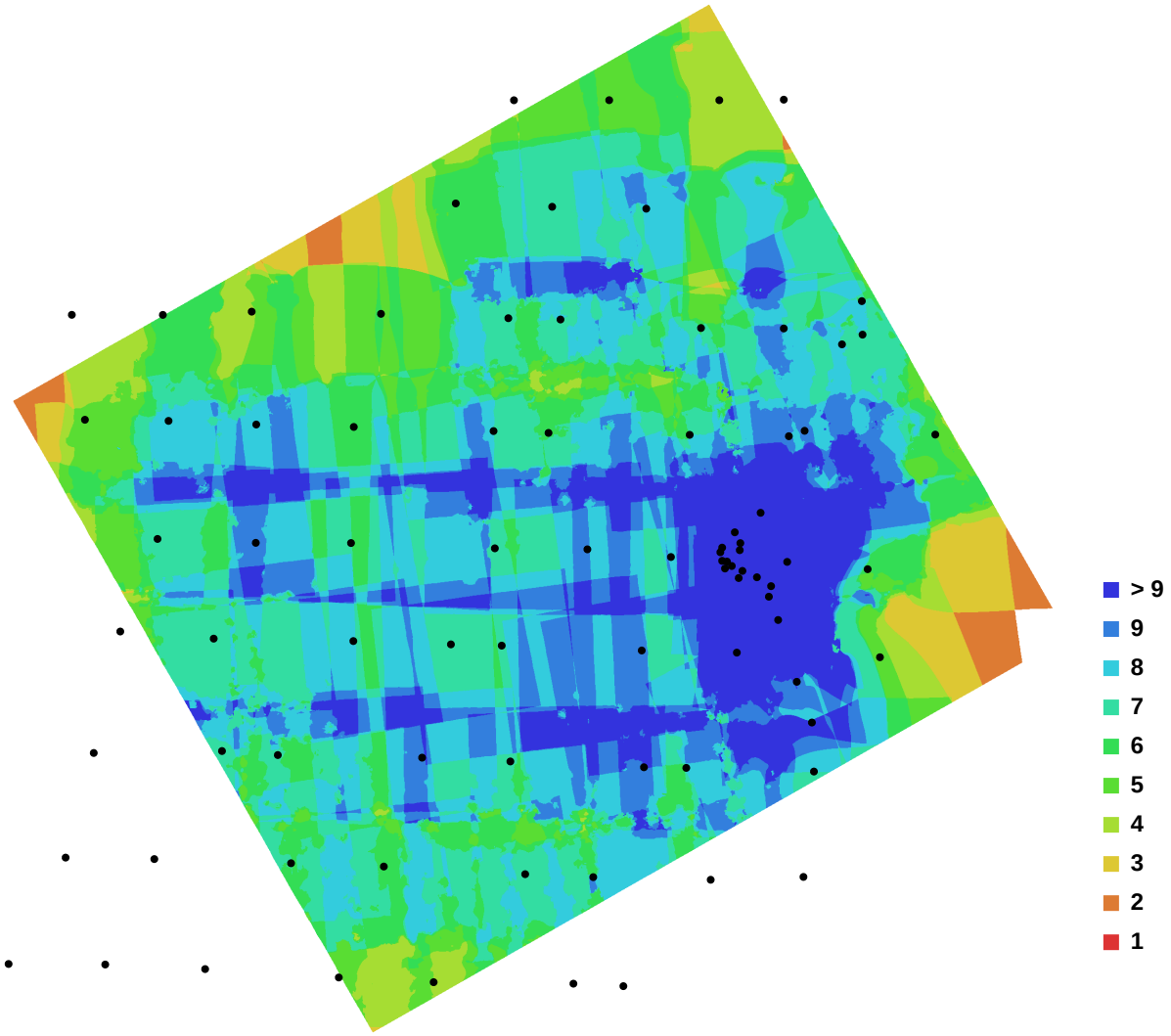

Fig. 1. Camera locations and image overlap.

Number of images:	147	Camera stations:	85
Flying altitude:	58.0884 m	Tie-points:	92749
Ground resolution:	0.0119593 m/pix	Projections:	228457
Coverage area:	0.0154552 sq km	Error:	0.606157 pix

Camera Model	Resolution	Focal Length	Pixel Size	Precalibrated
DMC-GF1 (20 mm)	4000 x 3000	20 mm	4.32666 x 4.32666 um	No

Table. 1. Cameras.

Camera Calibration

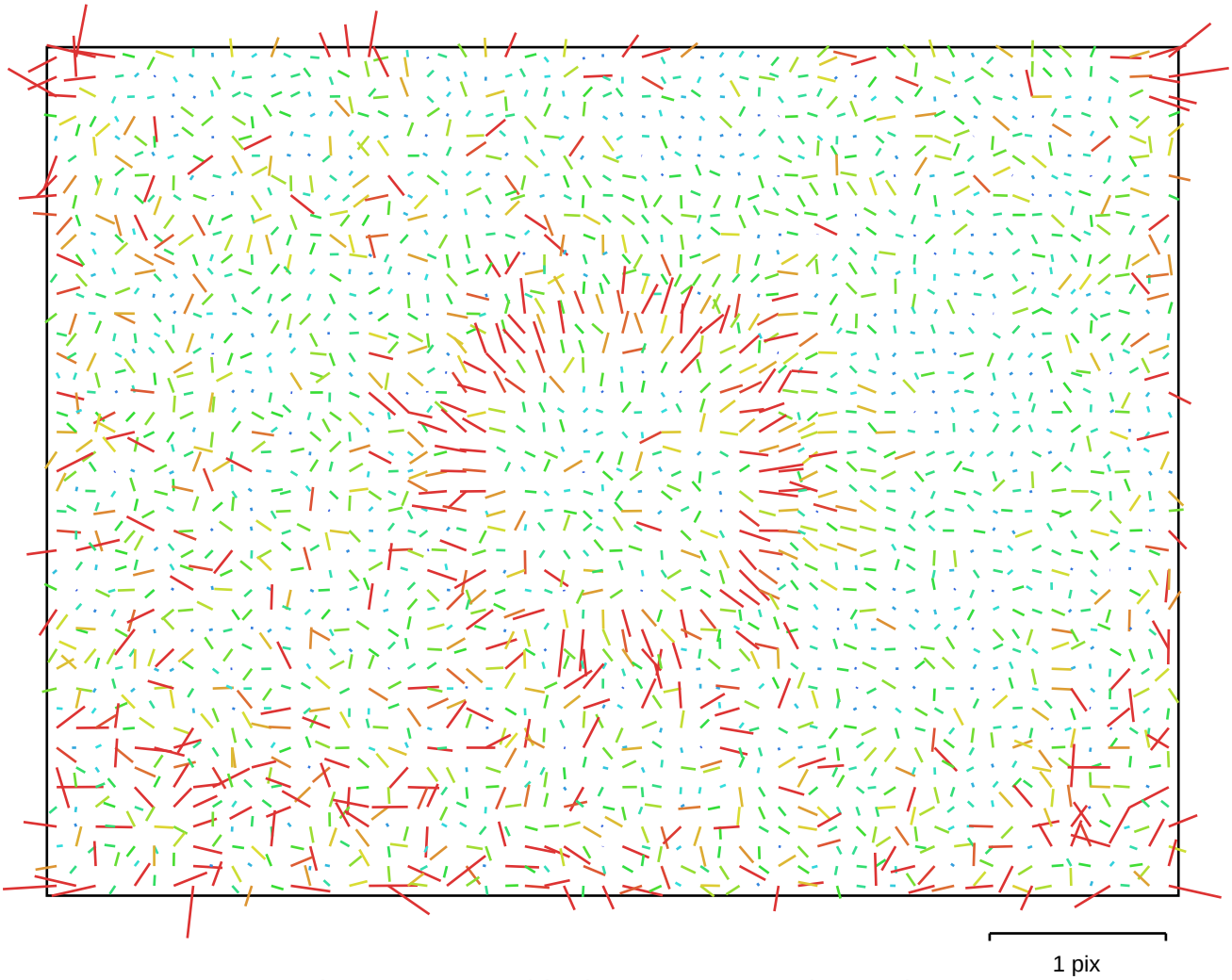

Fig. 2. Image residuals for DMC-GF1 (20 mm).

DMC-GF1 (20 mm)

Type:	Frame	K1:	-0.0164554
Fx:	4449.16	K2:	-0.0278829
Fy:	4449.16	K3:	0.109993
Cx:	2012.6	K4:	0
Cy:	1495.88	P1:	0
Skew:	0	P2:	0

Ground Control Points

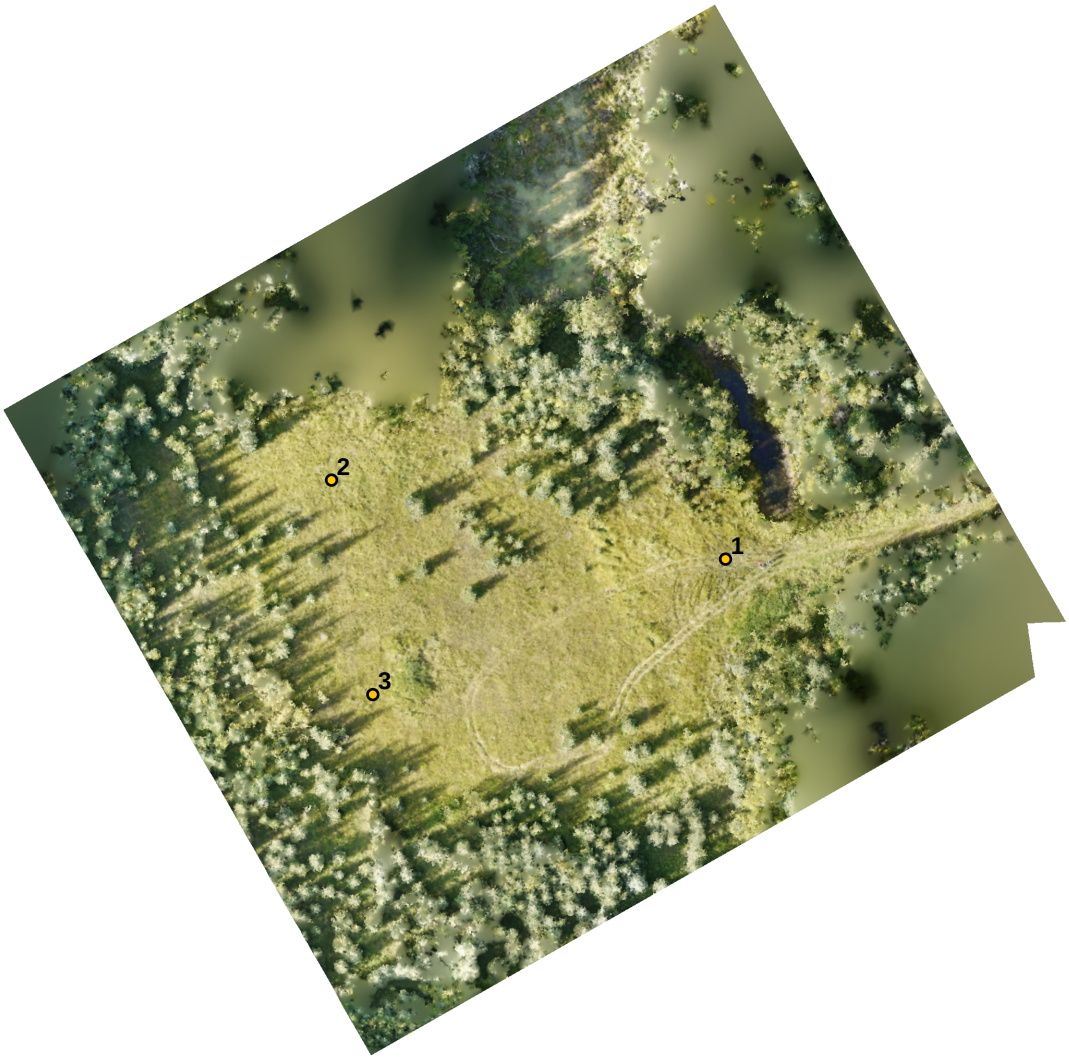

Fig. 3. GCP locations.

Label	X error (m)	Y error (m)	Z error (m)	Error (m)	Projections	Error (pix)
1	-0.617160	-0.331851	-0.003029	0.700729	23	2.679842
2	-0.382929	1.164339	0.050779	1.226743	8	0.419452
3	1.010303	-0.833321	-0.061229	1.311062	6	0.542352
Total	**0.718385**	**0.848574**	**0.045959**	**1.112775**	**37**	**2.133061**

Table. 2. Control points.

Digital Elevation Model

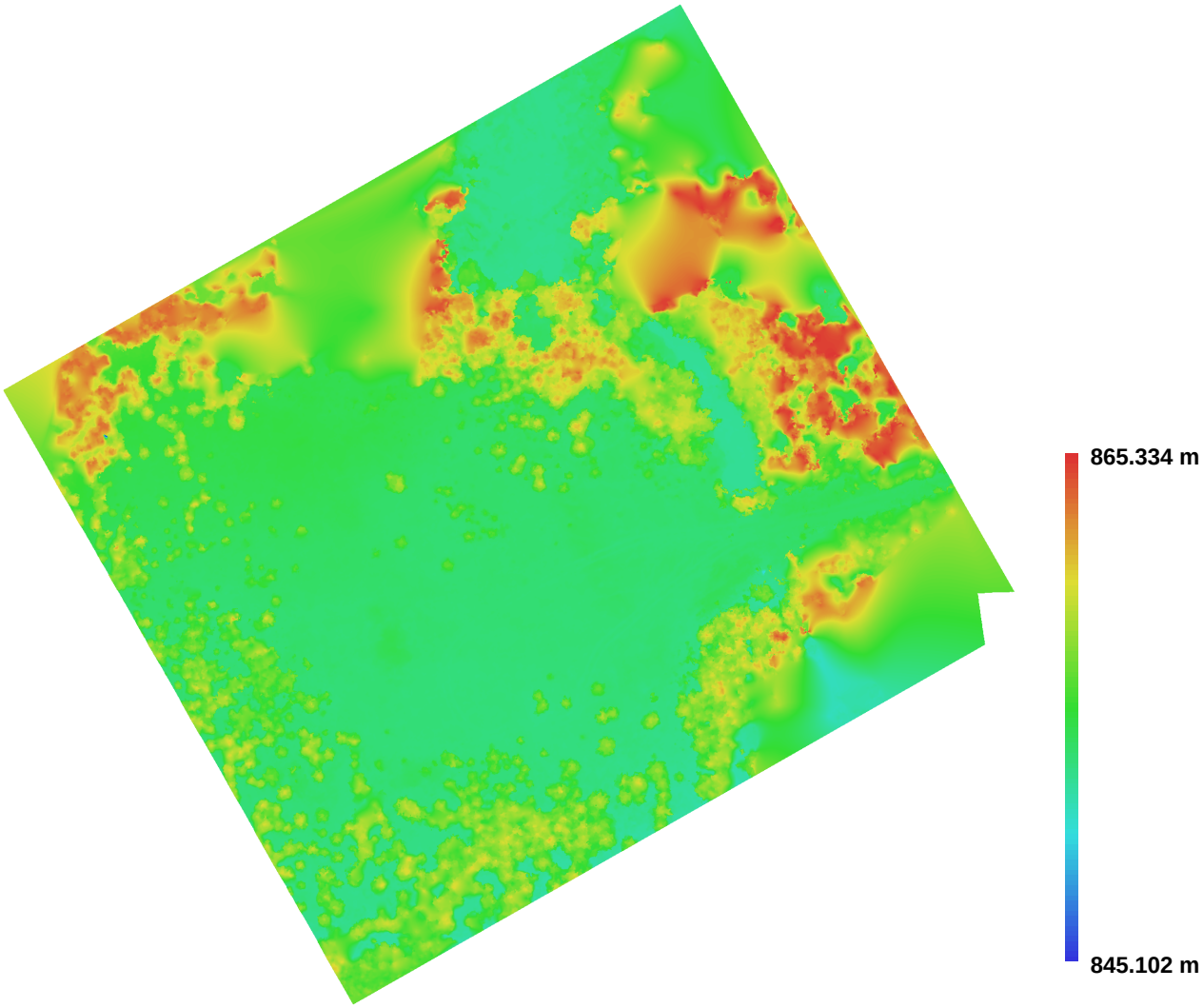

Fig. 4. Reconstructed digital elevation model.

Resolution:	0.0478373 m/pix
Point density:	436.985 points per sq m

Appendix A-ix: Agisoft PhotoScan UAV Image Processing Specifications for the Foot15 Wellsite

Agisoft PhotoScan

Processing Report

20 March 2015

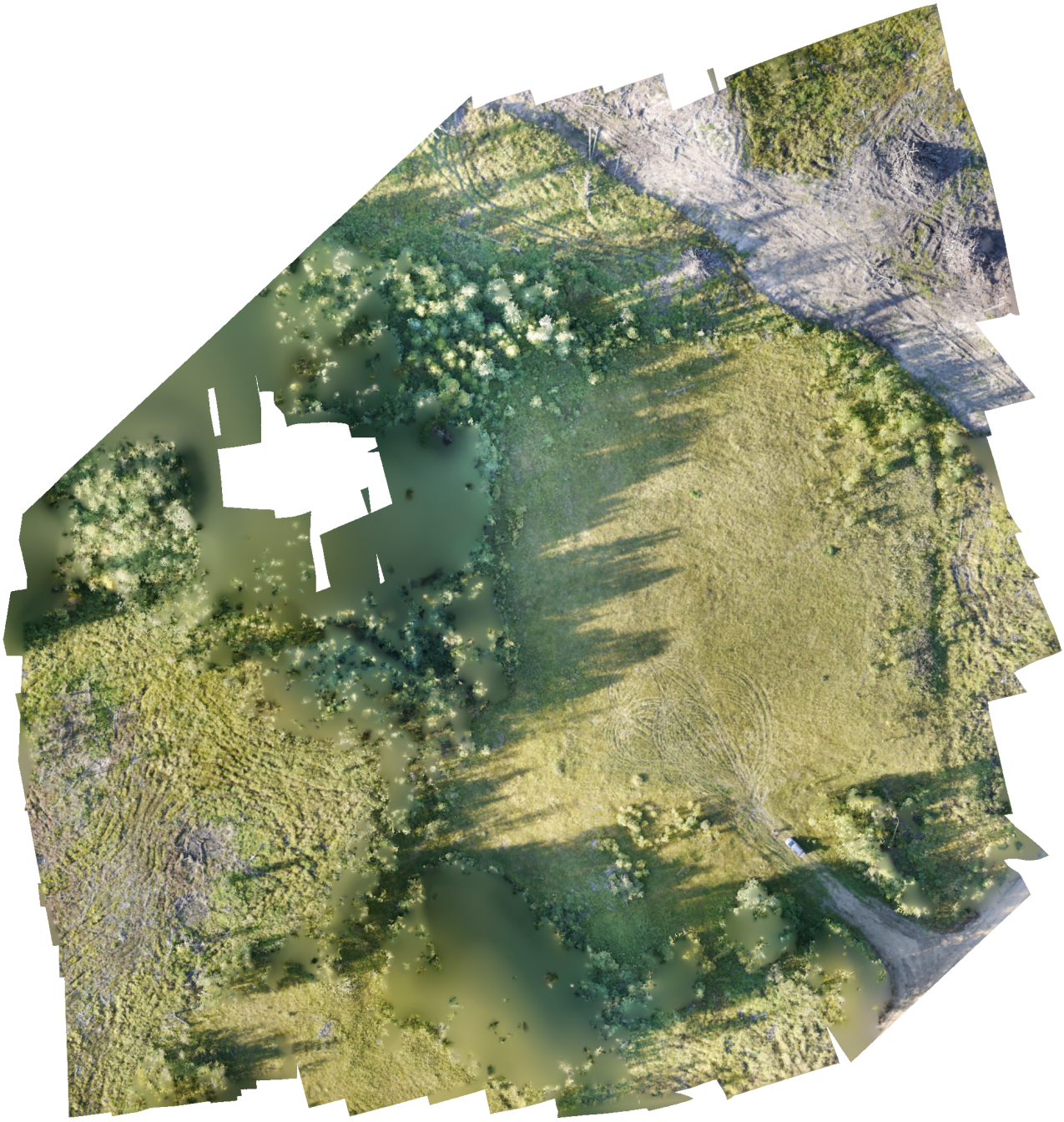

Survey Data

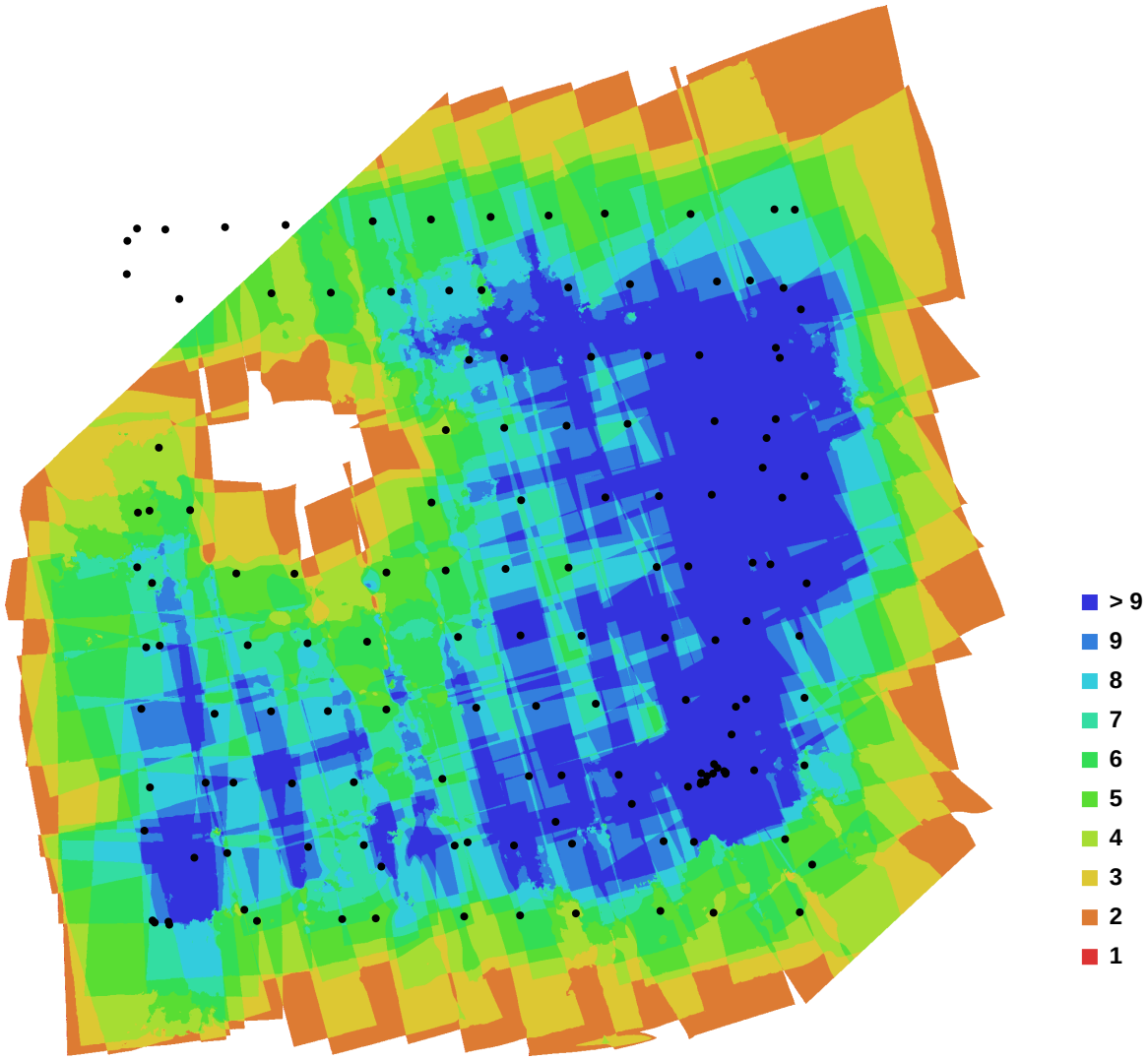

Fig. 1. Camera locations and image overlap.

Number of images:	157	Camera stations:	143
Flying altitude:	65.4497 m	Tie-points:	453042
Ground resolution:	0.0141272 m/pix	Projections:	1255545
Coverage area:	0.0506851 sq km	Error:	0.531815 pix

Camera Model	Resolution	Focal Length	Pixel Size	Precalibrated
DMC-GF1 (20 mm)	4000 x 3000	20 mm	4.32666 x 4.32666 um	No

Table. 1. Cameras.

Camera Calibration

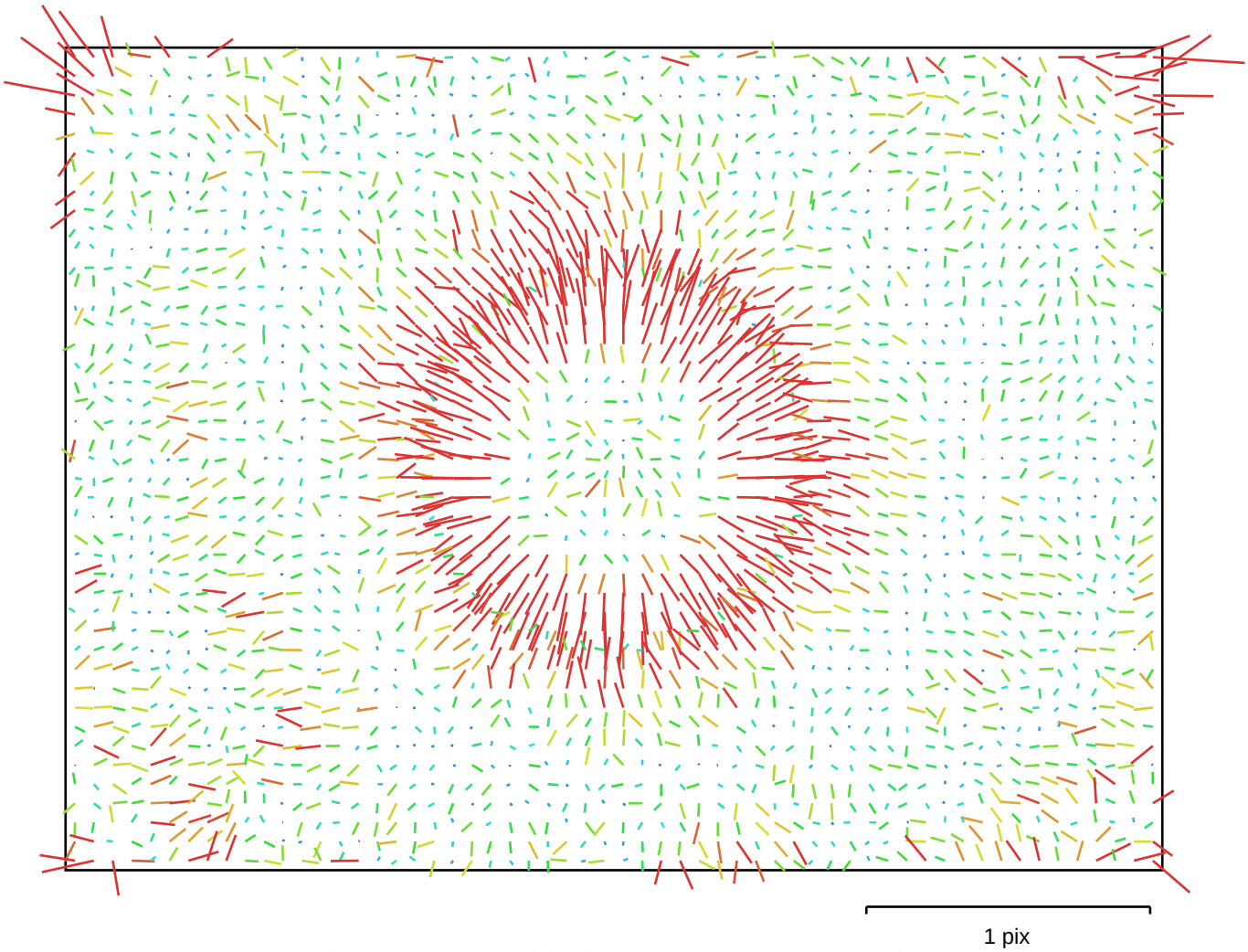

Fig. 2. Image residuals for DMC-GF1 (20 mm).

DMC-GF1 (20 mm)

Type:	Frame	K1:	-0.0187969
Fx:	4456.35	K2:	-0.00934355
Fy:	4456.35	K3:	0.0807776
Cx:	1995.86	K4:	0
Cy:	1495.18	P1:	0
Skew:	0	P2:	0

Ground Control Points

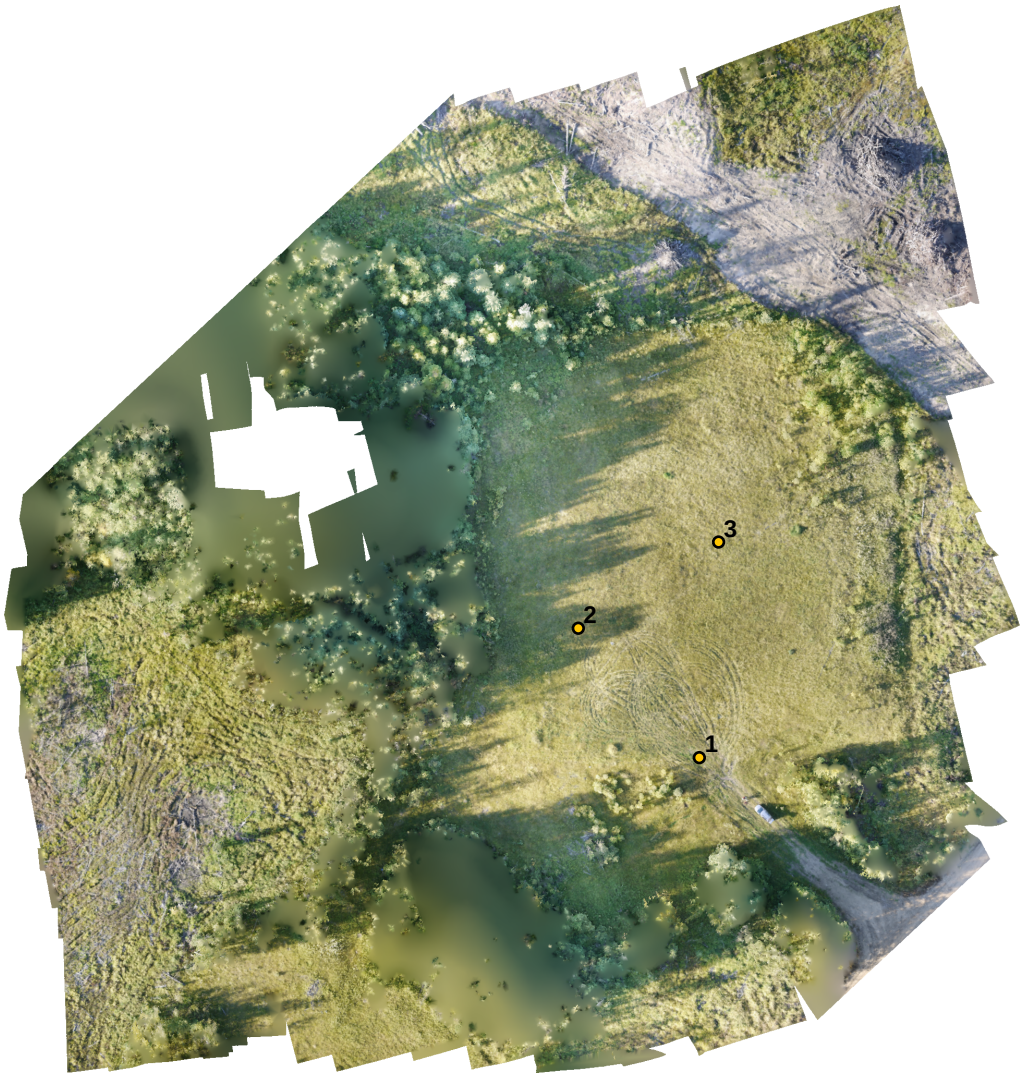

Fig. 3. GCP locations.

Label	X error (m)	Y error (m)	Z error (m)	Error (m)	Projections	Error (pix)
1	-0.803723	-0.034212	0.038533	0.805373	17	1.591507
2	0.674475	-0.824874	0.003120	1.065526	9	0.519792
3	0.134733	0.857170	-0.049272	0.869092	14	0.541850
Total	**0.610748**	**0.687102**	**0.036158**	**0.920017**	**40**	**1.113567**

Table. 2. Control points.

Digital Elevation Model

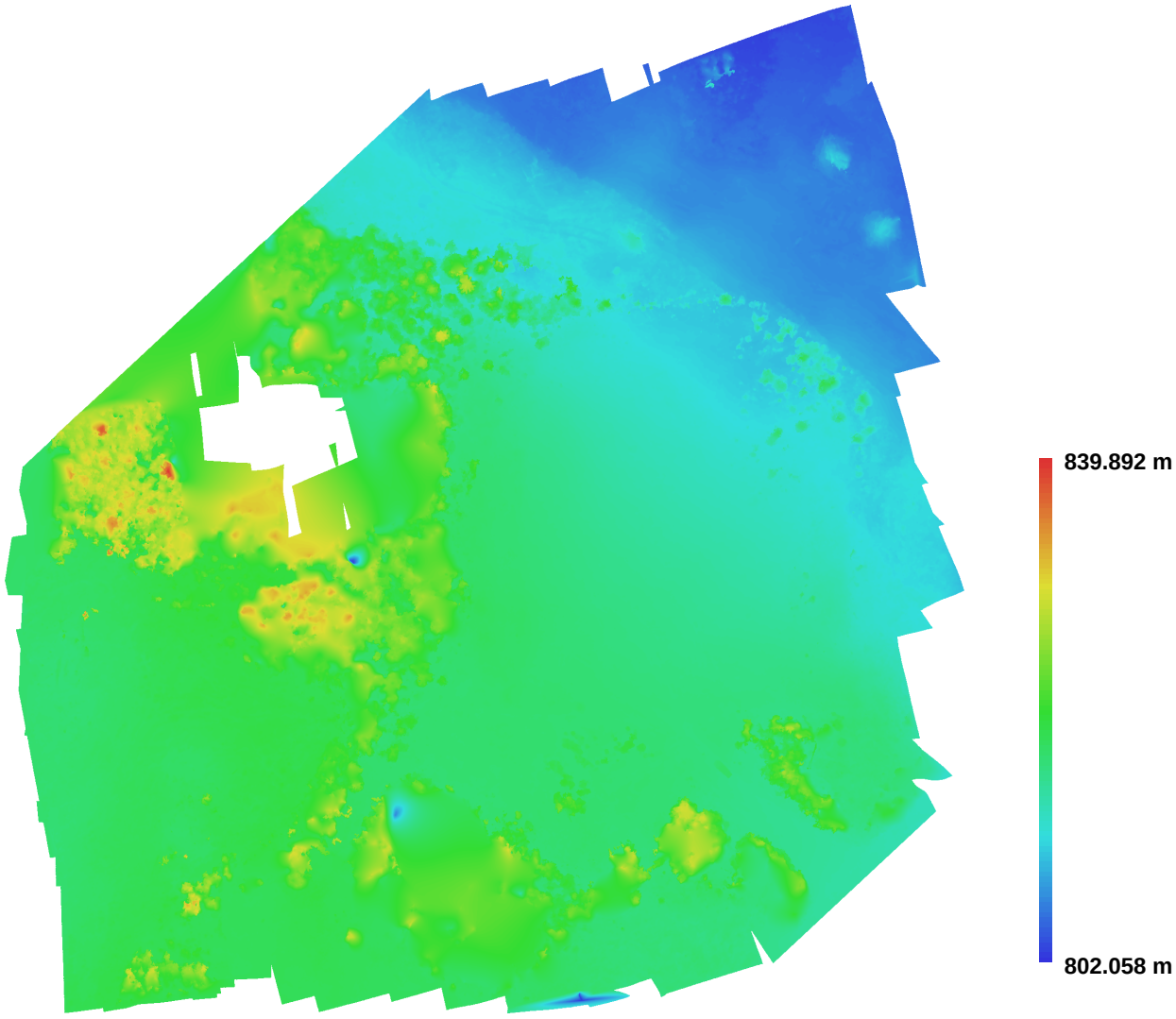

Fig. 4. Reconstructed digital elevation model.

Resolution:	0.0565088 m/pix
Point density:	313.161 points per sq m